Site U1307[1]

Expedition 303 Scientists[2]

Chapter contents

Background and objectives 1
Operations 2
Lithostratigraphy 2
Biostratigraphy 5
Paleomagnetism 7
Composite section 8
Geochemistry 9
Physical properties 11
References 13
Figures 15
Tables 49

Background and objectives

Integrated Ocean Drilling Program Site U1307 is located 53 km (28 nmi) northwest of Site U1306 (Fig. F1 in the "Site 1306" chapter) in 2575 m water depth, 300 m deeper than the water depth at Site U1306. The objective at Site U1307 was to recover the older part of the section on the Eirik Drift below the Quaternary sections recovered at Sites U1305 and U1306. Along seismic Line 25 (Fig. F1) of the multichannel seismic (MCS) network obtained over the Eirik Drift during *Knorr* cruise KN166-14, the Pliocene section is accessible at penetration depths less than ~300 m and is therefore recoverable with the advanced piston corer (APC). The MCS profile for Line 25 indicates a series of well-developed mudwaves with axes oriented approximately northwest–southeast (Fig. F2). The Quaternary sediment drape thins from northeast to southwest along this seismic line, bringing the Pliocene section closer to the sediment/water interface.

The oldest sediment recovered at Site U1306 (294.8 meters below seafloor [mbsf]) was uppermost Pliocene (~2 Ma). In Figure F2, we estimate the section recovered at Site U1306 transposed onto Line 25 (Fig. F1). Extrapolation of the Site U1306 penetration depth along Line 19 to Line 25 yields a corresponding thickness of 230 m and a mean sedimentation rate of 11 cm/k.y., whereas the mean sedimentation rate for the recovered section at Site U1306 was 15 cm/k.y. The 162 m penetration at Site U1307 succeeded in recovering sediments as old as 3.58 Ma, at a mean sedimentation rate of 4.5 cm/k.y.

Site U1307 (proposed Site LAB8C) was not a primary site for Expedition 303. It was necessary to remain in the vicinity of the Eirik Drift after termination at Site U1306 because of a severe storm along the intended transit to proposed Site IRD1A (Site U1308). Nonetheless, the two holes drilled at Site U1307 demonstrated the feasibility of recovering pre-Quaternary sediments on the Eirik Drift at penetration depths achievable with the APC. This will allow the high-resolution Quaternary climate record recovered at Site U1306 to be extended into the Pliocene. It will also contribute significantly to our understanding of the sedimentary architecture of the Eirik Drift and the formation of the mudwaves by providing detailed stratigraphic records of the pre-Quaternary sequence that can be correlated throughout the MCS network obtained during cruise KN166-14. The preservation of microfossils and the pristine magnetostratigraphic records at Sites U1305–

[1]Expedition 303 Scientists, 2006. Site U1307. *In* Channell, J.E.T., Kanamatsu, T., Sato, T., Stein, R., Alvarez Zarikian, C.A., Malone, M.J., and the Expedition 303/306 Scientists. *Proc. IODP,* 303/306: College Station TX (Integrated Ocean Drilling Program Management International, Inc.). doi:10.2204/iodp.proc.303306.107.2006
[2]Expedition 303 Scientists' addresses.

doi:10.2204/iodp.proc.303306.107.2006

U1307 indicate that the sediments have the required attributes for precise stratigraphic age control in the framework of a paleointensity-assisted chronology. The effort to recover the pre-Quaternary sequence, and hence pursue the pre-Quaternary sedimentation history of the Eirik Drift and extend the high-resolution environmental record into the Pliocene, is intended for continuation during Expedition 306.

Operations

The 28 nmi transit from Site U1306 to U1307 was accomplished in 3.1 h at an average speed of 9.2 kt. At 0824 h on 28 October 2004, the beacon was deployed initiating operations at Site U1307.

Hole U1307A

With the bit at 2586.4 meters below rig floor (mbrf), Hole U1307A was spudded with the APC at 1425 h on 28 October 2004. The recovery of the initial core was 9.48 m, suggesting an estimated seafloor depth of 2575.1 meters below sea level (mbsl) (2586.4 mbrf). Piston coring and drilling advanced the hole to a total depth of 162.6 mbsf, with an average recovery of 102.5% for the cored interval (Table **T1**). Core 6H was a partial stroke and only advanced 3 m (47.5–50.5 mbsf) before encountering a hard or debris-rich layer. The interval from 50.5 to 52.5 mbsf was drilled without coring to advance the bit beyond this layer. Core 9H also was a partial stroke that recovered only 2.2 m (71.5–73.7 mbsf), which resulted in drilling the interval from 73.7 to 77.7 mbsf to advance the bit beyond the layer. A total of five cores were advanced by recovery (Cores 6H, 9H, 13H, 15H, and 18H). No core barrels had to be drilled over. The bit clogged prior to Core 19H and required the deployment of the bit deplugger and several coring line round trips before the core could be obtained. Because our strategy at this site was to core until a weather window opened to allow a safe transit to Site U1308, the depth objective was limited by the available operational time and the desire to acquire a complete composite section. Operations in Hole U1307A ended when the bit cleared the seafloor at 1155 h on 29 October.

Hole U1307B

The ship was offset 30 m to the northwest, and Hole U1307B was spudded at 1250 h on 29 October 2004. With the bit positioned 4.5 m shallower than at Hole U1307A, we obtained a 4.83 m core, suggesting a seafloor depth of 2575.3 mbsl (2586.6 mbrf). Piston coring advanced the hole to a total depth of 154.6 mbsf, with an average recovery of 101.5% (Table **T1**). Unlike in Hole U1307A, only one core (Core 17H) was a partial stroke. Coring was terminated when the passing low-pressure system began to affect drilling operations because of excessive heave. The drill string was recovered and the ship was secured for transit. We departed Site U1307 at 1300 h on 30 October to safely navigate behind the storm, as the weather deteriorated to a Force 8 gale with winds gusting to 40 kt and 5.5 m seas.

Lithostratigraphy

Two holes were drilled at Site U1307 (Table **T1**). All cores were recovered using the APC, and recovery was good (102.0%). The sedimentary record at Site U1307 reflects the different degrees of mixing between terrigenous and biogenic material (primarily quartz, detrital carbonate, nannofossils, and foraminifers) (see **"Site U1307 smear slides"** in "Core Descriptions;" Fig. **F3**), so the most common lithologies are silty clay, silty clay with foraminifers, foraminifer silty clay, foraminifer sandy clay, foraminifer ooze, nannofossil silty clay, silty clay nannofossil ooze, and sandy clay (Fig. **F4**). The top of the succession is dominated by olive-brown and olive-gray colors, whereas different shades of greenish gray are more abundant toward the bottom. Variations in color between light gray and very dark gray are common and represent high to low nannofossil contents, respectively. Bioturbation is generally moderate to abundant, as indicated by the presence of numerous distinct pyritized silty clay-filled and sandy silt-filled burrows. Gradational and burrowed contacts between the various sediment types are much more common than well-defined, sharp boundaries. However, irregular, sharp contacts typically occur at the bases of foraminifer ooze layers.

Smear slide analyses recorded the abundances of terrigenous components, the most abundant of these being quartz, 2%–95%; detrital carbonate, 0%–35%; clay minerals, 0%–70%; and heavy minerals (especially hornblende), 0%–10% (Fig. **F3**). Among the biogenic components, nannofossils are widely distributed in the upper and lower intervals of the succession, whereas foraminifers are found predominantly in the upper part of the succession. The relative abundances of biogenic components are foraminifers, 0%–56%; nannofossils, 0%–70%; diatoms, 0%–12%; and sponge spicules, 0%–5%. Total carbonate content ranges from <1 to 58 wt% (see **"Geochemistry"**). Pyrite (usually associated with burrows) and iron oxide coatings on grains are present locally and were the only authigenic components observed.

Dropstones are present in low numbers throughout the entire cored interval. The dropstones display a

wide range of compositions, including acidic intrusive and metamorphic (granites and granitoids), basic igneous and/or metamorphic (basalts and metabasalts), and sedimentary and metasedimentary (sandstone, quartzite, and mudstone) rocks.

Large-scale patterns in the distribution of major lithologies at Site U1307 are represented in Figure F4. Of the 317 m recovered at this site, 279 m (88%) is silty clay, 16 m (5%) is nannofossil-dominated sediments (silty clay nannofossil ooze and nannofossil ooze), 16 m (5%) is foraminifer-dominated sediments (silty clay foraminifer ooze and foraminifer ooze), and 5.6 m (1.7%) is sandy clay. The sediments at Sites U1307 have been divided into three units: Unit I comprises Holocene–lower Pleistocene terrigenous and biogenic sediments that contain both nannofossil and foraminifers; Unit II is mainly composed of terrigenous materials of early Pleistocene–Late Pliocene age that lack biogenic carbonate; and Unit III comprises the nannofossil-bearing, but foraminifer-barren, lower Upper Pliocene succession.

Description of units

Unit I

Intervals: Sections 303-U1307A-1H-1, 0 cm, to 5H-7, 33 cm; and 303-U1307B-1H-1, 0 cm, to 6H-2, 102 cm

Depths: Hole U1307A: 0–46.6 mbsf and Hole U1307B: 0–45.1 mbsf (0 to 49.37–49.55 meters composite depth [mcd])

Age: Holocene–early Pleistocene

Unit I is composed predominantly of silty clay with foraminifers, foraminifer silty clay, foraminifer sandy clay, silty clay foraminifer ooze, foraminifer ooze, nannofossil ooze, silty clay nannofossil ooze with foraminifers, and nannofossil silty clay. Foraminifer silty sand and sandy foraminifer ooze beds are present as minor lithofacies. Colors are predominantly olive-brown (2.5Y 4/3 and 2.5Y 4/4), olive-gray (5Y 4/2), light olive-gray (5Y 6/2), gray (5Y 5/1), dark gray (5Y 4/1 and N/4), and very dark gray (5Y 3/1 and N/3), with lesser occurrences of light gray (5Y 6/1), which corresponds to foraminifer ooze. Contacts between these color changes are typically gradational or bioturbated (Fig. F5). The most common exceptions are the sharp contacts at the bases of the foraminifer silty sands and the sandy foraminifer oozes (Fig. F6). These coarser-grained intervals have irregular basal contacts and gradational or bioturbated upper contacts (Figs. F7, F8). A 1.1 m thick foraminifer ooze layer in Cores 303-U1307A-5H and 303-U1307B-6H marks the bottom of Unit I (Fig. F9) and its irregular base is the boundary between Units I and II. The boundary may represent a hiatus in the sedimentary record, although this has not been indicated by micropaleontologic analyses (see "Biostratigraphy"). Paleomagnetic data indicate that the foraminifer ooze layer is coeval with the base of the Jaramillo Subchron (see "Paleomagnetism") and may correlate with ~20 cm thick foraminifer ooze layer of the same age observed at Site U1306. Bioturbation is common to abundant through most of this unit; the most common indicators are diffuse centimeter-scale mottling and millimeter-scale sandy silt or pyritized burrow fills. In a few cases, discrete burrows or discrete macroscopic pyritized burrows were observed. Dropstones are present throughout Unit I in low numbers, and their distribution is plotted in Figure F6.

Unit II

Intervals: Sections 303-U1307A-5H-7, 33 cm, to 15H-CC, 20 cm; and 303-U1307B-6H-2, 102 cm, to 14H-4, 150 cm

Depths: Hole U1307A: 46.6–125.7 mbsf (49.37–49.55 mcd) and Hole U1307B: 45.1–124.8 mbsf (132.98–133.86 mcd)

Age: early Pleistocene–Late Pliocene

Unit II is composed almost exclusively of silty clay. Single layers of sandy silty clay and foraminifer ooze are the only other lithologies within this 80 m thick interval. The dominant colors are dark greenish gray (5GY 4/1), gray (5Y 5/1), dark gray (5Y 4/1 and N/4), and very dark gray (5Y 3/1 and N/3). Boundaries between these color variations are generally gradational or bioturbated. Common to abundant bioturbation occurs through most of this unit, as seen by the diffuse, centimeter-scale mottling; millimeter-scale sandy silt or pyritic burrow fills; and discrete macroscopic pyritized burrows. Dropstones are slightly less numerous than in the overlying unit (Fig. F10). Micropaleontological analyses point to a hiatus with a duration of ~0.24 m.y., or a condensed interval, between Samples 303-U1307A-7H-1, 10–11 cm, and 7H-5, 10–11 cm. There is, however, no visual evidence for an erosional truncation that could indicate the presence of a hiatus in this interval.

Unit III

Intervals: Sections 303-U1307A-16H-1, 0 cm, to 19H-CC, 27 cm; and 303-U1307B-14H-5, 0 cm, to 17H-5, 125 cm

Depths: Hole U1307A: 125.7–162.6 mbsf (0–131 mcd) and Hole U1307B: 124.8–154.6 mbsf (163.82–173.6 mcd)

Age: Late Pliocene

Unit III consists of at least 30–38 m of variable mixtures of terrigenous and biogenic material, dominated by quartz and nannofossils. The resulting lithologies are silty clay, silty clay with nannofossils,

silty clay nannofossil ooze, silty clay nannofossil ooze with diatoms, and nannofossil silty clay. Note that lithologies containing <25% nannofossils are not classified as nannofossil ooze and are represented with the symbol of the major lithology in Figure F4. Therefore, although Unit III in Hole U1307B contains nannofossils, these do not appear in the graphic representation. Contacts between the major lithologies are generally gradational and defined by progressive color changes. The main colors are greenish gray (5GY 5/1), dark greenish gray (5GY 4/1), gray (5Y 5/1), dark gray (5Y 4/1), and very dark gray (5Y 3/1). As in the younger units, bioturbation is common to abundant through most of this unit, represented by diffuse centimeter-scale mottling, millimeter-scale sandy silt or pyritized burrow fills, and distinct macroscopic pyritized burrows. The abundance of dropstones is rarely more than 1 per 10 cm (Fig. F10).

Discussion

The Holocene–Upper Pliocene sedimentary succession at Site U1307 records variations in the input rates of terrigenous and biogenic components. Pelagic and hemipelagic depositional patterns at this site are principally governed by the interplay between thermohaline contour currents and the regional seafloor morphology, leading to the formation of a field of accreting sedimentary waves in an area of focused sedimentation. Winnowing and/or erosion may have occurred during periods of intensified current velocities. Evidence for unconformities in the sedimentary record at this site were not observed, but further examination of micropaleontological and paleomagnetic data will provide more precise sedimentation rate estimates.

The sediment composition reflects changes in paleoceanographic conditions of the overlying and surrounding water masses, with these being translated into changes in the phytoplankton and zooplankton assemblages and the discharge and source of icebergs.

The relative input of terrigenous and biogenic components during the deposition of Units I and III appears to have varied on timescales of tens to hundreds of thousands of years, as indicated by repeated broad changes in the abundances of quartz, detrital carbonate, foraminifers, and nannofossils (as observed in smear slides) and in the distribution of dropstones. Unit II, however, represents a time when terrigenous supply clearly dominated over the biogenic component with little variation.

The top of the succession, corresponding to Unit I, is characterized by olive-brown, olive-gray, and varying shades of gray. The lighter colors generally indicate higher nannofossil and/or foraminifer content. In Units II and III, dark greenish gray and dark to very dark gray colors dominate. The origin of the diffuse dark greenish gray banding that influences the coloration of the lower part of the succession has not been discerned but may be diagenetic in origin.

Based on smear slide observations, nannofossil abundances are higher within Units I and III than within Unit II (Fig. F3). The quartz profile appears to show an inverse pattern to biogenic carbonate, and relatively high values are estimated throughout the two holes. Detrital carbonate content is low and values do not exceed 30%.

Gravel counts, defined as the number of clasts >2 mm in every 10 cm interval of each section, yielded a total of 305 clasts or ~2 clasts per 2 m of core. Thus, dropstones are more abundant at Site U1307 than at Sites U1305 and U1306 (~1.7 and ~1 clast for every 3 m of core, respectively). Dropstone distribution maxima occur at the same level as the foraminifer-rich layers of Unit I (15–22 mcd) and Unit II (85–95 mcd).

Sources of terrigenous input may be differentiated by the dominance of quartz and detrital carbonate in smear slides, supplemented by the composition of dropstones observed throughout the succession. Dropstone compositions include acidic intrusive and metamorphic rocks, basic volcanics and metavolcanics, and sedimentary rocks (mainly mudstones). The source of granitic and gneissic dropstones is uncertain, whereas dropstones with more basic lithologies could have been derived from sources to the northwest or in central eastern Greenland. The dominance of quartz in the sediment composition may also point toward eastern Greenland as a likely source of the terrigenous fraction. On the other hand, the low detrital carbonate content indicates that the input from Hudson Bay is either limited at Site U1307 or diluted by very high input from other source areas.

Lightness (L*) values at Site U1307 are similar to those at the two previous sites, ranging from 34% to 50%. The sediment lightness record was compared to $CaCO_3$ values to evaluate the effect of carbonate content on sediment color. In general, the two records show similar patterns, although the $CaCO_3$ record has much lower resolution than L*. As at Sites U1305 and U1306, carbonate content is low, with most $CaCO_3$ values lower than 12 wt% (see "Geochemistry;" Fig. F11). At ~50 mcd, a 1.1 m thick foraminifer ooze layer was observed in both holes that yielded a $CaCO_3$ content of 57.6 wt%, which produced a distinct peak in the L* curve (~49%).

Unit III reflects pulses of varying inputs of terrigenous and biogenic (mostly nannofossil dominated) components. The shift to terrigenous-dominated deposition in Unit II might reflect increased terrestrial dilution of the biogenic fraction or decreased surface water productivity. Micropaleontological analyses show that the foraminifer ooze layers in Unit I are well sorted, probably due to reworking, indicating frequent changes in bottom-current regime. Deposition of Unit I was dominated by pelagic and hemipelagic processes. Episodically, however, more pervasive bottom currents seem to have affected the area, scouring the seabed, leaving sharp and irregular contacts and depositing coarser-grained beds of foraminifer silty sand and sandy foraminifer ooze. Eight of these beds are observed and only two of them are thicker than 80 cm (Table **T2;** Fig. **F9**). These intervals yield high L* and carbonate values and their locations are indicated in Figure **F11.**

One of the main aims of Expedition 303 was to extend the record of Pleistocene millennial-scale change beyond that obtained from conventional piston cores. Site U1307 appeared to be a good candidate for coring the upper to middle part of the Pliocene succession using the APC to recover older strata than at the previous sites. A qualitative analysis indicates that the lithologic changes recorded in Units I, II, and III cannot be linked consistently to glacial–interglacial stages as interpreted from magnetic susceptibility and carbonate records (see **"Composite section"** and **"Physical properties"**). Extracting paleoclimatic records from the range of sedimentary characteristics will require a variety of detailed postcruise studies.

Biostratigraphy

Samples from Site U1307 yield common to rare calcareous, siliceous, and organic-walled microfossils moderate to poor in preservation (Tables **T3, T4, T5, T6, T7, T8, T9, T10, T11**). Twenty datum events of calcareous nannofossils, diatoms, planktonic foraminifers, and dinocysts provide a preliminary age model at Site U1307 (Fig. **F12**). According to these events, at Site U1307 we recovered an Upper Pliocene–Pleistocene sequence spanning at least the last 3.4 m.y. An unconformity with ~0.24 m.y. duration, or a highly condensed section, is likely between Samples 303-U1307A-7H-1, 10–11 cm, and 7H-5, 10–11 cm (56.15–62.15 mcd). The hiatus is implied by absence of calcareous nannofossil marker species *Gephyrocapsa* spp. (large form).

Floral and faunal assemblages of planktonic organisms provide some insight into paleoceanographic conditions. Species abundance is generally low (Fig. **F13**). Assemblages of all groups are characterized by the presence of species indicative of subpolar to polar conditions during the Pleistocene. In particular, planktonic foraminifer assemblages are characterized by the dominance of *Neogloboquadrina pachyderma* (sinistral). In the early Late Pliocene (before 2.74 Ma), the sediments contain warm-water species such as the calcareous nannofossil *Discoaster asymmetricus, Discoaster brouweri, Discoaster pentaradiatus, Discoaster surculus,* and *Discoaster tamalis*.

Calcareous nannofossils

Calcareous nannofossils were examined in all core catcher samples from Holes U1307A and U1307B. Additional samples from interval 303-U1307A-5H-1, 10–11 cm, to 8H-6, 10–11 cm (1 sample/section), were also studied to determine if an unconformity exists between Samples 303-U1307A-7H-1, 10–11 cm, and 7H-5, 10–11 cm, and other stratigraphic issues in the sequences. Nannofossils are generally few to common in most samples and abundant or barren in a small number of samples. Preservation is poor to moderate and rarely good in some samples, and diversity is comparatively low. However, most of datum planes described by Sato et al. (1999) have been identified in the sedimentary sequence. The nannofossil datum events are listed in Tables **T3** and **T4,** and the correlations between holes and to the magnetostratigraphy are shown in Figure **F12.**

The first occurrence (FO) of *Emiliania huxleyi* (0.25 Ma) and the LO of *Pseudoemiliania lacunosa* (0.41 Ma) occur between Samples 303-U1307A-1H-CC and 2H-CC and 303-U1307B-1H-CC and 3H-CC. *Reticulofenestra asanoi,* which ranges from 1.16 to 0.85 Ma, is found just below and above the Jaramillo Subchron, between Samples 303-U1307A-5H-1, 10–11 cm, and 6H-1, 10–11 cm, and in Sample 303-U1307B-5H-CC. The FO of *Gephyrocapsa parallela* (0.95 Ma), which lies just above the Jaramillo Subchron of the Matuyama Chron, is found between Samples 303-U1307A-5H-2, 10–11 cm, and 5H-6, 10–11 cm.

Large-form *Gephyrocapsa* spp. (>6 m), which usually occurs between 1.45 and 1.21 Ma, was absent throughout the section. This indicates a hiatus or inferred condensed sequence with a duration of ~0.24 m.y. (minimum) between Samples 303-U1307A-7H-1, 10–11 cm, and 7H-5, 10–11 cm. Samples 303-U1307A-7H-5, 10–11 cm, to 9H-CC and 303-U1307B-8H-CC are characterized by the presence of *Gephyrocapsa oceanica, Gephyrocapsa caribbeanica,* and *P. lacunosa* and the absence of large-form *Gephyrocapsa* spp. This indicates an age of 1.45–1.65 Ma. Samples 303-U1307A-10H-CC and 303-U1307B-10H-CC are correlated to the latest Pliocene (1.73–2.74

Ma) because of the absence of *G. oceanica, G. caribbeanica,* and *D. tamalis* and rare presence of *Reticulofenestra* spp. (small). Samples 303-U1307A-15H-CC to 19H-CC and 303-U1307B-14H-CC to 17H-CC contain the Late Pliocene marker species such as *D. asymmetricus, D. brouweri, D. pentaradiatus, D. surculus, D. tamalis, Reticulofenestra ampla,* and *P. lacunosa*. Moreover, the occurrence of *R. ampla* and *D. tamalis* indicates this interval has an age of 2.74–3.85 Ma in the Late Pliocene. From these observations, we concluded that the Pliocene/Pleistocene boundary is situated between Samples 303-U1307A-9H-CC and 11H-CC and 303-U1307B-8H-CC and 10H-CC. Part of the Lower Pleistocene (1.21–1.45 Ma) may be missing or condensed at this site.

Although the assemblages found in the Quaternary sequences are characterized by low species diversity and by absence or rare occurrence of warm-water species, the lower Upper Pliocene assemblages (2.74–3.85 Ma) contain warm-water species such as *D. asymmetricus, D. brouweri, D. pentaradiatus, D. surculus,* and *D. tamalis*. This indicates that this area was strongly influenced by the drastic increase in arctic ice that occurred at 2.74 Ma (Jansen et al., 1988; Whiteman and Berger, 1992; Thiede and Myhre, 1996; Sato et al., 2004).

Planktonic foraminifers

Planktonic foraminifers were examined in all core catcher samples from Holes U1307A and U1307B (Table **T5, T6**). The upper core catchers of each hole contain soft sediment that was washed with tap water. Sediments of the lower sections were treated with H_2O_2 before washing. Planktonic foraminifers are mostly common to rare in abundance in the upper half of both holes and rare or barren in the lower half (Table **T5**). Preservation of tests is moderate to poor throughout the cored interval.

The FO of encrusted *N. pachyderma* (sinistral) generally occurs in the top of the Oludvai Subchron (Weaver and Clement, 1987) and is found in Samples 303-U1307A-10H-CC and 303-U1307B-9H-CC. In the Pleistocene section, *N. pachyderma* (dextral) typically occurs with 2%–4% of the frequency of *N. pachyderma* (sinistral). In the Pliocene, *N. pachyderma* (sinistral) is rare and not encrusted. In Sample 303-U1307A-15H-CC and 303-U1307B-14H-CC and below, *Neogloboquadrina atlantica* (sinistral) is the most abundant species, which indicates the *N. atlantica* Zone of the Upper Pliocene (Weaver and Clement, 1987). *Globigerina bulloides* and *Turborotalita quinqueloba* are occasionally present.

Benthic foraminifers

Benthic foraminifers were examined in all core catcher samples from Holes U1307A and U1307B (Table **T7**). Benthic foraminifers are rare in most sections of both holes and abundant only in the middle part (Samples 303-U1307A-11H-CC and 303-U1307B-10H-CC). Small-sized species *Bolivina translucens* species, small *Cassidulina* species, and *Epistominella exigua* are most commonly present.

Diatoms

Diatom assemblages were investigated in 36 core catcher samples and 39 additional samples from Holes U1307A and U1307B (Tables **T8, T9**). Diatoms are rare to common in the lowermost and uppermost part of the sequence (173–125 and 10–0 mcd, respectively) and mostly rare to barren between 125 and 33 mcd (Fig. **F13**). The sequence between 33 and 14 mcd is barren of diatoms. The preservation of diatom valves varies greatly throughout the sedimentary sequence. Valves appear better preserved in the lower and upper part of the sequence (163–125 and 65–0 mcd, respectively), whereas they show strong signs of dissolution between 110 and 65 mcd (Tables **T8, T9**). Silicoflagellates and the siliceous dinoflagellate *Actiniscus pentasterias* are present only in a few samples below 100 mcd (Tables **T8, T9**).

Because of low abundance of diatom valves at the site, only two datum events were recognized with low reliability. The LO of *Neodenticula seminae* (0.84–0.85 Ma, marine isotope Stage [MIS] 21; Koç et al., 1999) is tentatively placed between Samples 303-U1307A-3H-CC and 4H-CC and 303-U1307B-3H-CC and 4H-CC (Fig. **F12**). The FO of this species (1.25–1.26 Ma, MIS 37; Koç et al., 1999) is implied between Samples 303-U1307A-6H-CC and 7H-CC and 303-U1307B-6H-CC and 7H-CC. These stratigraphic placements do not reflect the true LO and FO of the species.

Seventy-two diatom species were identified at Site U1307 (Tables **T8, T9**). The diatom assemblage is dominated throughout by resting spores of *Chaetoceros,* mirroring high-nutrient content and low temperature of surface waters. The *Chaetoceros* community is accompanied by a few diatom species indicative of different ecological conditions. The main association, composed of spores of *Thalassiosira gravida,* forms of *Rhizosolenia hebetata, Actinocyclus curvatulus,* and abundant fragments of the *Thalassiothrix/Lioloma* complex, indicates subarctic–arctic waters (Andersen et al., 2004). Minor influence of sea-ice cover is revealed by the occurrence of *Fragilariopsis oceanica* and *Bacterosira fragilis*.

Radiolarians

Radiolarians were examined in all core catcher samples from Hole U1307A (Table **T10**). Radiolarian specimens occur in most samples examined. Their preservation is moderate to poor. The abundance of radiolarians is rare to trace because of both dissolution and dilution by detritus. Species diversity is low.

Cycladophora davisiana davisiana occurs in only three core catcher samples of Hole U1307A (Samples 303-U1307A-5H-CC, 6H-CC, and 12H-CC), and these samples are thus assigned to the Upper Pliocene–Pleistocene *C. davisiana davisiana* Zone of Goll and Bjørklund (1989). In the lower part of the sequence, from Samples 303-U1307A-13H-CC to 19H-CC, there is no occurrence of key species.

Palynomorphs

Palynological assemblages were examined in all core catcher samples from Hole U1307A (Table **T11**). The concentration of palynomorphs is low in most samples. Dinocysts are present in low numbers down to ~120 mcd. A few samples are barren (303-U1307A-2H-CC, 3H-CC, and 10H-CC). The interval below 120 mcd contains common to abundant marine palynomorphs including dinocysts *Cymatiosphaera* and incertae sedis, which probably belong to prasinophytes. In all studied samples, *Tasmanites* occurs below ~120 mcd. Terrestrial palynomorphs are present except in Sample 303-U1307A-2H-CC, which is barren. Pollen of *Pinus* and *Picea* are dominant. Pollen grains of angiosperms, spores of pteridophytes, and *Sphagnum* are also present in significant numbers in a few samples (notably in Sample 303-U1307A-1H-CC). Colonies of the freshwater algae *Pediastrum* are present in many samples. Reworked pre-Neogene palynomorphs are present in most samples. They are dominated by trilete spores but pollen, dinocyst, and acritarchs also occur. The acritarchs are mainly represented by small-sized species of *Pterospermella*. Among reworked dinocysts, specimens of the genera *Deflandrea* and *Oligosphaeridinium* were identified.

In the upper part of the sedimentary section (Samples 303-U1307A-1H-CC to 13H-CC), the dinocyst assemblages are characterized by moderately poor preservation, low concentrations, and low species diversity. The discontinuity of the sampled record and the presence of reworking prevents interpretations in terms of paleoceanography or biostratigraphy. The lower part of the section (below ~120 mcd), however, shows a different facies. Concentrations are higher and *Nematosphaeropsis* sp. 1, *Cymatiosphaera* ?*invaginata,* and incertae sedis sp. 1 occur in significant numbers. These three groups are characteristic of the Pliocene at Ocean Drilling Program (ODP) Site 646 (cf. de Vernal and Mudie, 1989). *Nematosphaeropsis* sp. 1 and incertae sedis sp. 1 are small-sized taxa (25–30 and 12–25 µm, respectively). They are not reported elsewhere, possibly because of sieving procedures (often 20 µm) or because these taxa are endemic to the northwestern North Atlantic. In any case, correlations with the palynological record of Site 646 allow some biostratigraphic conclusions, at least on regional scale. The distribution of marine palynomorphs in Hole 646B has been dated using age interpolations between the paleomagnetic reversal boundaries in the same hole (Clement et al., 1989). On these grounds, the LO of *Nematosphaeropsis* sp. 1 (Sample 303-U1307A-13H-CC) is dated 2.4 Ma and the LO of incertae sedis sp. 1 (Sample 303-U1307A-16H-CC) is dated ~2.6 Ma. In addition, the lowermost sample (Sample 303-U1307A-19H-CC) contains diversified assemblages of *Operculodinium* ?*eirikianum* and *Barssidinium pliocenum,* with LOs at ~3.3 Ma at Site 646.

Paleomagnetism

The natural remanent magnetization (NRM) of all undisturbed Site U1307 archive-half core sections were measured and remeasured after alternating-field (AF) demagnetization in peak fields of 10 mT. Additionally, Sections 303-U1307B-6H-2, 12H-4, 12H-5, and 16H-1 to 16H-4 were demagnetized at 15 mT. Sections 303-U1307A-8H-2, 8H-4, 13H-1, 13H-2, 17H-6, and 18H-1 to 18H-6 and Sections 303-U1307B-8H-4, 9H-1 to 9H-3, and 10H-3 were demagnetized at 20 mT. Sections 303-U1307A-3H-3 to 3H-5, and 4H-2 and Sections 303-U1307B-4H-5, 5H-3 to 5H-6, 6H-6, 13H-5 to 13H-6, and 16H-5 to 16H-7 were demagnetized at both 15 and 20 mT. The number of demagnetization steps and the peak fields used reflected the magnetic characteristics of the sediments, the severity of the drill string magnetic overprint, the shipboard protocol of not exceeding peak fields of 20 mT, and the need to maintain core flow through the laboratory. Sections completely affected by drilling disturbance were not measured. The NRM intensities, inclinations, and declinations from Site U1307 are shown in Figures **F14, F15,** and **F16,** respectively. Data associated with intervals identified as drilling slurry, deformation, and exceptionally coarse deposits (see **"Lithostratigraphy"**) are not shown. Average NRM intensities are strong and variable both before and after demagnetization. Intensities prior to demagnetization are generally in the 10^{-1} A/m range and occasionally as low as 1×10^{-2} A/m. Intensity variations occur at both the meter and tens of meters scales with longer variations having greater amplitude than the shorter ones (Fig. **F14**). After AF

demagnetization at peak fields of 10 or 20 mT, NRM intensities are reduced (low 10^{-1} A/m range) and the pattern of variability changes. The amplitude of the meter-scale variability becomes greater, whereas the longer-period variability is reduced. Below ~25 mcd, average values are lower and the general character of the meter-scale intensity variability changes with a downhole trend of decreasing peak values (Fig. **F14**).

Steep positive inclinations observed prior to demagnetization and caused by the drill string magnetic overprint are generally removed by peak AF demagnetization of 10 mT (Fig. **F15**). Demagnetization at higher peak fields (15 or 20 mT) results in little difference in either direction or intensity, indicating that the majority of the drill string overprint was successfully removed. Inclinations associated with normal and reversed polarities vary around the expected values (approximately ±73°) for a geocentric axial dipole. Declinations show within-core consistency and, when Tensor tool-corrected, facilitate polarity interpretations (Fig. **F16**). The directional record from Holes U1307A and U1307B document an almost-continuous sequence of polarity transitions, allowing correlation to the geomagnetic polarity timescale (Cande and Kent, 1995; Channell et al., 2002; 2003) (Figs. **F15, F16, F17**). Identification of the Brunhes, Matuyama, and Gauss Chronozones is unambiguous. Within the Matuyama Chronozone, the Jaramillo, Olduvai, and Reunion Subchronozones are identified. The lower Jaramillo polarity transition is truncated by a thick (1.1 m) sand layer in both holes (see **"Lithostratigraphy"**). A thinner sand layer was observed at the same stratigraphic interval at Site U1306 (see **"Paleomagnetism"** in the "Site U1306" chapter).

Below the Jaramillo Subchronozone, three normal polarity subchronozones are indicated by positive inclinations (Fig. **F15**) and reversed declinations (Fig. **F16**). Assuming constant sedimentation rates between the base of the Jaramillo and top of the Olduvai Subchronozones, a normal to reverse transition underlain by a core break at ~54 mcd is consistent with the top of the Cobb Mountain Subchronozone (Fig. **F17**). The missing base of the Cobb Mountain Subchronozone could reflect a hiatus, as suggested by nannofossil biostratigraphy. Two normal polarity subzones, each ~1.0 m thick, were observed at ~72.7 and 79.25 mcd in Hole U1307B (Figs. **F15, F16**). Based on constant sedimentation rates, these subzones are consistent with the Gardar (1.472–1.480 Ma) and Gilsa (1567–1575 Ma) magnetic excursions (Channell et al., 2002) (Fig. **F17**). Within the Gauss Chronozone, the Kaena and Mammoth Subchronozones are identified, though the normal polarity interval (C2An.2n) between them is thinner than would be expected based on constant sedimentation rates (Fig. **F17**). Figures **F15** and **F16** and Tables **T12** and **T13** document the polarity zonations and corresponding age interpretations.

Composite section

Cores were depth-shifted on the basis of magnetic susceptibility data collected with the "Fast Track" magnetic susceptibility core logger (MSCL) soon after recovery. Magnetic susceptibility proved most useful for correlating between holes at Site U1307 (Fig. **F18**). There were only two holes cored at Site U1307, and, with poor recovery of several intervals in Hole U1307A, it was impossible to construct a complete spliced record for the entire recovered section. There were, however, several long intervals of overlap between holes where cores could be correlated. The correlated segments have been appended to one another in the record. The offsets and composite depths are listed in Table **T14.** Correlation between Holes U1307A and U1307B was generally good down to the bottom of Core 303-U1307B-6H (56.5 mcd). Core 303-U1307A-6H was disturbed, had low recovery, and could not be correlated to Core 303-U1307B-6H. Consequently, Core 303-U1307B-7H was appended to Core 303-U1307B-6H. It correlated with Core 303-U1307B-7H but covered an almost identical interval, so Core 303-U1307B-8H was further appended and correlated with Core 303-U1307A-8H.

The tie between Core 303-U1307A-8H and Core 303-U1307B-9H at 76.4 mcd is tenuous but is supported by application of the average growth factor for Site U1307. Core 303-U1307A-9H was a partial APC stroke that recovered only 2.2 m and could not be correlated with any of the rest of the section. Correlation between holes is good from 76.4 mcd to 104.7 mcd. There is another tenuous correlation at 104.7 mcd (i.e., the base of Core 303-U1307B-11H to the top of Core 303-1307A-12H). Another good floating splice extends from Core 303-U1307A-12H to the base of Core 303-U1307B-15H (146.2 mcd), which cannot be matched to the top of Core 303-U1307A-17H.

The bottom few cores from each hole are poorly matched, but there is reasonable correlation between the middle segments of Cores 303-1307A-17H and 303-1307B-16H. Natural gamma ray (NGR) data suggest a correlation between the bottom of Core 303-U1307B-16H and the top of Core 303-U1307A-18H.

The sections of core used for the splice are identified in Table **T15.** We avoided using the first (top) section of each core wherever possible because it was often disturbed and contained gravel-sized ice-rafted de-

bris. The cores from Site U1307 provide a discontinuous stratigraphic sequence to ~160 mcd with the problematic intervals described above.

A growth factor (GF) of 1.06 is calculated by linear regression for both holes at Site U1307, indicating a 6% increase in mcd relative to mbsf (Fig. F19). We used this value of GF to calculate corrected meters composite depth (cmcd) presented in Table T14 to aid in the calculation of mass accumulation rates.

We calculated sedimentation rates using paleomagnetic and biostratigraphic datums. Linear regression provides a mean sedimentation rate of 4.9 cm/k.y. for the entire section cored at Site U1307 (Fig. F20). Using only paleomagnetic datums, interval sedimentation rates are still relatively uniform, varying between 2.7 and 7.6 cm/k.y., with a short interval between 148.3 and 148.9 mcd having a sedimentation rate of only 0.5 cm/k.y. (Table T16).

Geochemistry

Volatile hydrocarbons

Headspace gas analysis was performed as a part of the standard protocol required for shipboard safety and pollution prevention monitoring. From Hole U1307A, a total of 19 headspace samples were collected and analyzed at a sampling resolution of one per core (Table T17). Methane (C_1) concentrations decrease from 216 ppmv in the uppermost sample at 1.5 mbsf to 33 ppmv at 30 mbsf (Fig. F21). Between 30 and 63.5 mbsf, C_1 concentrations are relatively constant at ~31–35 ppmv. C_1 concentrations increase sharply downhole from 89 ppmv at 79.2 mbsf to 10,459 ppmv at 107.7 mbsf. From 107.7 mbsf toward the bottom of the recovered section, C_1 concentrations increase gradually and remain at relatively high levels ranging between 7,186 and 26,015 ppmv. Ethane (C_2) is present in sediments from 98.2 mbsf and below (Fig. F21), generally increasing downhole from 2 to 7 ppmv. No hydrocarbons higher than C_2 were detected. C_1 in the sediments at Site U1307 appears to have a biogenic origin, as indicated by the high C_1/C_2 ratios, which range between 2566 and 4023 (not shown; see Table T17 for data), and the absence of measurable higher volatile hydrocarbons.

Sedimentary geochemistry

A total of 31 sediment samples were collected for analysis of solid-phase geochemistry (inorganic carbon and elemental C, N, and S) at a sampling resolution of two per core from Hole U1307A. Figure F22 shows calcium carbonate ($CaCO_3$) concentrations, total organic carbon (TOC) contents, N elemental concentrations, and organic C/N ratios for Site U1307. Results of coulometric and elemental analyses are reported in Table T18.

$CaCO_3$ contents for Site U1307 samples are low, ranging from 0.3 to 12 wt%, except for Sample 303-U1307A-5H-6, 3–4 cm (45.5 mbsf), with 57.6 wt% $CaCO_3$ (Fig. F22). This sample was taken from a ~1 m thick foraminiferal sand layer (see "Lithostratigraphy"). The average value for $CaCO_3$ at Site U1307 is 3.8 wt% (excluding the sample from the foraminiferal sand layer at 45.5 mbsf). TOC contents at Site U1307 range between 0.01 and 0.42 wt% (average = 0.16 wt%) (Fig. F22). The mean total N content at Site U1305 is 0.04 wt% (Fig. F22). TOC and N records show no notable downhole trends. C/N values at Site U1307 are generally low, mostly ranging from 1 to 5 (Fig. F22), indicating preservation of marine organic matter in the recovered sediments. However, C/N ratios must be considered with care because the total N contents are low (i.e., <0.1 wt%). None of the analyzed samples contain measurable S.

Interstitial water chemistry

A total of 11 whole-round samples were collected from Hole U1307A for shipboard interstitial water geochemical analyses. In addition to whole-round sections, interstitial waters for shore-based studies were collected from small plug (~10 cm^3) sediment samples from the upper ~100 mbsf. Results of interstitial water analyses for Site U1307 are reported in Table T19 and Figure F23.

Chloride, sodium, salinity, pH, and dissolved boron

Chloride (Cl^-) concentrations increase from 560 mM in the shallowest sample (1.5 mbsf) to 575 mM in the deepest sample (154.6 mbsf) (Fig. F23). The overall Cl^- profile at Site U1307, with changes in slope at ~20 and 80 mbsf, is similar to that at Site U1306. The downhole increasing trend in Cl^- at Site U1307 suggests hydration reactions involving clay mineral alteration in the sediments. A similar downhole Cl^- profile is reported from Site 984 in the North Atlantic (Shipboard Scientific Party, 1996). Pore fluid sodium (Na^+) concentrations, calculated by charge balance, range from 485 to 493 mM (Fig. F23). Similar to the Cl^- profile, the highest Na^+ concentration is recognized in the deepest sample. Salinity (not shown) decreases downhole from 35 g/kg in the uppermost sample (1.45 mbsf) to 33 g/kg at 79.15 mbsf, below which the values increase to 34 g/kg.

pH generally increases downhole in the upper 53.95 mbsf, from 7.2 to 7.9 (Fig. F23). Between 53.95 and 154.55 mbsf, pH values decrease downhole to 7.32. Interstitial boron concentrations, mostly as boric acid

(H_3BO_3), range from 321 to 428 µM at Site U1307 (Fig. F23) and negatively correlate with pH (r = –0.94). Previous workers have reported that increasing boron concentrations with pH enhance the degree of boron adsorption by clay minerals (e.g., Keren and Mezuman, 1981; Palmer et al., 1987). Thus, the antithetic relationship between pore fluid pH and boron concentrations recognized at Site U1307, as well as the other Eirik Drift Sites U1305 and U1306, may be partly explained by pH control on boron adsorption by clay minerals. Along with the downhole increasing trends in interstitial water Cl^-, the antithetical pH and boron trends at the Eirik Drift sites appear to reflect reactions with the clay-rich sediments (see "Lithostratigraphy").

Alkalinity, sulfate, ammonium, and dissolved silica

Alkalinity increases with depth from 2.9 to 10.1 mM in the upper 79.2 mbsf, followed by a slight decrease to 8.9 mM toward the lowermost sample at 154.6 mbsf (Fig. F23). Sulfate (SO_4^{2-}) concentrations decrease linearly in the upper 79.2 mbsf from 29.1 to 1.6 mM and remain lower than 1 mM to the deepest sample (Fig. F23). Ammonium (NH_4^+) concentrations increase linearly (r = 0.99) over the entire recovered sequence, ranging from 11 to 1895 µM (Fig. F23).

The downhole decrease in SO_4^{2-} and increase in alkalinity and NH_4^+ in the upper 79.2 mbsf at Site U1307 reflect the effects of bacterial SO_4^{2-} reduction. The linear SO_4^{2-} profile in the upper 79.2 mbsf (r = 0.99) implies diffusion of SO_4^{2-} through the SO_4^{2-} reduction zone and focused consumption of SO_4^{2-} at the sulfate/methane interface (SMI), probably by anaerobic methane oxidation. The depletion of SO_4^{2-} to ~1.6 mM at 79.2 mbsf coincides with a sharp increase in interstitial C_1 concentration (Fig. F24). Such downhole trends in the SO_4^{2-} and C_1 profiles are common at all the other Eirik Drift sites drilled during Expedition 303 and support the inferred biogenic origin of C_1 (Claypool and Kvenvolden, 1983; Capone and Klein, 1988). The presence of C_1 (up to 216 ppmv) above the SMI at Site U1307 indicates simultaneous SO_4^{2-} reduction and methanogenesis, suggesting possible consumption of noncompetitive substrates for the methanogens (Mitterer et al., 2001). The coincident alkalinity maximum at the SMI also suggests anaerobic methane oxidation because bicarbonate is a by-product of this reaction. The downhole increase in alkalinity of ~7.2 mM within the SO_4^{2-} reduction zone is much smaller than the magnitude expected from the degree of SO_4^{2-} reduction (i.e., ~55 mM), implying diagenetic consumption of alkalinity in the sediments. The continuing downhole linear trend in NH_4^+ across the SMI at Site U1307 suggests that decomposition of organic matter and the resulting NH_4^+ production persist into the methanogenic zone.

Dissolved silica (H_4SiO_4) concentrations generally increase downhole from 338 µM in the shallowest sample to 885 µM in the lowermost sample (average = 569 µM) (Fig. F23). The downhole variability in the dissolved H_4SiO_4 profile may reflect varying degrees of dissolution and/or the presence of biogenic silica in the sediments.

Calcium, strontium, lithium, and barium

Pore fluid calcium (Ca^{2+}) concentrations increase by ~0.7 mM to 10.8 mM in the upper 20.5 mbsf and decrease steadily to 5.3 mM between 20.5 and 79.2 mbsf (Fig. F23). Below 79.2 mbsf, Ca^{2+} concentrations remain relatively constant with a slight increase toward the bottom of the recovered section. Strontium (Sr^{2+}) concentrations decrease downhole in the upper 79.2 mbsf from 86.6 to 75.9 µM (Fig. F23). Below 79.2 mbsf, Sr^{2+} concentrations increase with depth to 83.0 µM in the lowermost sample. Lithium (Li^+) concentrations decrease in the upper 23 mbsf from 22.9 to 10.4 µM and increase downhole to 23.5 µM in the deepest sample (Fig. F23).

Ca^{2+} shows an antithetic relationship to alkalinity (r = –0.97). Furthermore, the most depleted Ca^{2+} value at 79.2 mbsf (Fig. F23) coincides with the SMI (Fig. F24). This coincidence in Ca^{2+}, SO_4^{2-}, and alkalinity suggests precipitation of carbonate and associated consumption of alkalinity within the SO_4^{2-} reduction zone down to ~79.2 mbsf. The similar downhole trends recognized in the Ca^{2+} and Sr^{2+} profiles within the SO_4^{2-} reduction zone suggest the uptake of Sr^{2+} in the same diagenetic phase.

Unlike other Eirik Drift sites cored during Expedition 303 (i.e., Sites U1305 and U1306) and Site 646 (Shipboard Scientific Party, 1987), the Ca^{2+} profile at Site U1307 does not exhibit a downhole increasing trend below the SO_4^{2-} reduction zone. Downhole increases in Ca^{2+} (and decreases in Mg^{2+} and K^+) are generally interpreted as the result of the addition of Ca^{2+} ions into pore fluids associated with alteration of silicate minerals in the sediments and/or basement and subsequent diffusion (Gieskes and Lawrence, 1981). At Site U1307, the relatively constant Ca^{2+} values below the SO_4^{2-} reduction zone imply that the effect of silicate alteration is masked by removal of pore fluid Ca^{2+} associated with precipitation of carbonate (Fig. F23).

The downhole trend in Li^+ (Fig. F23) does not parallel the Ca^{2+} or Sr^{2+} trends at Site U1307, although the Li/Ca and Sr/Ca ratios between 11 and 79.2 mbsf appear to correlate well (r = 0.95). This implies that Li^+

concentrations in pore fluid are not solely controlled by diagenetic uptake by a carbonate phase. The downhole increasing trend in Li^+ below 30 mbsf suggests that silicate phases and/or clay mineral alteration may act as a major source for Li^+.

Interstitial water barium (Ba^{2+}) concentrations are relatively low (0.3–0.7 µM) in the upper 54 mbsf (Fig. F23). Between 54 and 79.2 mbsf, Ba^{2+} concentrations increase downhole from 0.5 to 5.9 µM. The sample with elevated Ba^{2+} at 79.2 mbsf is also characterized by depleted SO_4^{2-}. The relatively high Ba^{2+} concentrations, up to 10.8 µM, persist to the bottom of the recovered section. As commonly observed at the other Eirik Drift sites (Sites U1305 and U1306), increasing Ba^{2+} concentrations below the SO_4^{2-} reduction zone reflect dissolution of barite under conditions of SO_4^{2-} depletion. Similar trends in interstitial water Ba^{2+} profiles are reported from regions of high-sedimentation-rate depositional environments on continental margins and are often associated with "barite fronts" at the SMI (e.g., Torres et al., 1996a, 1996b; Dickens, 2001).

Magnesium, potassium, manganese, and iron

Magnesium (Mg^{2+}) and potassium (K^+) concentrations decrease downhole at Site U1307 (Fig. F23). The total decrease throughout the cored interval is 28% for Mg and 22% for K^+. However, it appears that the negative downhole Mg gradient is higher in the upper 79.2 mbsf (–0.17 mM/m) than the underlying sediments (0.01 mM/m). This implies a possible change in the mechanism governing the consumption of Mg^{2+} ions across the depth of alkalinity maximum. A similar trend in the Mg^{2+} profile is observed at Site U1305 where the gradient decreases between 60 and 140 mbsf but increases downhole. As inferred from interstitial Ca^{2+} and Sr^{2+} profiles, carbonate precipitation is indicated at the SMI at Site U1307. The higher gradient in the Mg^{2+} profile above this zone may reflect incorporation of ions into a carbonate mineral phase, whereas the lower gradient below 79.2 mbsf may reflect a decreased rate of removal. Although not documented at Site U1307 because of shallower penetration, the downhole decrease in pore fluid Mg^{2+} may persist in the sediments below ~155 mbsf, as observed at Site U1305, which cored to ~260 mbsf. The linear K^+ profile at Site U1307 (r = 0.98 overall) indicates that K^+ is being consumed by reactions within or below the cored interval, probably associated with silicate reaction (i.e., silicate diagenesis or alteration of basement) and subsequent diffusion.

Pore fluid manganese (Mn^{2+}) concentrations increase sharply downhole from 0.17 µM at 1.5 mbsf to 93.5 µM at 11 mbsf (Fig. F23). Below this maximum, Mn^{2+} concentrations decrease gradually toward the bottom of the cored section to 2.7 µM. The Mn^{2+} maximum at 11 mbsf suggests Mn^{2+} production within the Mn^{2+} reduction zone. Iron (Fe^{2+}) concentrations range from 0.08 µM in the uppermost sample to 19.6 µM in the deepest sample but do not show any significant downhole trend (Fig. F23). The lowest Fe^{2+} concentration at 1.5 mbsf indicates an oxidized condition evident in the other redox-sensitive element, Mn^{2+}, and sediment color. In general, the overall low interstitial Fe^{2+} concentrations indicate sequestration of dissolved ions into iron sulfides, which are commonly observed in the sediments (see "Lithostratigraphy").

Physical properties

Physical property data at Site U1307 were measured on both whole-round sections and discrete samples from split-core sections. Whole cores were measured every 5 cm. Samples were collected from each core in Hole U1307A for moisture and density (MAD) property measurements.

Whole-core magnetic susceptibility measurements

Magnetic susceptibility records are highly variable, responding to lithologic and/or mineralogic changes. Magnetic susceptibility measurements were obtained from the Fast Track MSCL and from the multisensor track (MST) system. There is an offset in susceptibility values between the MSCL and the MST records (see "Physical properties" in the "Site U1302–U1308 methods" chapter), but both records show the same variability downcore.

The magnetic susceptibility record shows multiple excursions toward high values (Fig. F25), with an average magnetic susceptibility of ~411 × 10^{-5} SI. No clear long-term trend is evident in the data, although there is some hint that the upper 10 m records lower magnetic susceptibility values. High-frequency variations occur at scales of a meter or less throughout the Site U1307 records. The amplitude of these meter-scale fluctuations is variable downcore. The largest peaks in magnetic susceptibility commonly correspond to darker layers (see "Lithostratigraphy"). Lower magnetic susceptibility values of 70 × 10^{-5} to 280 × 10^{-5} SI were observed and, in general, correspond to sediment of lighter color. An interval of exceptionally low magnetic susceptibility was recorded at 154–64 mcd (Cores 303-U1307A-18H and 303-1307B-16H). Here, values shifted abruptly to 27 × 10^{-5} to 30 × 10^{-5} SI (Fig. F26). This excursion to low values does not correlate with any major lithologic change (see "Lithostratigraphy"). X-ray diffraction (XRD)

analysis of sediments immediately above and within this low-magnetic susceptibility interval show identical bulk mineralogic records.

Density

Gamma ray attenuation (GRA) density values record a general increase downcore from ~1.55 to ~1.76 g/cm^3. Discrete bulk density values generally fall within the range of GRA density values, recording a similar downhole increase (Fig. F27). This density increase is typical of Expedition 303 sites and results from sediment compaction. Superimposed on this long-term increase are meter-scale fluctuations of ~0.2 g/cm^3. In most cases, single-point peaks correspond to large clasts (>2 cm) in the core (see **"Lithostratigraphy"**).

Natural gamma radiation

NGR counts generally increase downcore (Fig. F28). Much of the downhole increase in NGR values appears to occur within two intervals: 50–60 mcd and 115–130 mcd (roughly corresponding to lithologic Unit II; ~50–134 mcd) with average NGR counts of 25.9 and 31.7 cps, respectively. Below 130 mcd, average NGR is 34.3 cps. A steep decrease in NGR values occurs below ~157 mcd in Core 303-U1307B-17H. This trend is not recorded in Hole U1307A; however, Core 303-U1307B-17H is disturbed, which may account for the discrepancy between Holes U1307A and U1307B.

P-wave velocity

P-wave velocities range from 1543 to 1604 m/s at the top of the sedimentary sequence (upper 80–85 mcd) (Fig. F29). Velocity records from the MST (*P*-wave logger [PWL]) and the split-core measurements from the *P*-wave sensor number 3 (PWS3) are discontinuous, which may be a function of gas content in the sediments. Signal strength deteriorated below ~85–90 mcd in Hole U1307A and below ~90 mcd in Hole U1307B, often generating readings with values lower than that of seawater. This deterioration coincides with a rapid downhole increase in methane at ~85 mcd (see **"Geochemistry"**). PWL and PWS3 measurements also show an offset in values throughout the entire section. This is apparently a long-standing "calibration" problem not unique to Expedition 303 (see **"Physical properties"** in the "Site U1302–U1308 methods" chapter).

Porosity

Porosity was calculated using MST GRA density measurements (see **"Physical properties"** in the "Site U1302–U1308 methods" chapter) and spot-checked with discrete pycnometer measurements (Fig. F30). The GRA density-derived porosity and discrete MAD measurements (Fig. F30) agree well. Although highly variable, porosity decreases from values of 65%–40% to ~42%–39% at the bottom of Hole U1307A. At the bottom of Hole U1307B, a steep increase in porosity to values >70% coincides with disturbed Core 303-U1307B-17H.

Discussion

Site U1307 was placed in an area where the Quaternary sedimentation rates were lower, thus allowing the older record to be recovered by APC coring. All three Eirik Drift sites (Sites U1305–U1307) have similar long-term NGR, density, and porosity records, whereas magnetic susceptibility values show distinct differences among the sites. The average magnetic susceptibility value at Site U1307 is 425 × 10^{-5} SI. This average is very similar to the average value at Site U1305 (436 × 10^{-5} SI), but much lower than the average value at Site U1306 (626 × 10^{-5} SI). This is surprising because Site U1307 has a similar water depth and is located closer to Site U1306; hence, they might be expected to have similar depositional patterns.

The lowest range of magnetic susceptibility variation at Site U1307 appears to be recorded in the uppermost 10 m. Farther downhole, numerous high magnetic susceptibility peaks generally correspond to darker sediment layers, several of which contain large terrigenous particles (>2 cm), whereas lighter-color sediments are usually characterized by low magnetic susceptibility values. This is particularly evident in intervals characterized by high carbonate content such as nannofossil ooze layers (e.g., at 20, 24.5, and 147.7–148.5 mcd) and in the interval corresponding to gray foraminiferal sand (47.9–50 mcd). These foraminiferal sands are also characterized by low NGR values and high density, unlike most of the other carbonate-rich levels. There is an apparent increase in the high-frequency variability of magnetic susceptibility values from 110 to 125 mcd that may in part be related to an increase in the deposition of terrigenous-dominated sediments (see **"Lithostratigraphy"**), thus diluting the other sediment components. Hence, we suggest that the terrigenous versus carbonate content of the sediments is an important control on magnetic susceptibility values at Site U1307.

One of the most interesting features of the magnetic susceptibility record is an interval of exceptionally low magnetic susceptibility values between 154 and 164 mcd, whereas NGR shows little or no change in character. This interval is also generally characterized by low density values. Identical bulk mineralogic

records were obtained from XRD within and outside the low-magnetic susceptibility interval. Postcruise analyses are required to fully understand the causes of the variability within the physical property records and to interpret them in the context of paleoclimate change.

At Site U1307, a high-frequency signal is evident in all of the physical properties. The NGR records covary with magnetic susceptibility records in some intervals, but in other intervals they are out of phase with magnetic susceptibility records. More detailed studies are required to determine the relationships among the sedimentary record and these forcing factors.

References

Andersen, C., Koç, N., and Moros, M., 2004. A highly unstable Holocene climate in the subpolar North Atlantic: evidence from diatoms. *Quat. Sci. Rev.,* 23(20–22):2155–2166. **doi:10.1016/j.quascirev.2004.08.004**

Cande, S.C., and Kent, D.V., 1995. Revised calibration of the geomagnetic polarity timescale for the Late Cretaceous and Cenozoic. *J. Geophys. Res.,* 100(B4):6093–6095. **doi:10.1029/94JB03098**

Capone, D.G., and Klein, R.P., 1988. Comparison of microbial dynamics in marine and freshwater sediments: contrast in anaerobic carbon catabolism. *Limnol. Oceanogr.,* 33:725–749.

Channell, J.E.T., Labs, J., and Raymo, M.E., 2003. The Reunion Subchronzone at ODP Site 981 (Feni Drift, North Atlantic). *Earth Planet. Sci. Lett.,* 215(1–2):1–12. **doi:10.1016/S0012-821X(03)00435-7**

Channell, J.E.T., Mazaud, A., Sullivan, P., Turner, S., and Raymo, M.E., 2002. Geomagnetic excursions and paleointensities in the Matuyama Chron at ODP Sites 983 and 984 (Iceland Basin). *J. Geophys. Res.,* 107(B6):10.1029/2001JB000491. **doi:10.1029/2001JB000491**

Claypool, G.E., and Kvenvolden, K.A., 1983. Methane and other hydrocarbon gases in marine sediment. *Annu. Rev. Earth Planet. Sci.,* 11:299–327. **doi:10.1146/annurev.ea.11.050183.001503**

Clement, B.M., Hall, F.J., and Jarrard, R.D., 1989. The magnetostratigraphy of Ocean Drilling Program Leg 105 sediments. *In* Srivastava, S.P., Arthur, M.A., Clement, B., et al., *Proc. ODP, Sci. Results,* 105: College Station, TX (Ocean Drilling Program), 583–595. **[PDF]**

de Vernal, A., and Mudie, P.J., 1989. Pliocene and Pleistocene palynostratigraphy at ODP Sites 646 and 647, eastern and southern Labrador Sea. *In* Srivastava, S.P., Arthur, M.A., Clement, B., et al., *Proc. ODP, Sci. Results,* 105: College Station, TX (Ocean Drilling Program), 401–422. **[PDF]**

Dickens, G.R., 2001. Sulfate profiles and barium fronts in sediment on the Blake Ridge: present and past methane fluxes through a large gas hydrate reservoir. *Geochim. Cosmochim. Acta,* 65(4):529–543. **doi:10.1016/S0016-7037(00)00556-1**

Gieskes, J.M., and Lawrence, J.R., 1981. Alteration of volcanic matter in deep-sea sediments: evidence from the chemical composition of interstitial waters from deep sea drilling cores. *Geochim. Cosmochim. Acta,* 45(10):1687–1703. **doi:10.1016/0016-7037(81)90004-1**

Goll, R.M., and Bjørklund, K.R., 1989. A new radiolarian biostratigraphy for the Neogene of the Norwegian Sea: ODP Leg 104. *In* Eldholm, O., Thiede, J., Taylor, E., et al., *Proc. ODP, Sci. Results,* 104: College Station, TX (Ocean Drilling Program), 697–737. **[PDF]**

Jansen, E., Bleil, U., Henrich, R., Kringstad, L., and Slettemark, B., 1988. Paleoenvironmental changes in the Norwegian Sea and Northeast Atlantic during the last 2.8 m.y.: Deep Sea Drilling Project/Ocean Drilling Program Sites 610, 642, 643, and 644. *Paleoceanography,* 3:563–581.

Keren, R., and Mezuman, V., 1981. Boron adsorption by clay minerals using a phenomenological equation. *Clays Clay Miner.,* 29:198–204.

Koç, N., Hodell, D.A., Kleiven, H., and Labeyrie, L., 1999. High-resolution Pleistocene diatom biostratigraphy of Site 983 and correlations with isotope stratigraphy. *In* Raymo, M.E., Jansen, E., Blum, P., and Herbert, T.D. (Eds.), 1999. *Proc. ODP, Sci. Results,* 162: College Station, TX (Ocean Drilling Program), 51–62. **[HTML]**

Mitterer, R.M., Malone, M.J., Goodfriend, G.A., Swart, P.K., Wortmann, U.G., Logan, G.A., Feary, D.A., and Hine, A.C., 2001. Co-generation of hydrogen sulfide and methane in marine carbonate sediments. *Geophys. Res. Lett.,* 28(20):3931–3934. **doi:10.1029/2001GL013320**

Palmer, M.R., Spivack, A.J., and Edmond, J.M., 1987. Temperature and pH controls over isotopic fractionation during adsorption of boron on marine clay. *Geochim. Cosmochim. Acta,* 51(9):2319–2323. **doi:10.1016/0016-7037(87)90285-7**

Sato, T., Kameo, K., and Mita, I., 1999. Validity of the latest Cenozoic calcareous nannofossil datums and its application to the tephrochronology. *Earth Sci.,* 53:265–274.

Sato, T., Yuguchi, S., Takayama, T., and Kameo, K., 2004. Drastic change in the geographical distribution of the cold-water nannofossil *Coccolithus pelagicus* (Wallich) Schiller at 2.74 Ma in the Late Pliocene, with special reference to glaciation in the Arctic Ocean. *Mar. Micropaleontol.,* 52(1–4):181–193. **doi:10.1016/j.marmicro.2004.05.003**

Shipboard Scientific Party, 1987. Site 646. *In* Srivastava, S.P., Arthur, M., Clement, B., et al., *Proc. ODP, Init. Repts.,* 105: College Station, TX (Ocean Drilling Program), 419–674. **[PDF]**

Shipboard Scientific Party, 1996. Site 984. *In* Jansen, E., Raymo, M.E., Blum, P., et al., *Proc. ODP, Init. Repts.,* 162: College Station, TX (Ocean Drilling Program), 169–222.

Thiede, J., and Myhre, A.M., 1996. Introduction to the North Atlantic-Arctic gateways: plate tectonic-paleoceanographic history and significance. *In* Thiede, J., Myhre, A.M., Firth, J.V., Johnson, G.L., and Ruddiman, W.F. (Eds.), *Proc. ODP, Sci. Results,* 151: College Station, TX (Ocean Drilling Program), 3–23.

Torres, M.E., Bohrmann, G., and Suess, E., 1996a. Authigenic barites and fluxes of barium associated with fluid seeps in the Peru subduction zones. *Earth Planet. Sci. Lett.,* 144(3–4):469–481. **doi:10.1016/S0012-821X(96)00163-X**

Torres, M.E., Brumsack, H.-J., Bohrmann, G., and Emeis, K.C., 1996b. Barite fronts in continental margin sediments: a new look at barium remobilization in the zone of sulfate reduction and formation of heavy barites in diagenetic fronts. *Chem. Geol.,* 127(1–3):125–139. **doi:1016/0009-2541(95)00090-9**

Weaver, P.P.E., and Clement, B.M., 1987. Magnetobiostratigraphy of planktonic foraminiferal datums, DSDP Leg 94, North Atlantic. *In* Ruddiman, W.F., Kidd, R.B., Thomas, E., et al., *Init. Repts. DSDP,* 94: Washington (U.S. Govt. Printing Office), 815–829.

Whiteman, J.M., and Berger, W.H., 1992. Pliocene–Pleistocene oxygen isotope record, Site 586, Ontong Java Plateau. *Mar. Micropaleontol.,* 18(3):171–198. **doi:10.1016/0377-8398(92)90012-9**

Publication: 9 September 2006
MS 303-107

Figure F1. Map of multichannel seismic lines collected during *Knorr* cruise KN166-14 in 2002, relative to the seismic lines collected in 1977 by BGR1 and BGR2. The location of the deepwater site (Site U1305) and the shallower-water sites (Sites U1306 and U1307) are shown relative to the location of Site 646 (Mountain et al., unpubl. data).

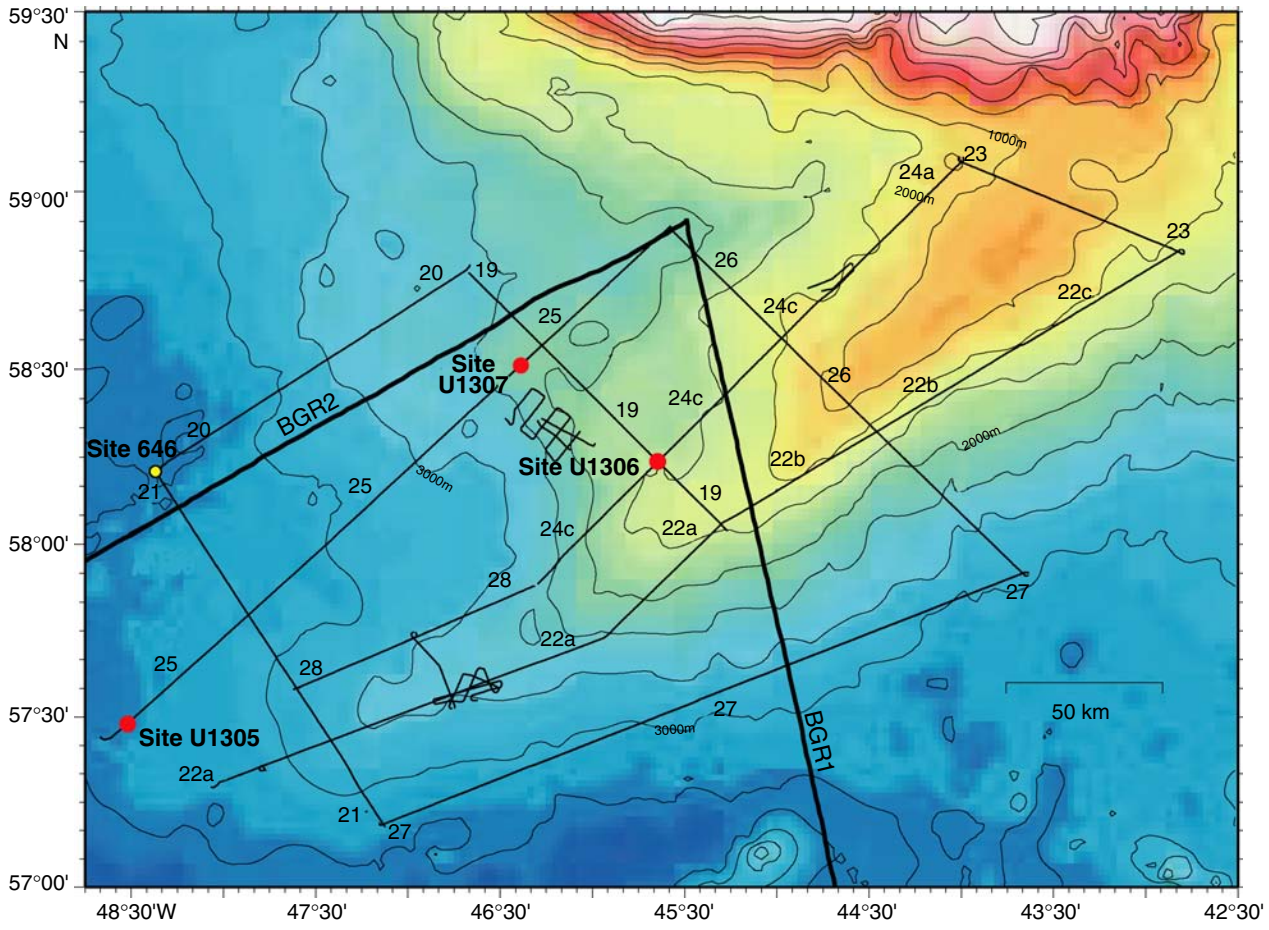

Figure F2. Seismic Line 25a from *Knorr* cruise KN166-14 in the vicinity of Site U1307, showing penetration depth. The equivalent penetration at Site U1306, correlated to Line 25a along Line 19, is indicated (see Fig. F1) (Mountain et al., unpubl. data).

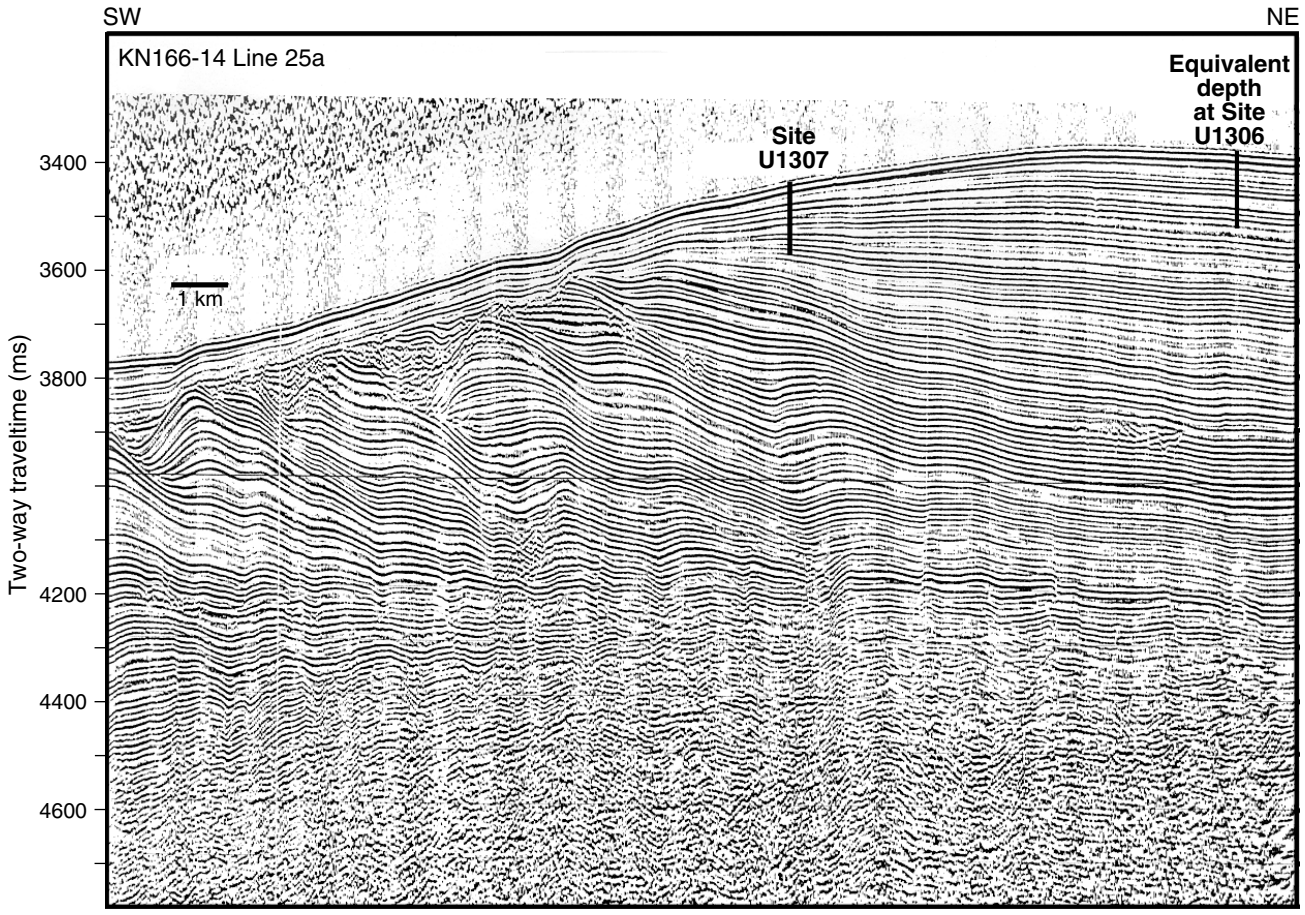

Figure F3. Abundances of quartz, detrital carbonate, and nannofossils. Circles = Hole U1307A data, squares = Hole U1307B data.

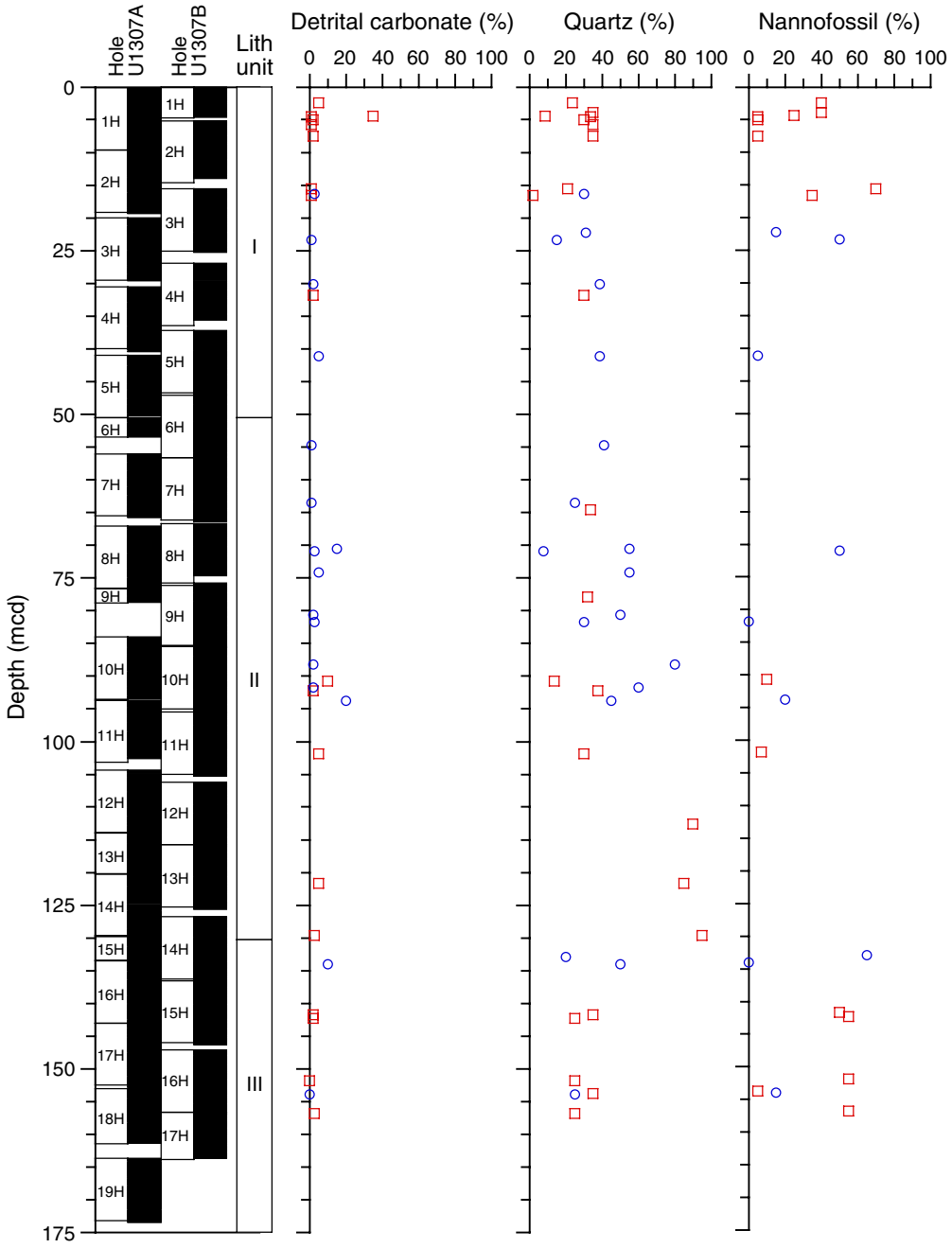

Figure F4. Graphic summary of the lithologies recovered at Site U1307.

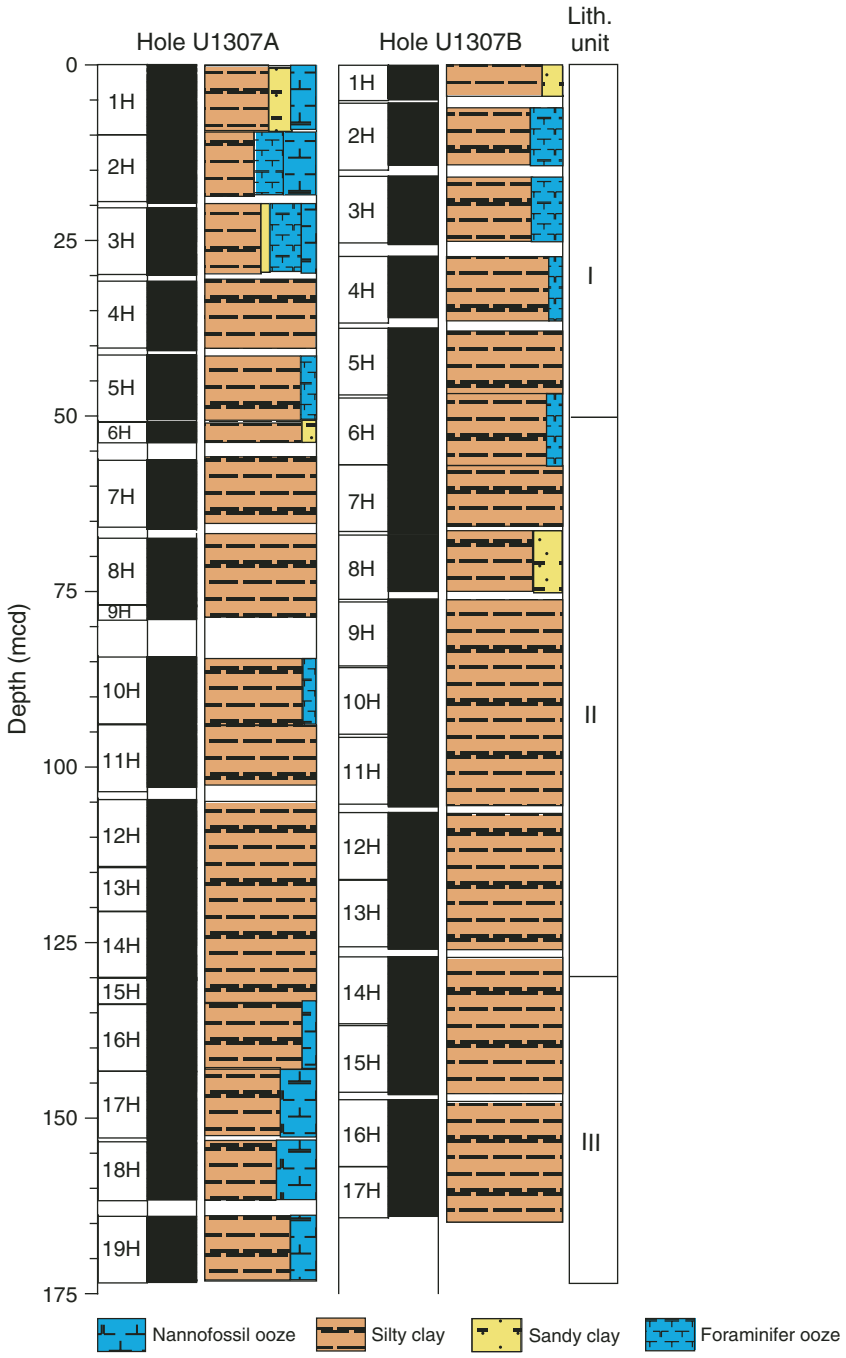

Figure F5. Gray silty clay nannofossil ooze bed with upper gradational contact passing into olive-brown silty clay (interval 303-U1307A-2H-4, 125–145 cm).

Figure F6. Foraminifer nannofossil ooze with silty clay bed with irregular base and gradational top (interval 303-U1307A-1H-3, 115–135 cm).

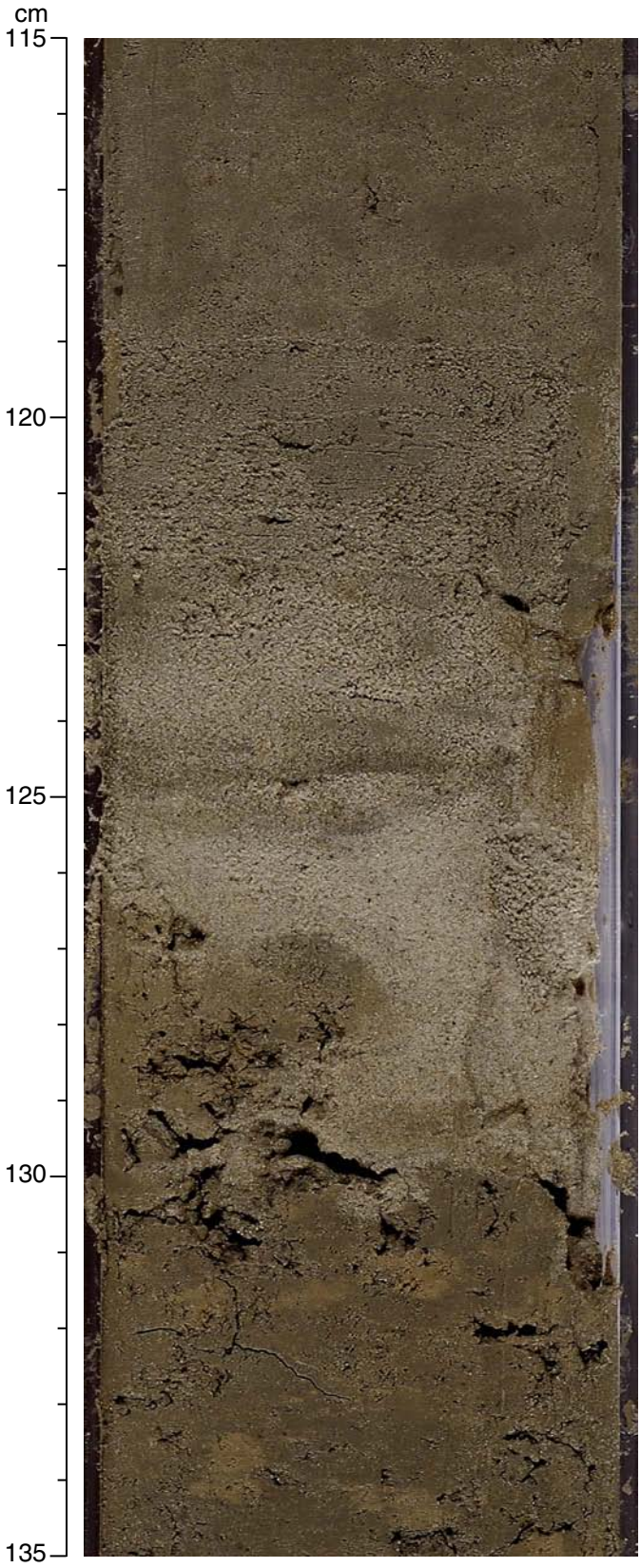

Figure F7. Gray foraminifer ooze showing a bioturbated contact with the overlying dark gray silty clay foraminifer ooze (interval 303-U1307A-2H-5, 80–100 cm).

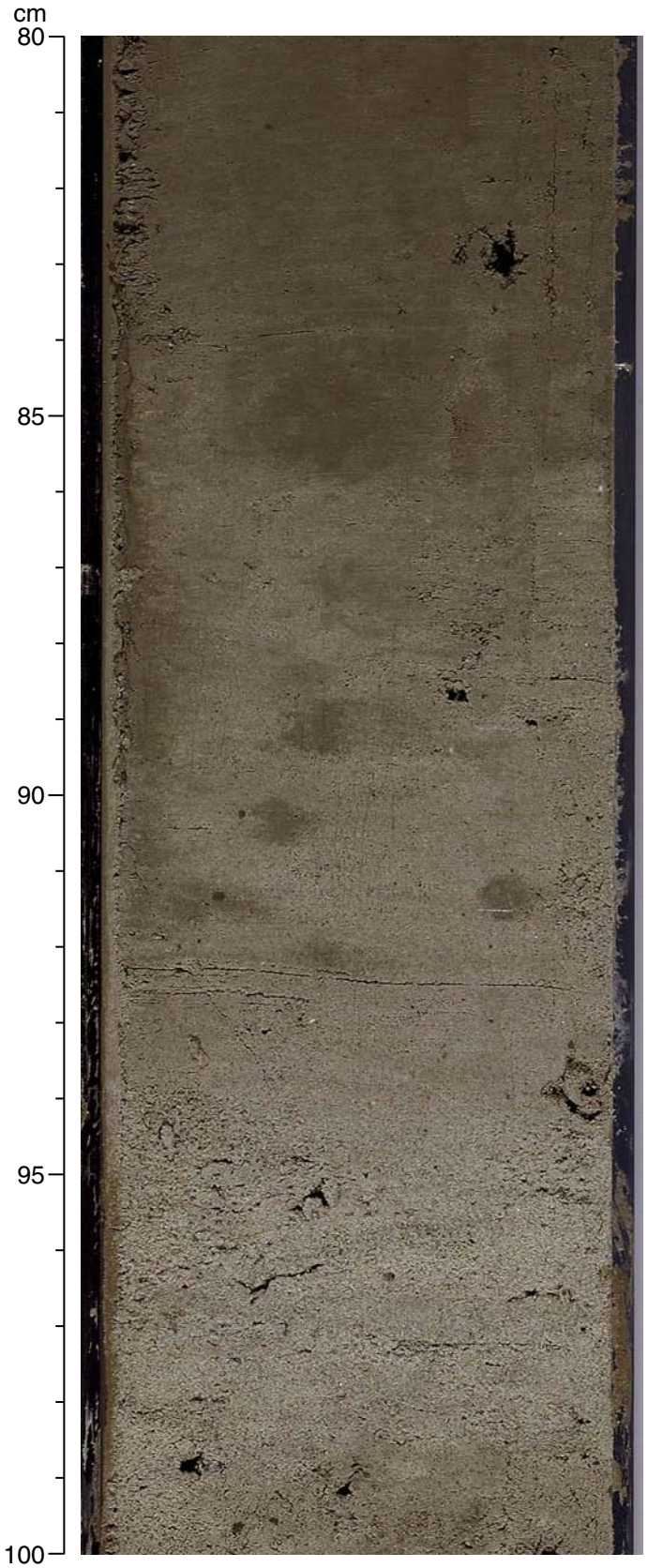

Figure F8. Irregular bottom contact of the gray foraminifer ooze bed of Figure F7, with the underlying olive-gray silty clay foraminifer ooze (interval 303-U1307A-2H-5, 100–115 cm).

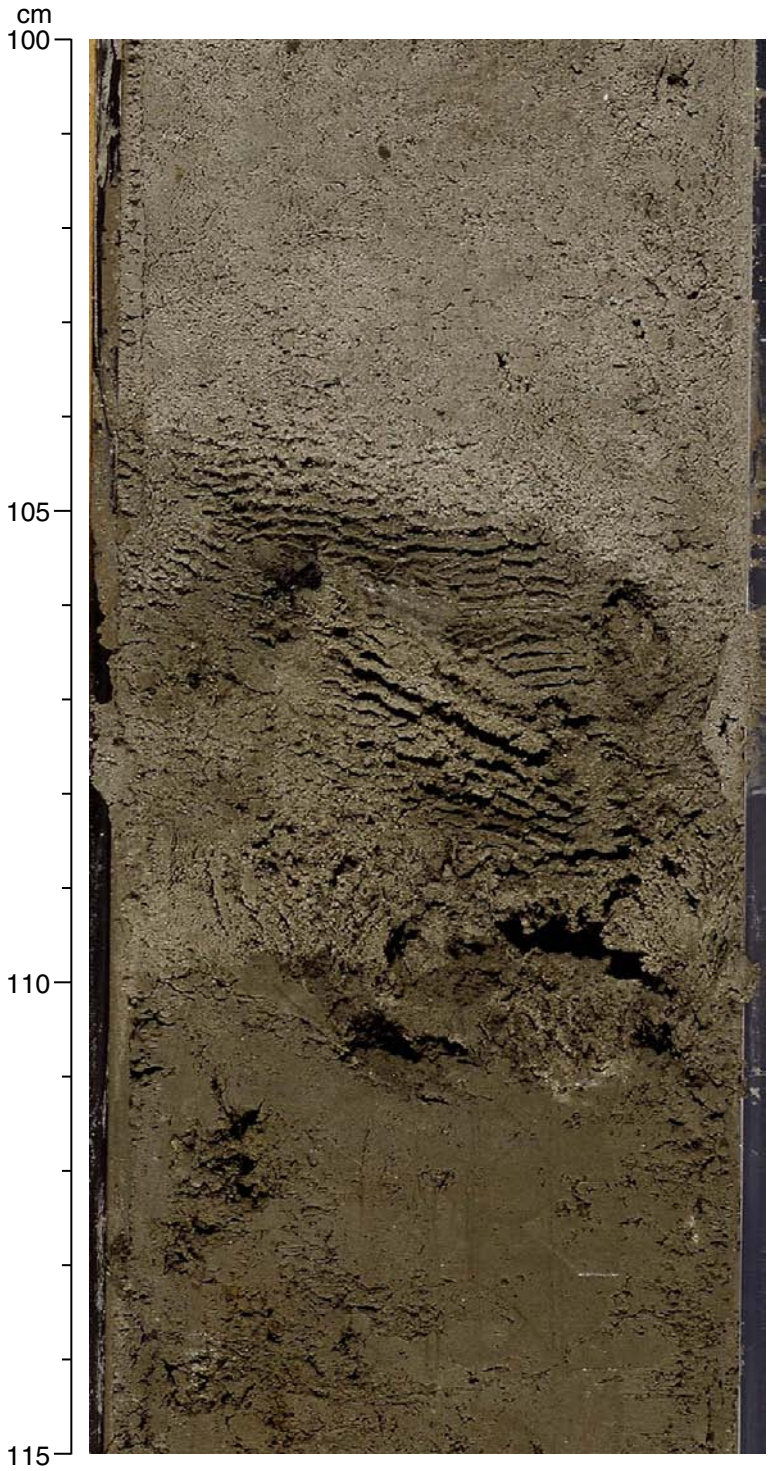

Figure F9. Foraminifer ooze layer present in interval 303-U1307A-5H-6, 15–40 cm.

Figure F10. Abundance of gravel-sized grains (number of grains/10 cm length of core).

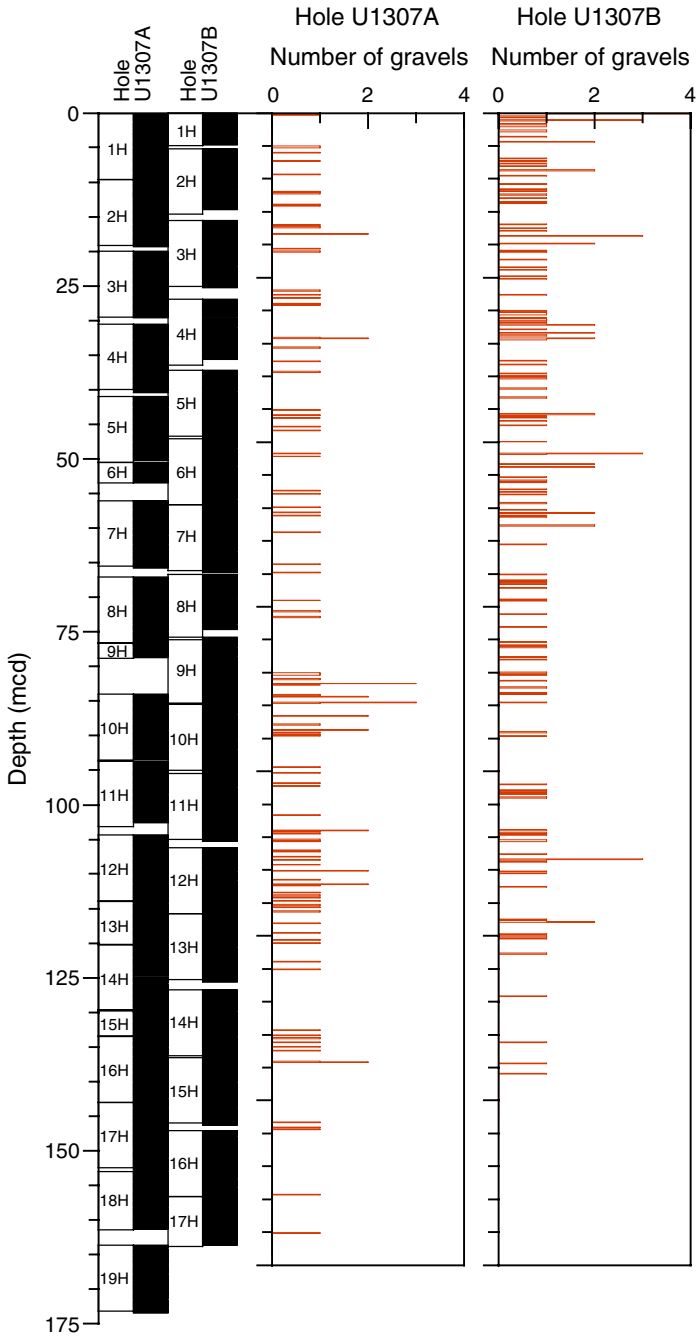

Figure F11. Variation of the sediment lightness (L* smoothed) and $CaCO_3$. Peak numbers from 1 to 8 represent the location of the foraminifer ooze layers of Unit I.

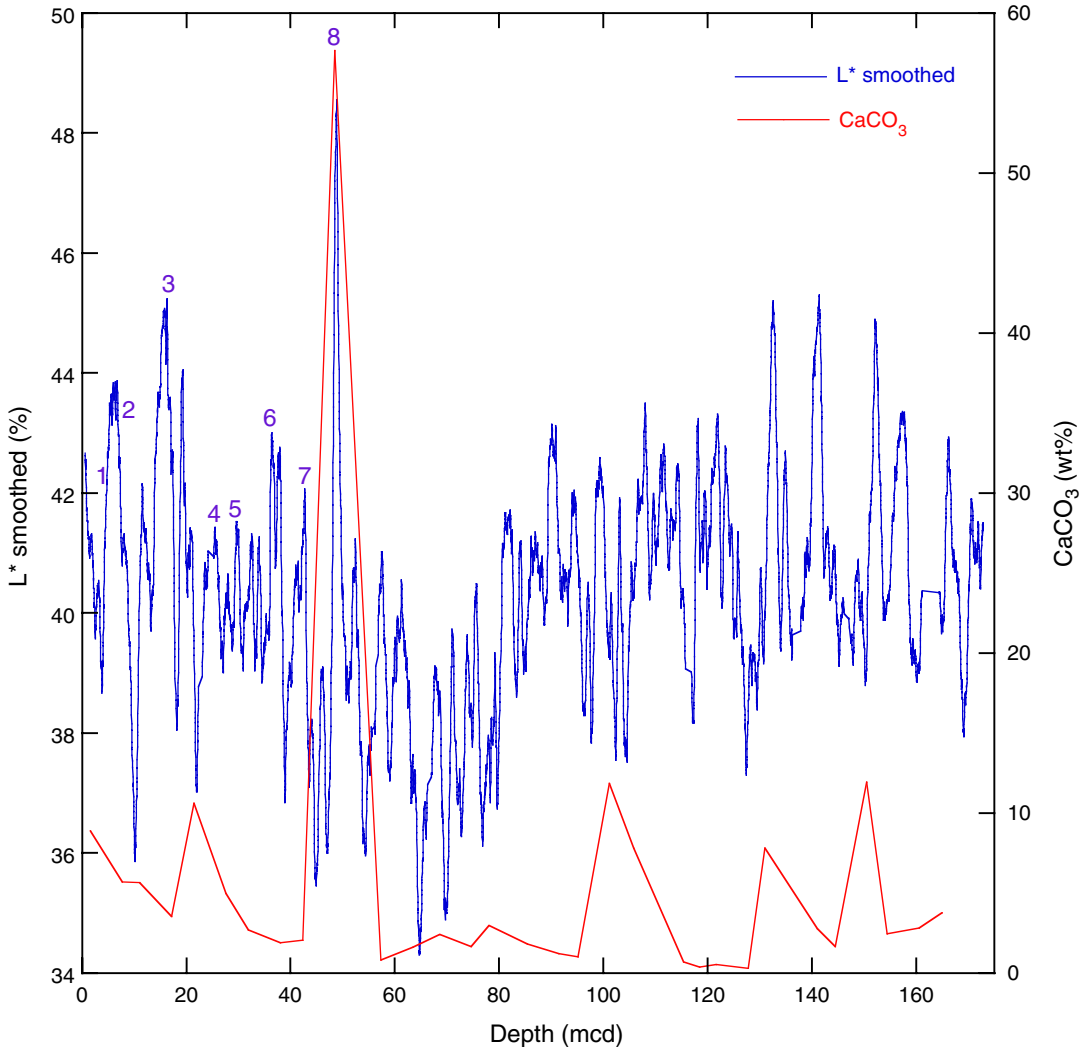

Figure F12. Chronostratigraphic correlation of Holes U1307A and U1307B based on calcareous nannofossils, diatoms, planktonic foraminifers, and dinocysts. Relationship to magnetostratigraphy is shown in the left panel. Bar at 56–62 mcd indicates tentatively identified hiatus. MIS = marine isotope stage, LO = last occurrence, FO = first occurrence.

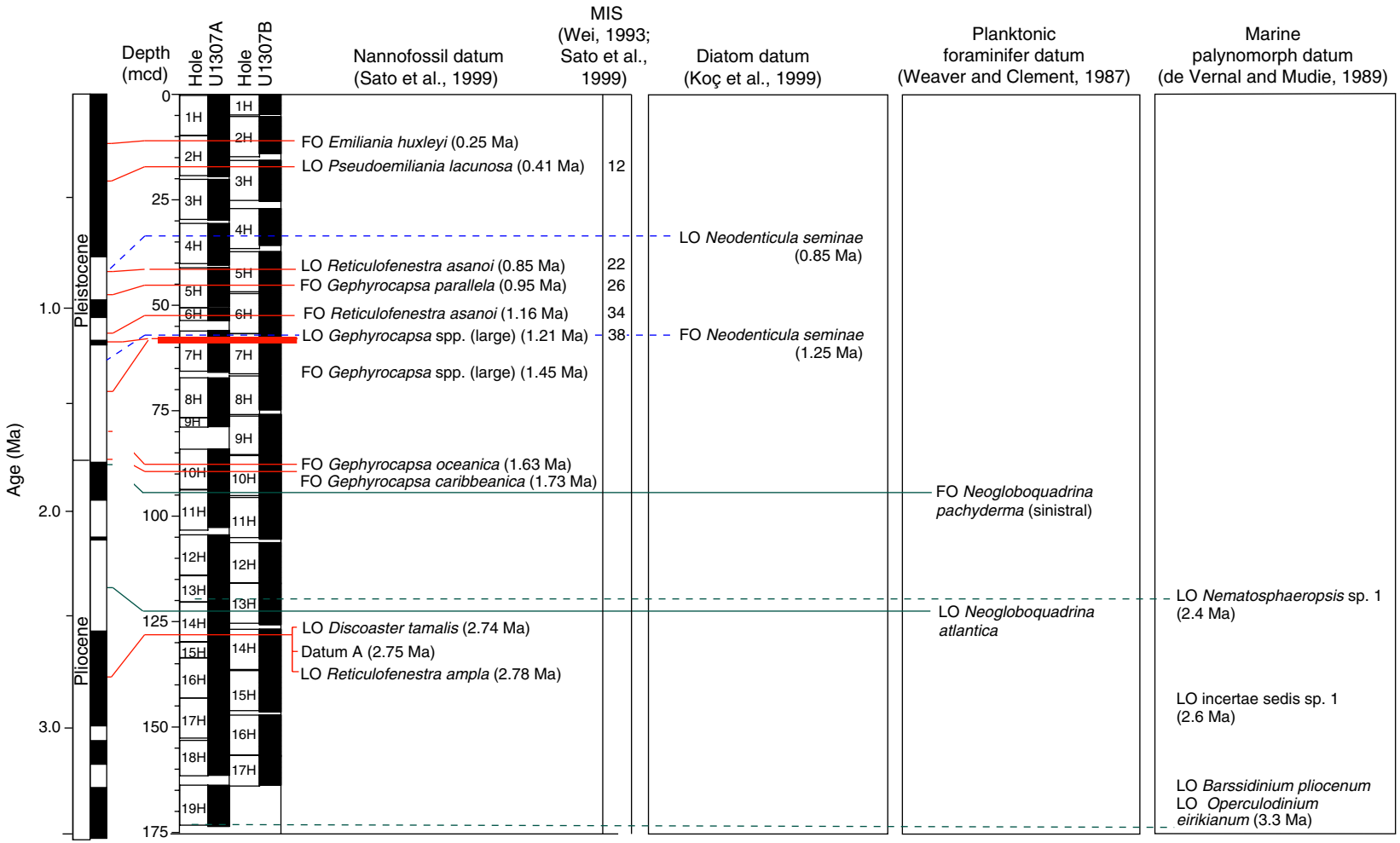

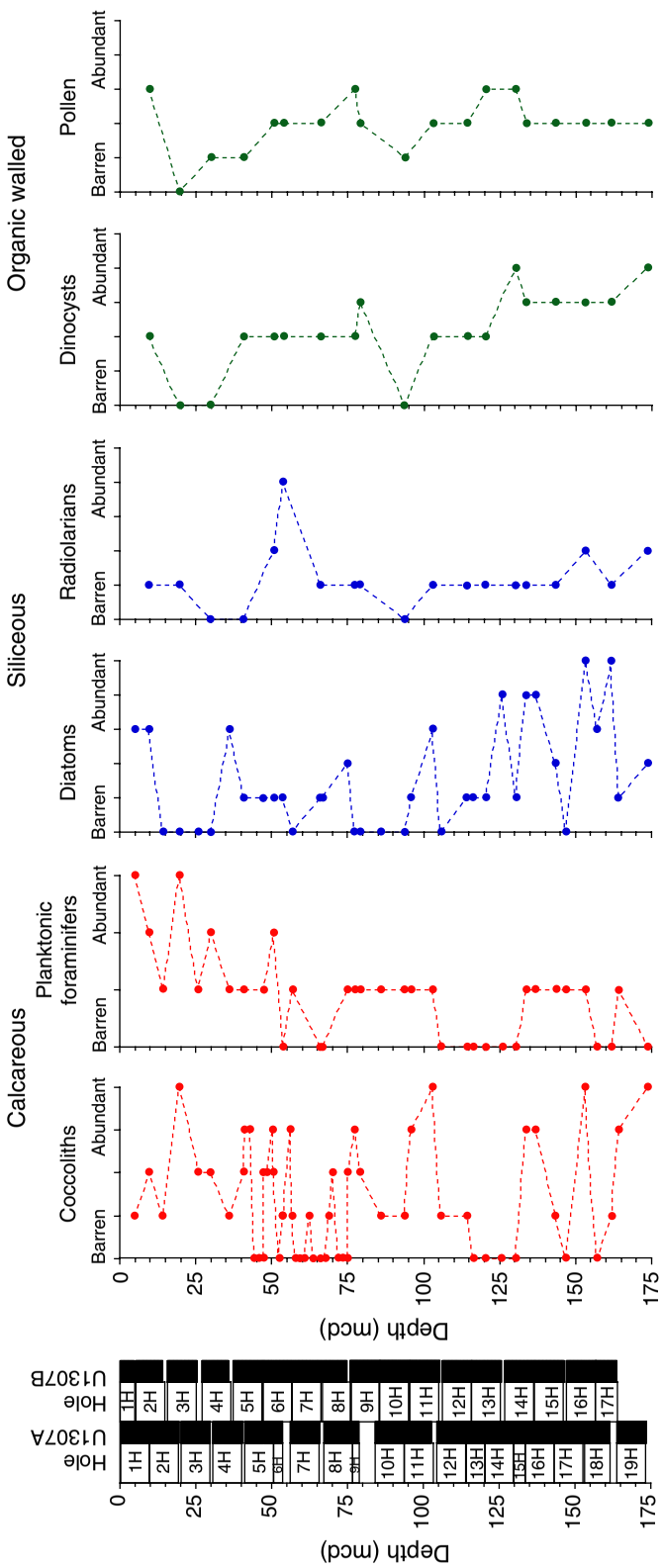

Figure F13. Site U1307 downcore relative abundance of calcareous nannofossils, planktonic foraminifers, diatoms, radiolarians, dinocysts, and pollen.

Figure F14. Site U1307 NRM intensity before (black) and after 10 mT (blue) and 20 mT (red) peak AF demagnetization versus depth. Core recovery is shown in the left panel.

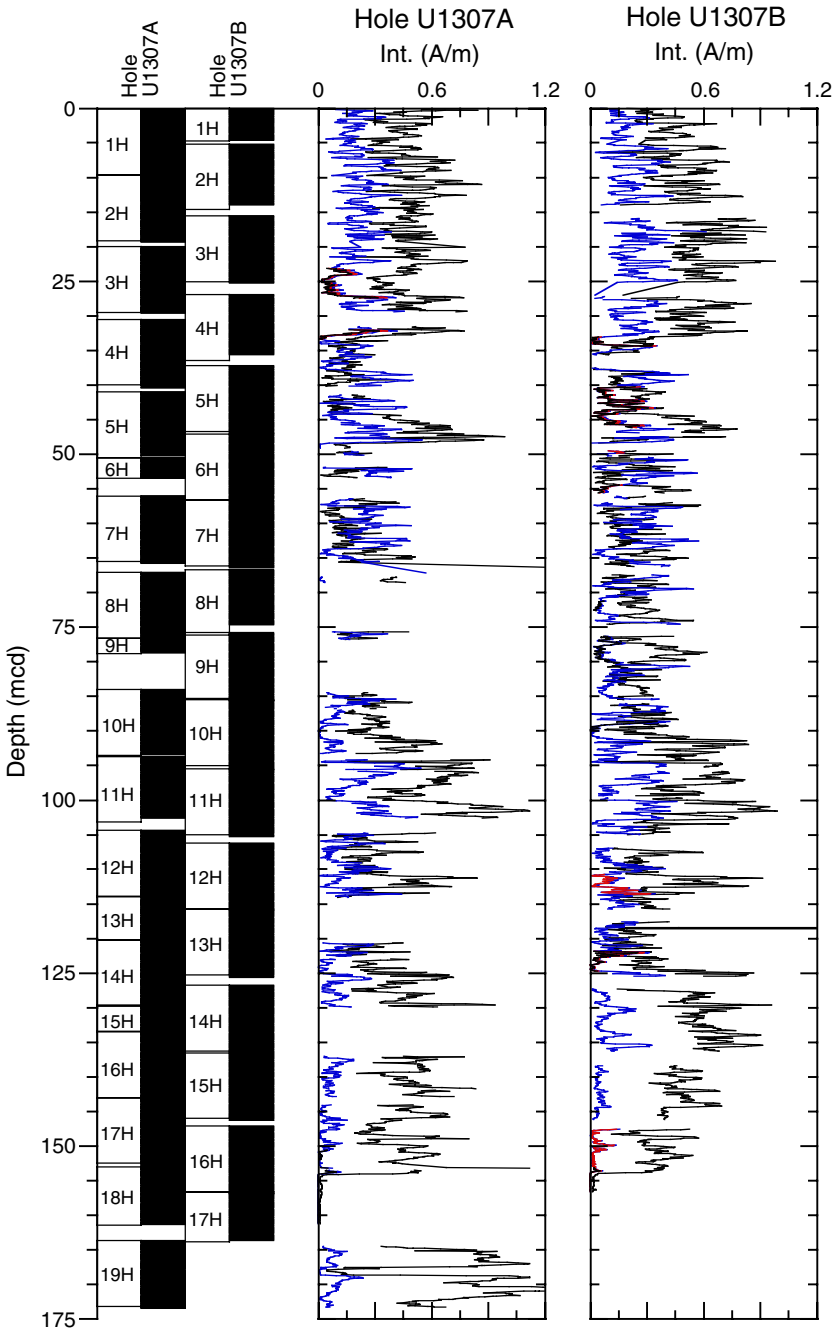

Figure F15. Site U1307 inclination after peak AF demagnetization (10 mT = black, 20 mT = red) versus depth with accompanying polarity interpretations. Core recovery is shown in the left panel.

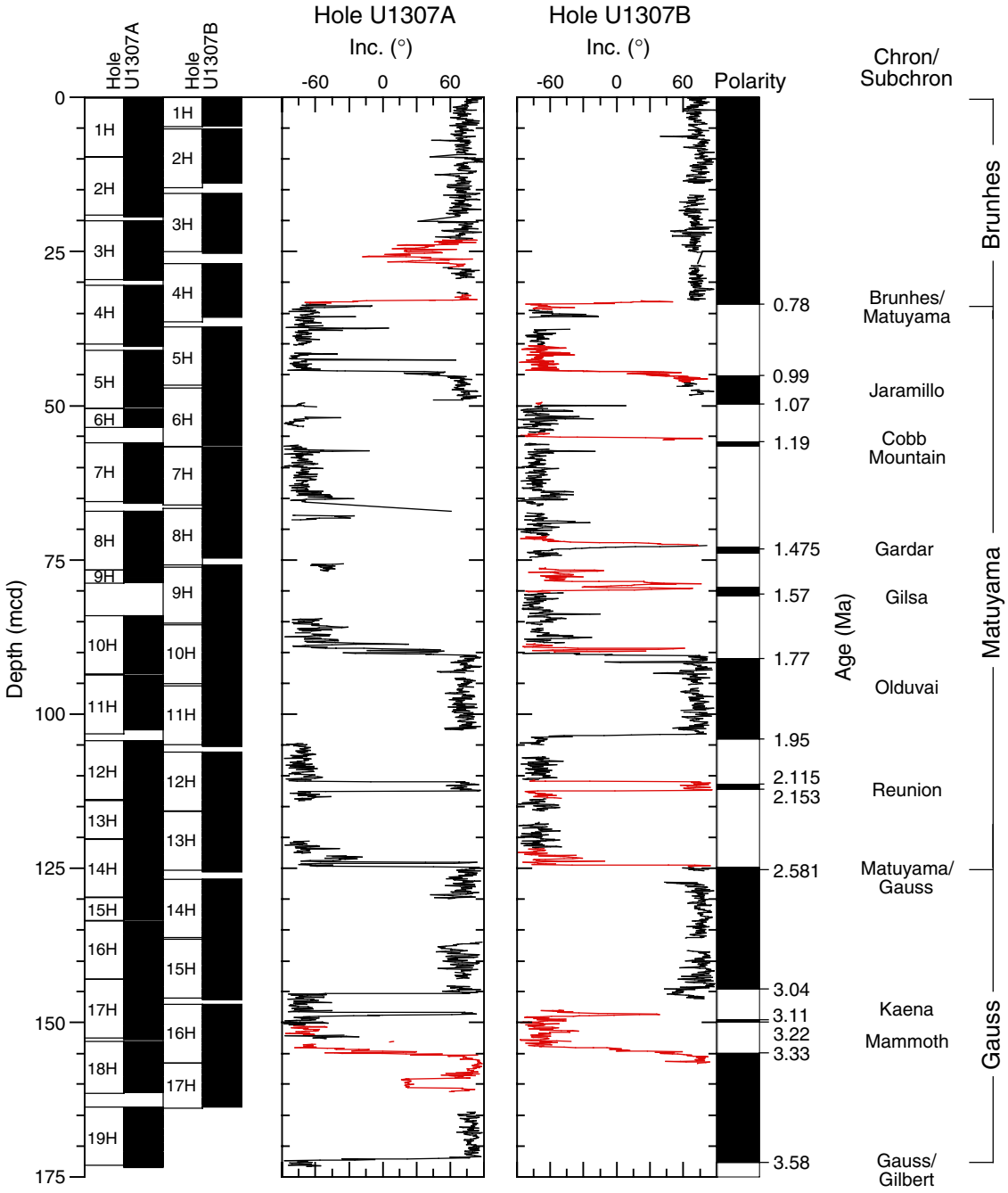

Figure F16. Site U1307 declination after peak AF demagnetization (10 mT = gray, 20 mT = red) and after Tensor tool correction (black) versus depth with accompanying polarity interpretations. Core recovery is shown in the left panel.

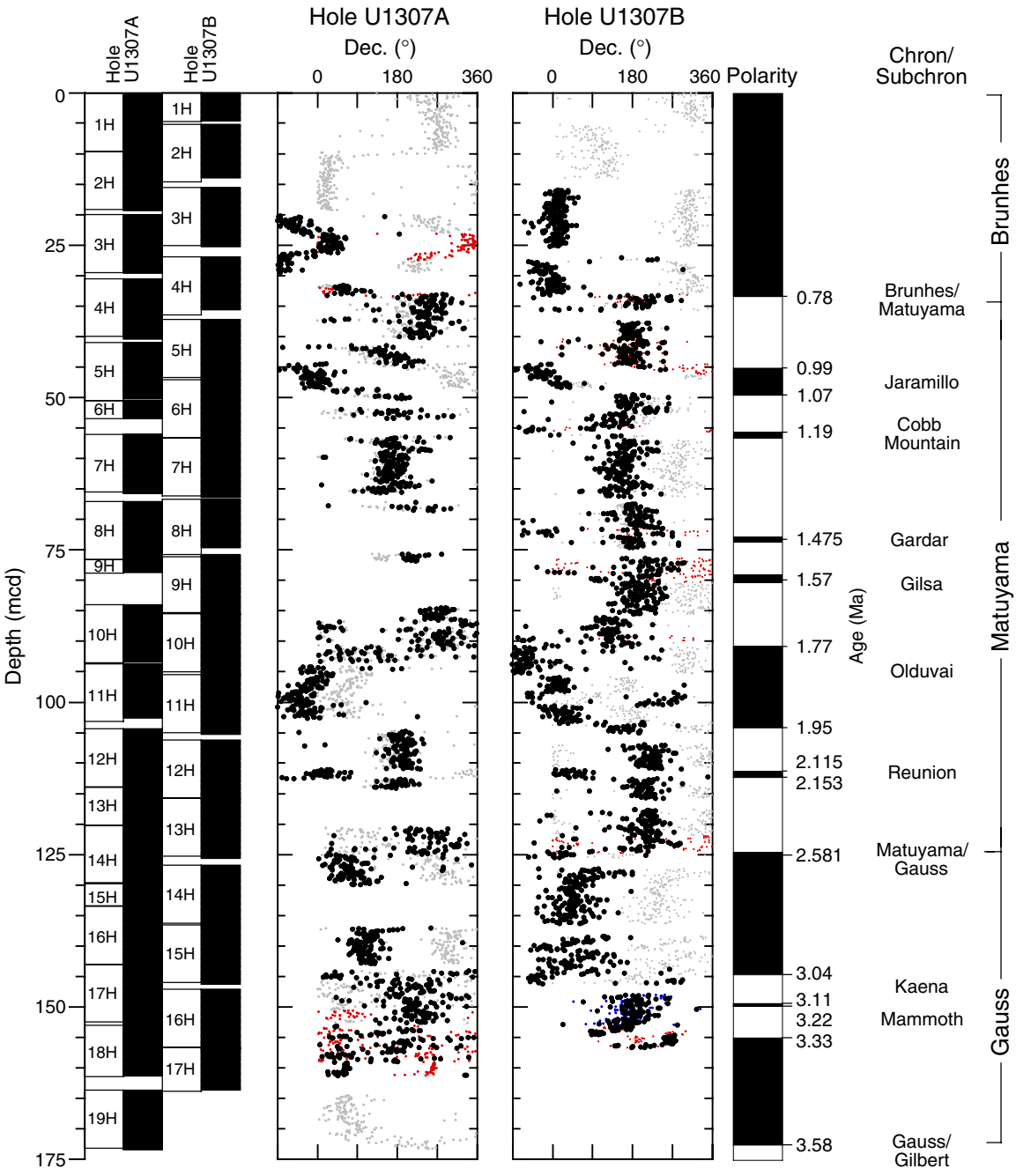

Figure F17. Age-depth curve for Site U1307 derived from the magnetic stratigraphy shown in Figures F15 and F16. Average sedimentation rates in meters per million years are also plotted using the geomagnetic polarity timescale of Cande and Kent (1995) with ages for the Reunion Subchronozone from Channell et al. (2003). Red squares mark polarity boundary interpretations (Table T13), and blue triangles denote the position of the upper Cobb Mountain transition and the Gilsa and Gardar magnetic excursions (Figs. F15, F16) with ages from Channell et al. (2002).

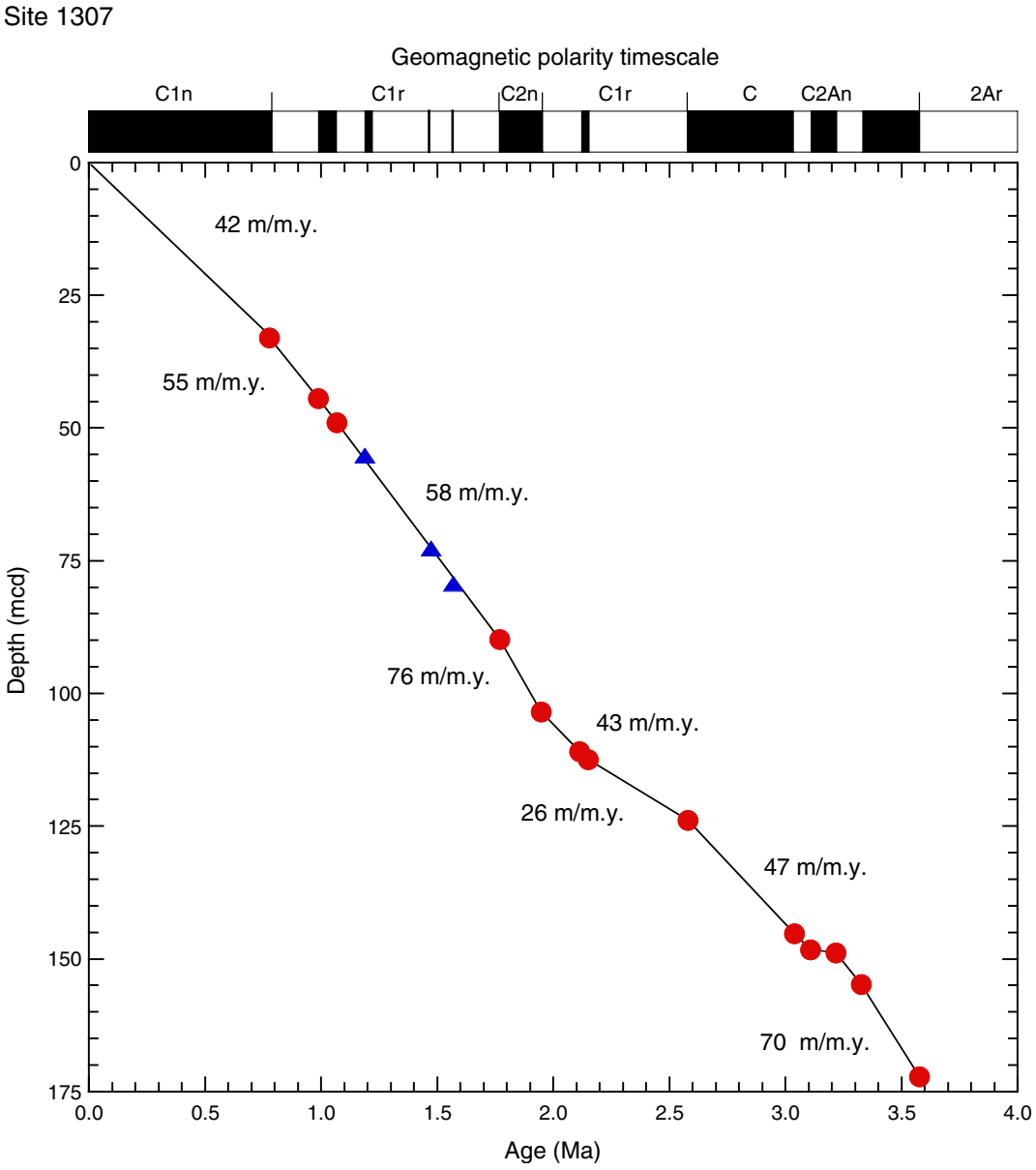

Figure F18. Magnetic susceptibility (MS), Site U1307. Numbers shown below MS records refer to core from which the record was taken. Lower panel: Magnetic susceptibility versus mcd for each hole drilled at Site U1305. Upper panel: Composite magnetic susceptibility record indicating hole numbers used to form the splice. **A.** 0–60 mcd. (Continued on next two pages.)

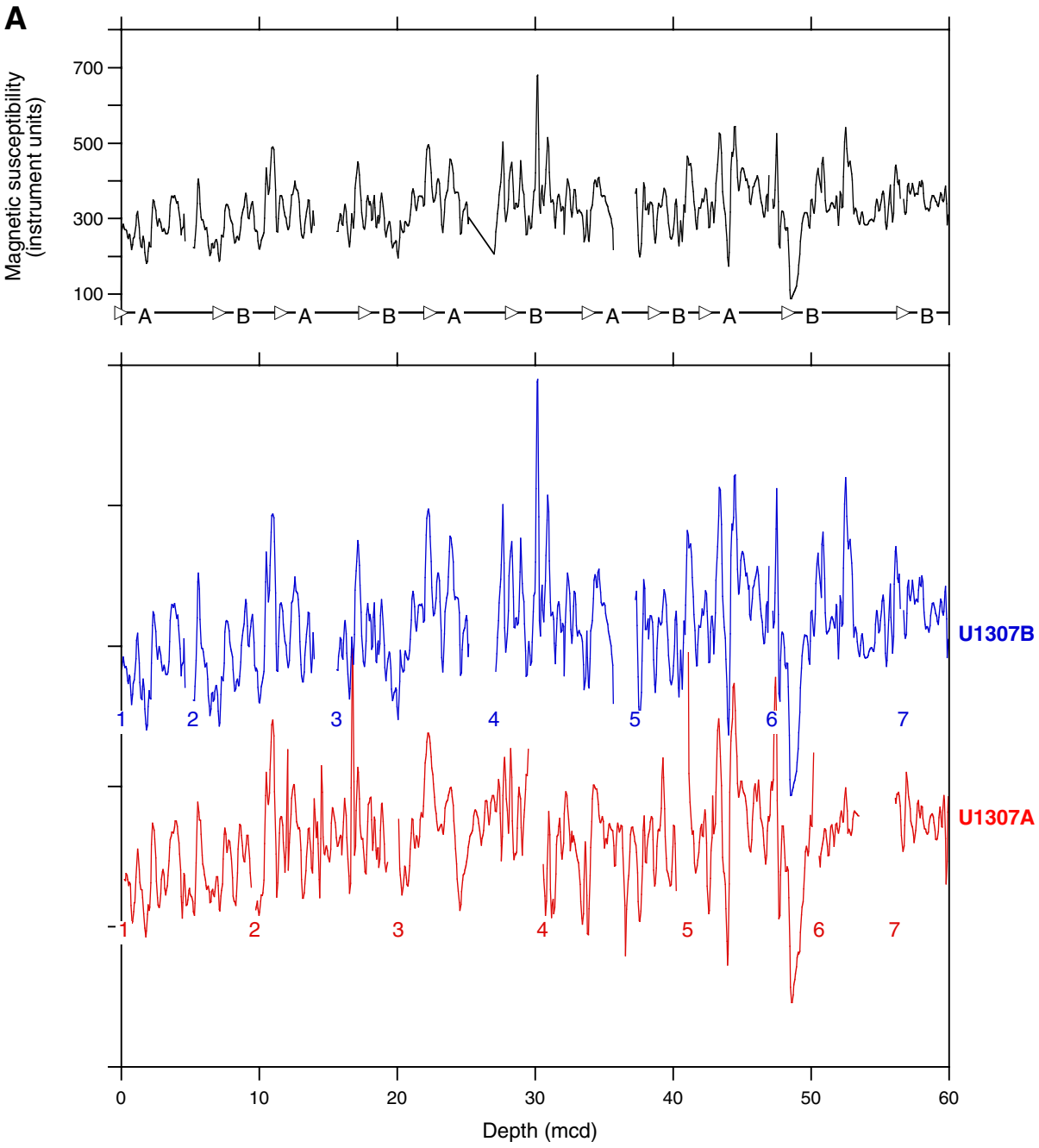

Figure F18 (continued). B. 60–120 mcd.

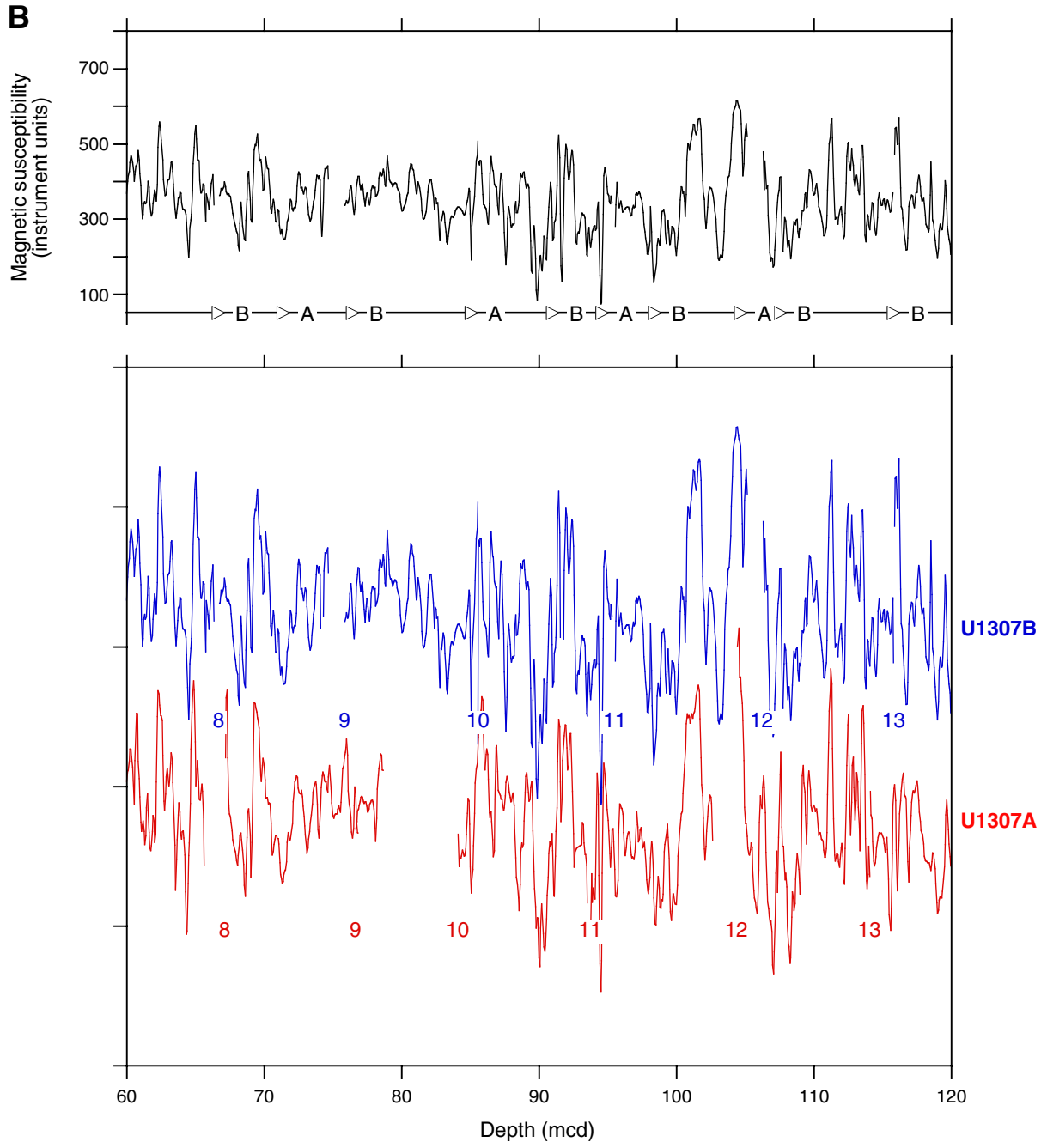

Figure F18 (continued). C. 120–180 mcd.

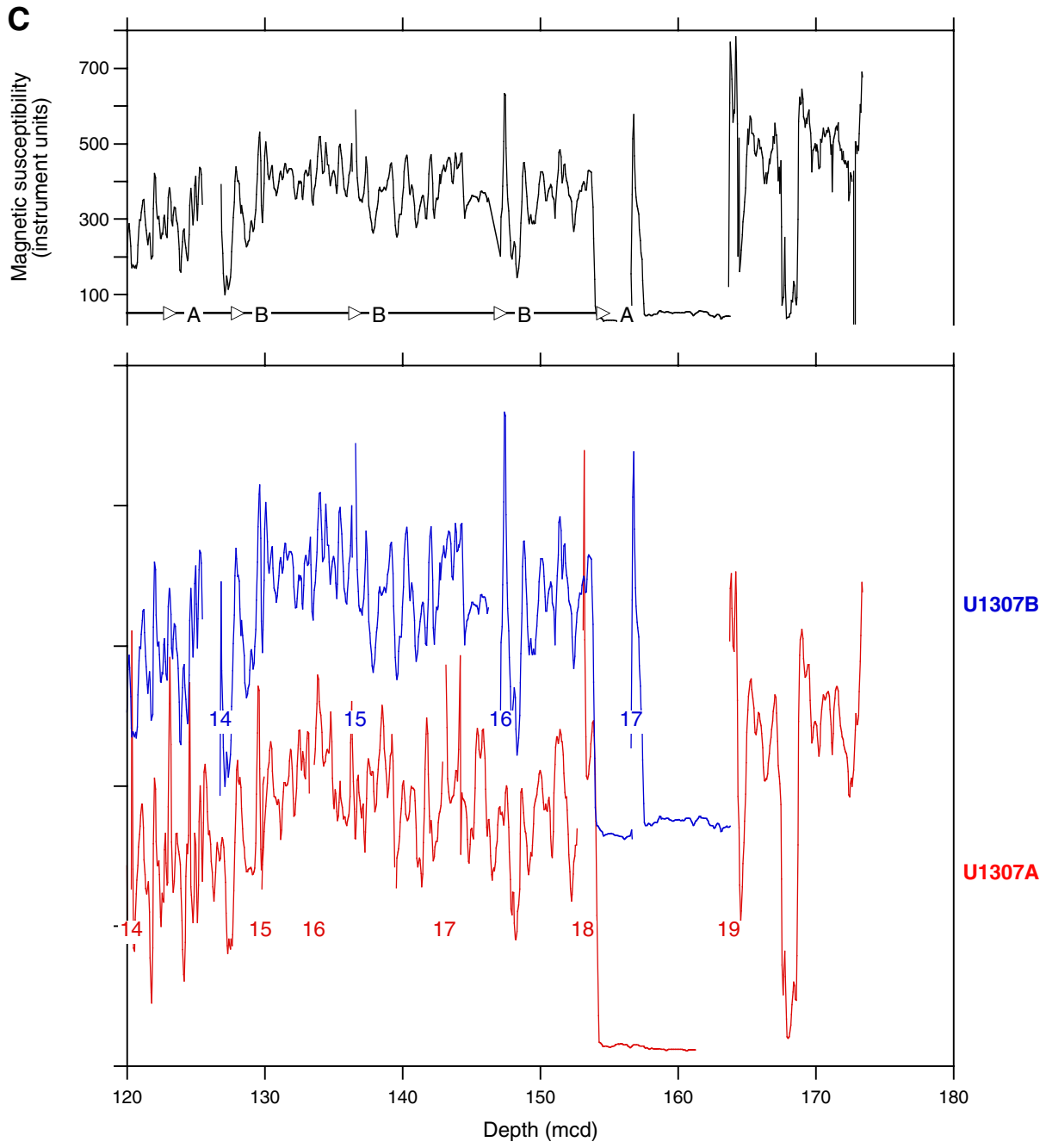

Figure F19. Meters composite depth versus meters below seafloor depth for tops of cores at Site U1307. The growth factor (GF) is the slope of the regression line. Average mcd of the spliced section is 6% greater than meters below seafloor.

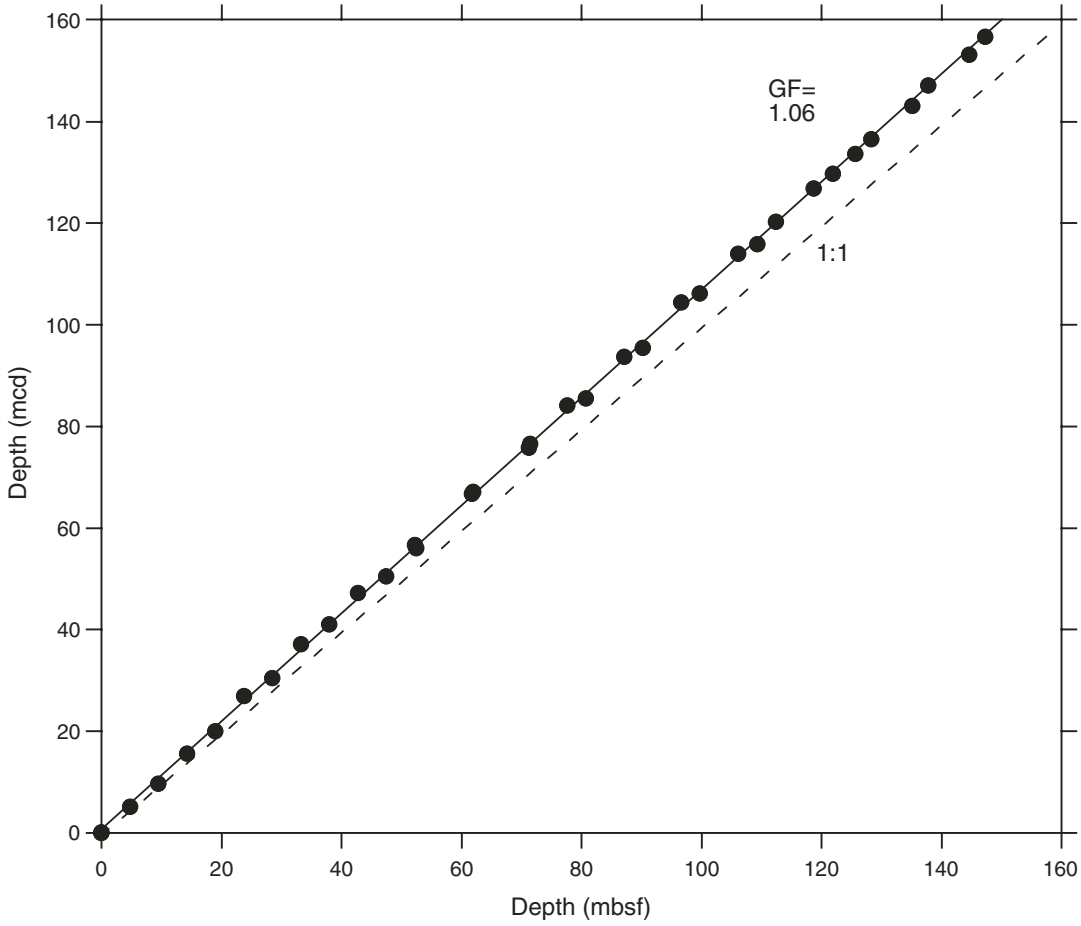

Figure F20. A. Age versus depth for paleomagnetic and biostratigraphic datums for Site U1307. A mean sedimentation rate of 5.0 cm/k.y. was calculated by linear regression. **B.** Datums shown with the interval sedimentation rates derived from the paleomagnetic datums only.

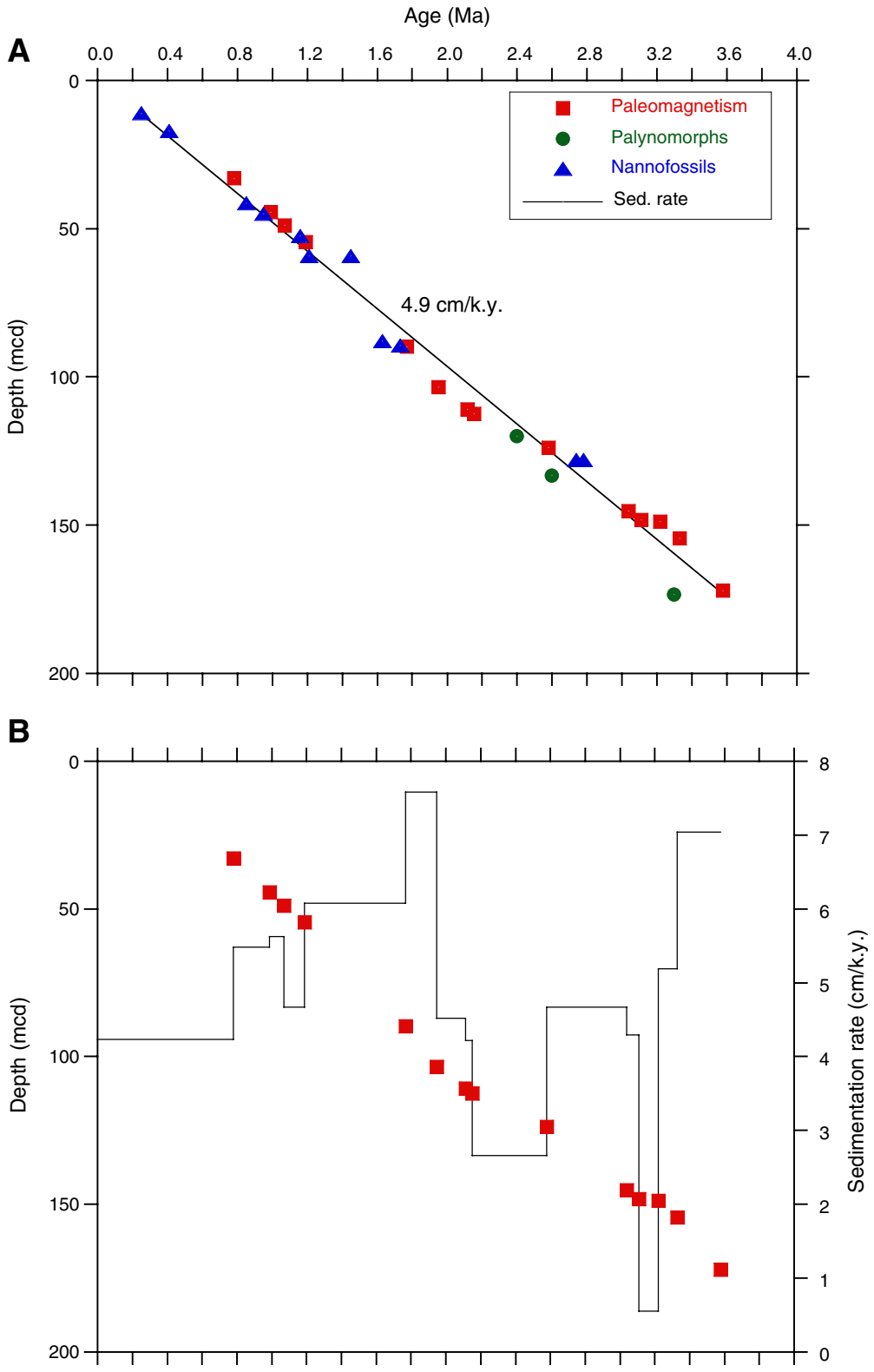

Figure F21. Headspace methane concentrations for Hole U1307A.

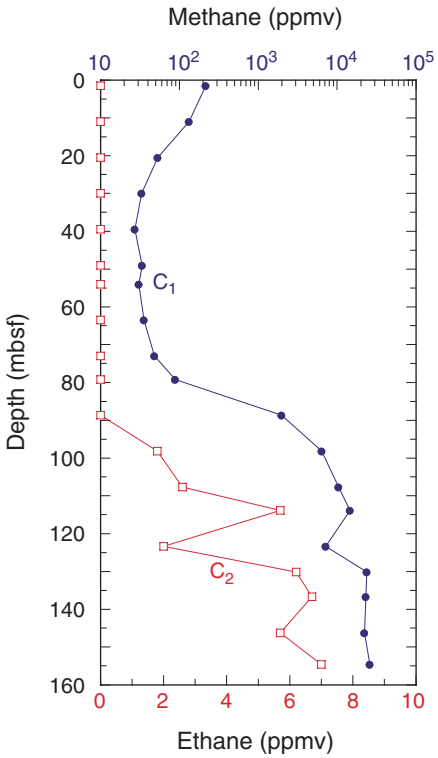

Figure F22. Site U1307 carbonate contents and elemental compositions. **A.** Calcium carbonate. **B.** Total organic carbon (TOC). **C.** Elemental nitrogen. **D.** Organic C/N ratio.

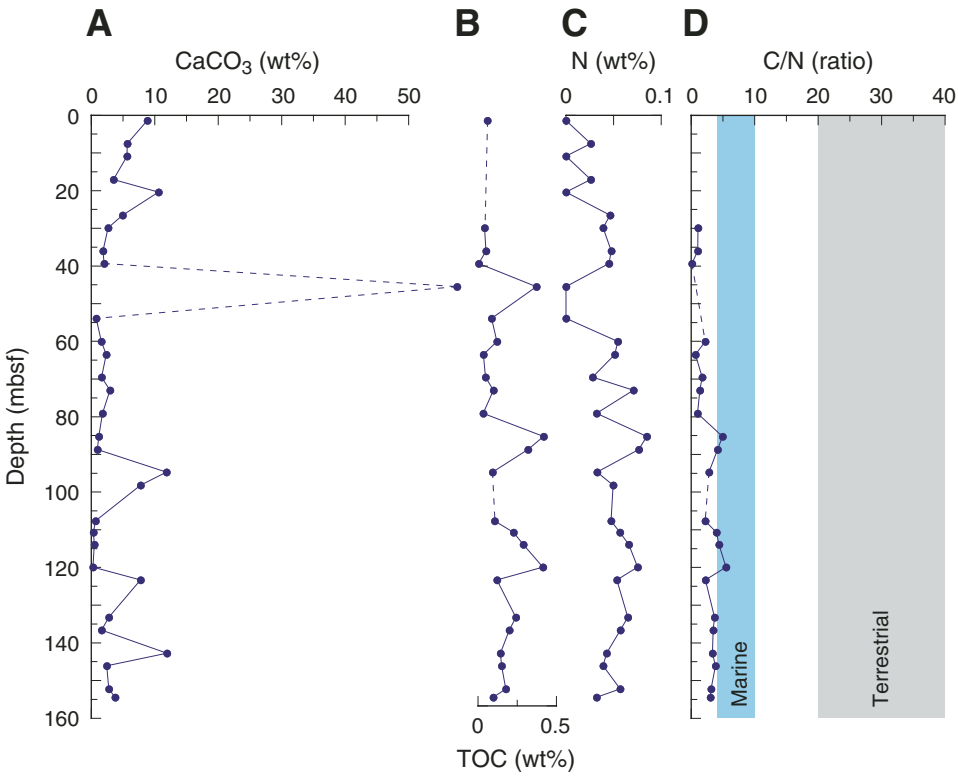

Figure F23. Profiles of chemical constituents in interstitial waters from Hole U1307A. **A.** Chlorinity. **B.** Sodium. **C.** pH. **D.** Boron. **E.** Alkalinity. **F.** Sulfate. **G.** Ammonium. **H.** Dissolved silica. **I.** Calcium. **J.** Strontium and Sr/Ca ratio. **K.** Lithium and Li/Ca ratio. **L.** Barium. **M.** Magnesium. **N.** Potassium. **O.** Manganese. **P.** Iron.

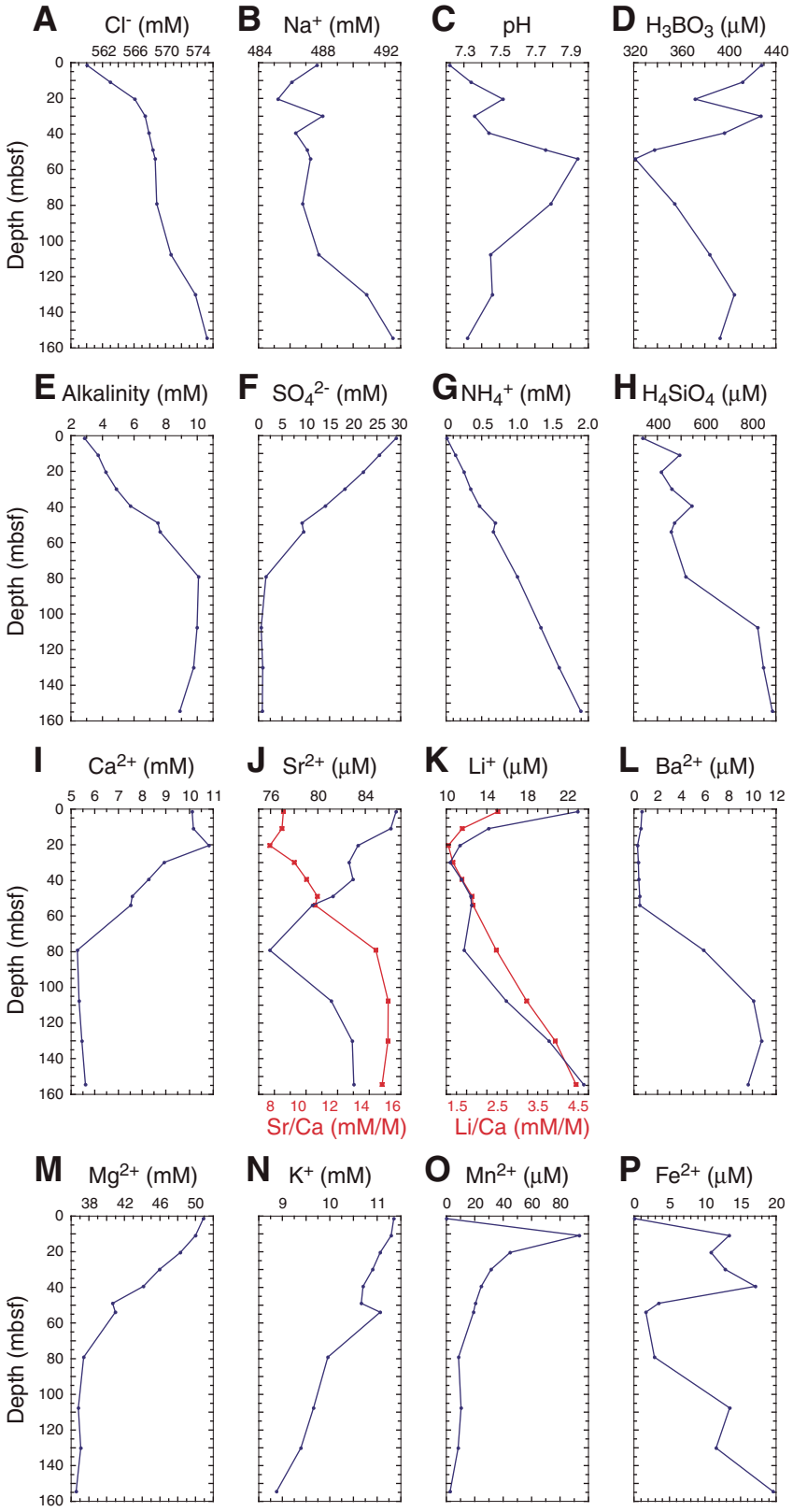

Figure F24. Headspace methane and interstitial water sulfate profiles for Hole U1307A.

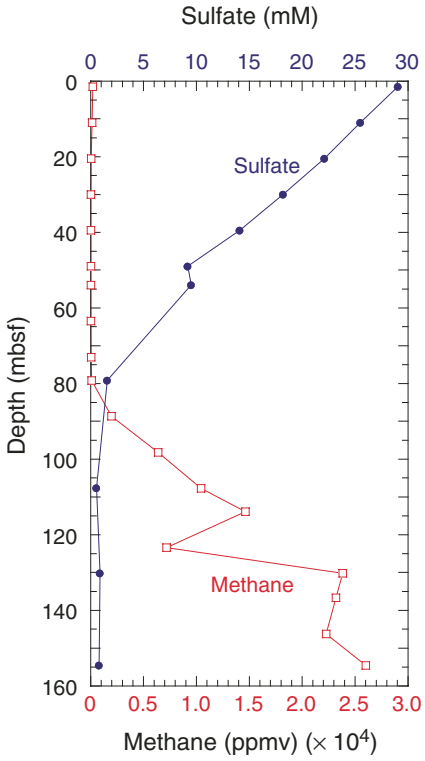

Figure F25. Site U1307 magnetic susceptibility (MS) records. Core recovery columns are represented on the left side of each plot. Black = multisensor track (MST) record, red = magnetic susceptibility core logger (MSCL) record.

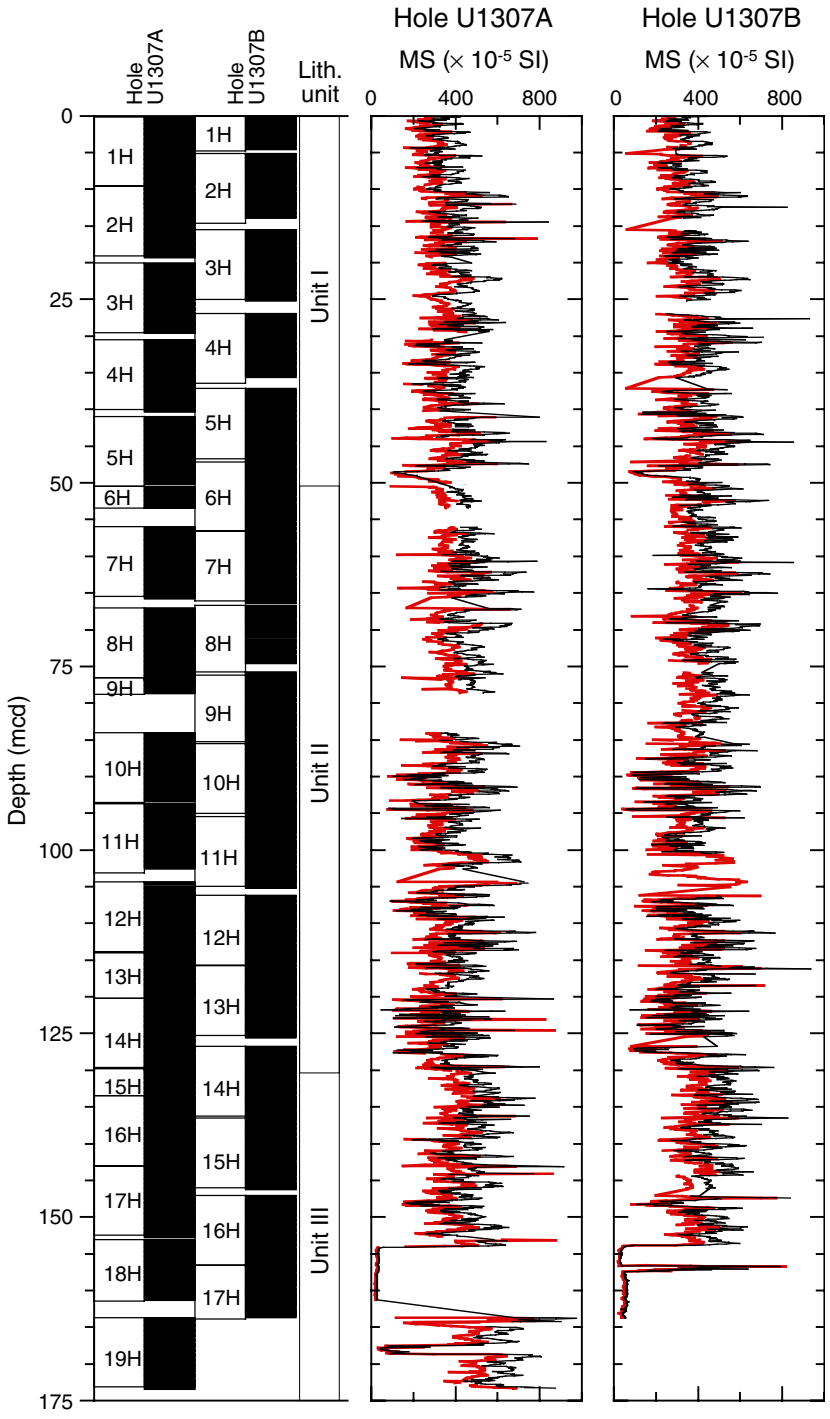

Figure F26. Combined plots of the spliced records of multisensor track–derived magnetic susceptibility (MS), gamma ray attenuation (GRA) density, and natural gamma ray (NGR), Site U1307. **A.** 0–50 mcd. (Continued on next two pages.)

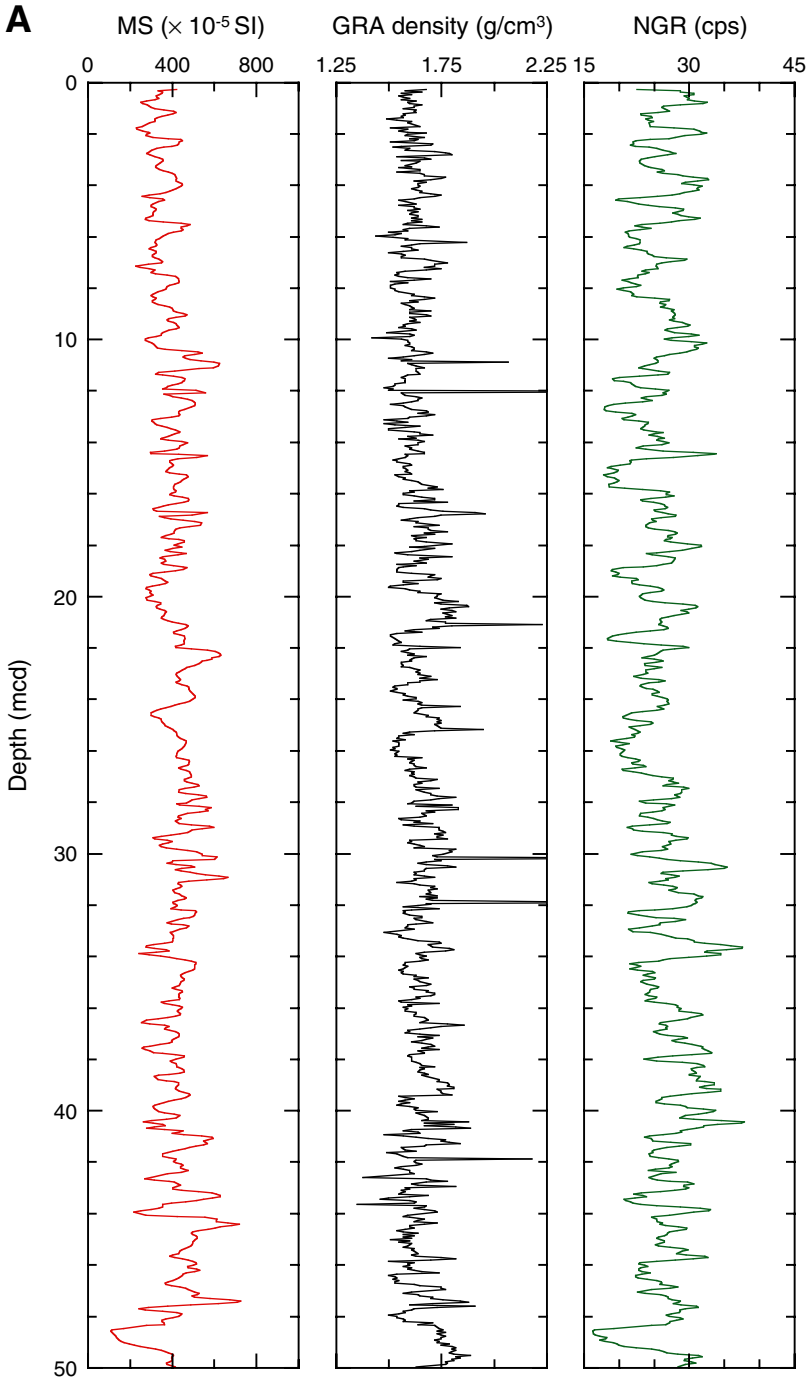

Figure F26 (continued). B. 50–100 mcd.

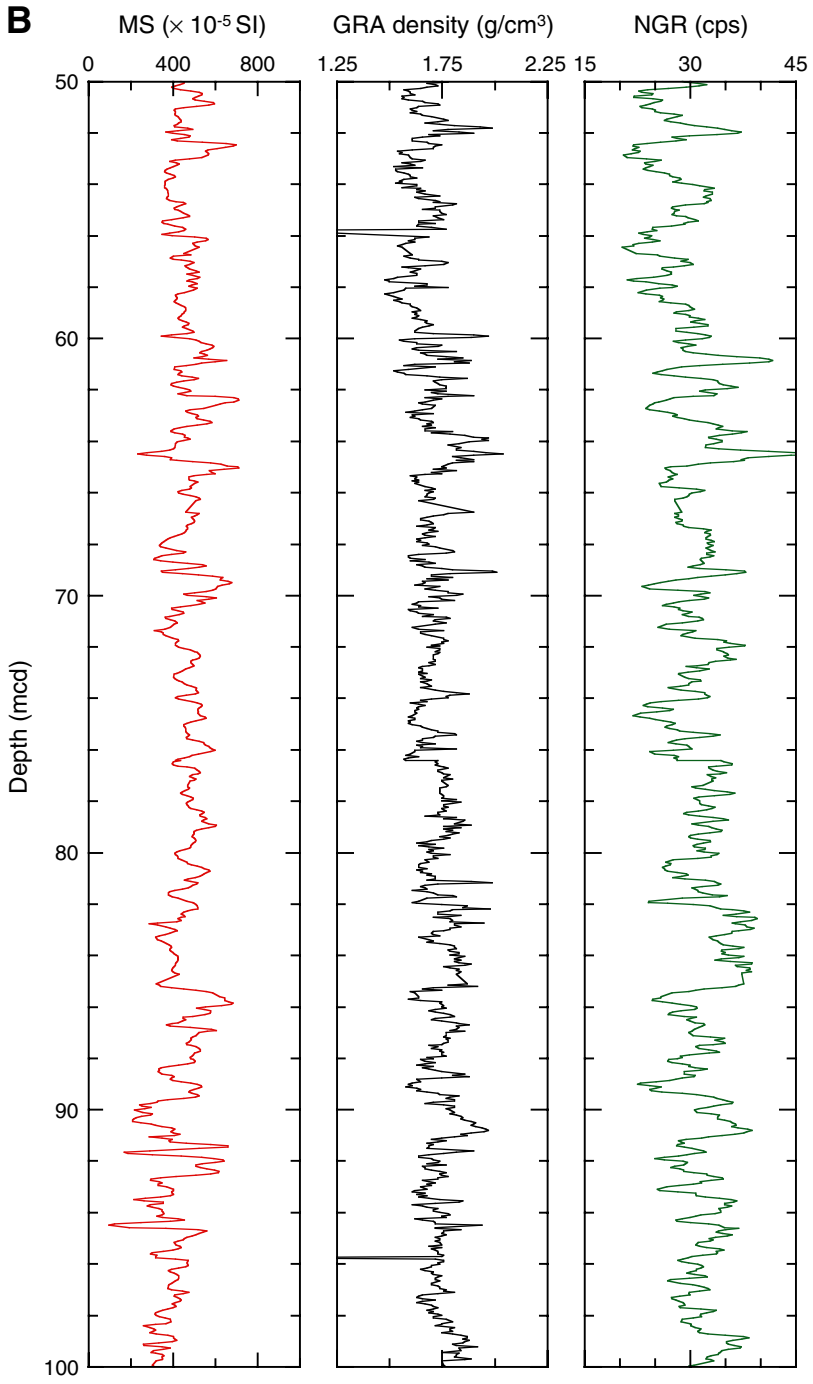

Figure F26 (continued). C. 100–175 mcd.

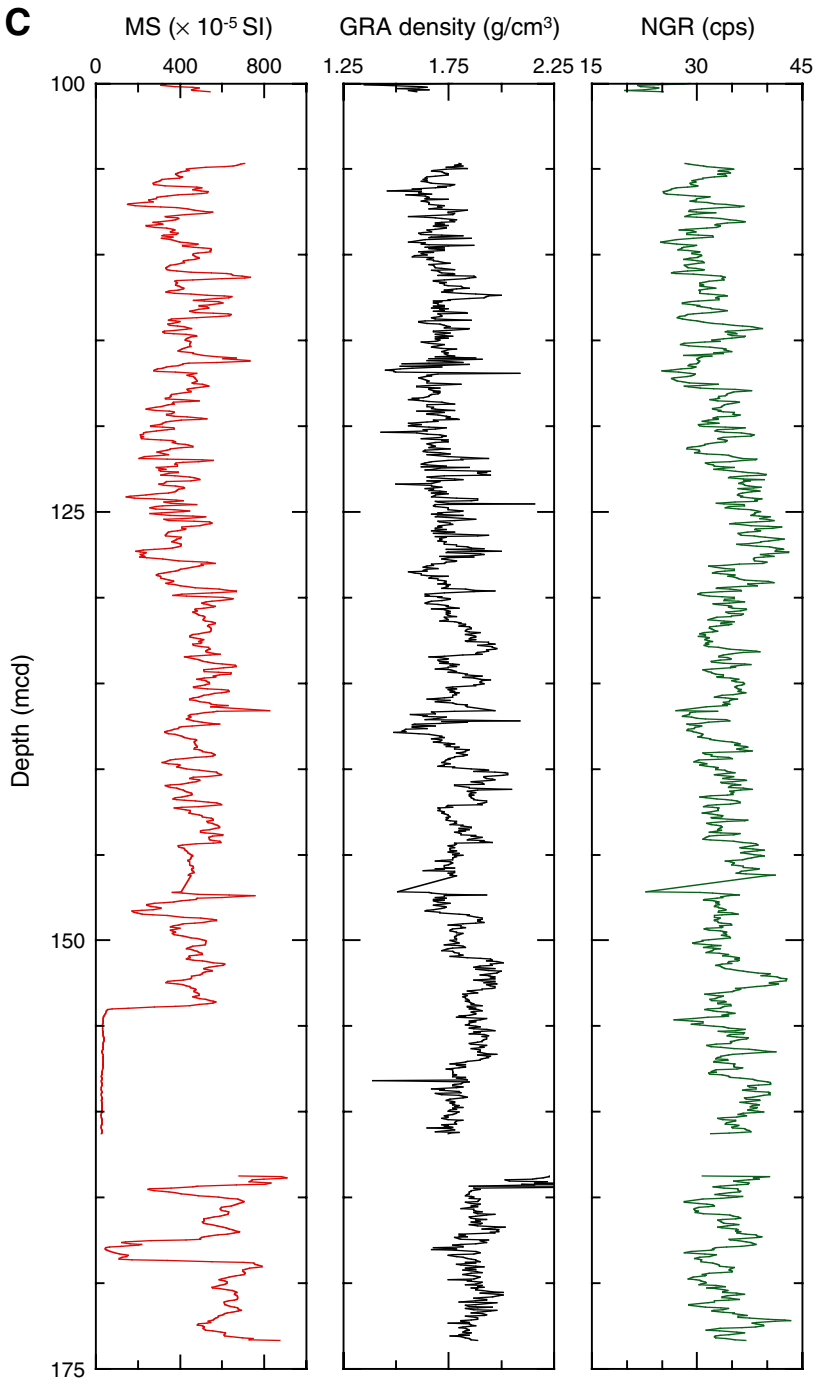

Figure F27. Combined gamma ray attenuation density measurements from the multisensor track and bulk density from discrete measurements (red circles), Site U1307.

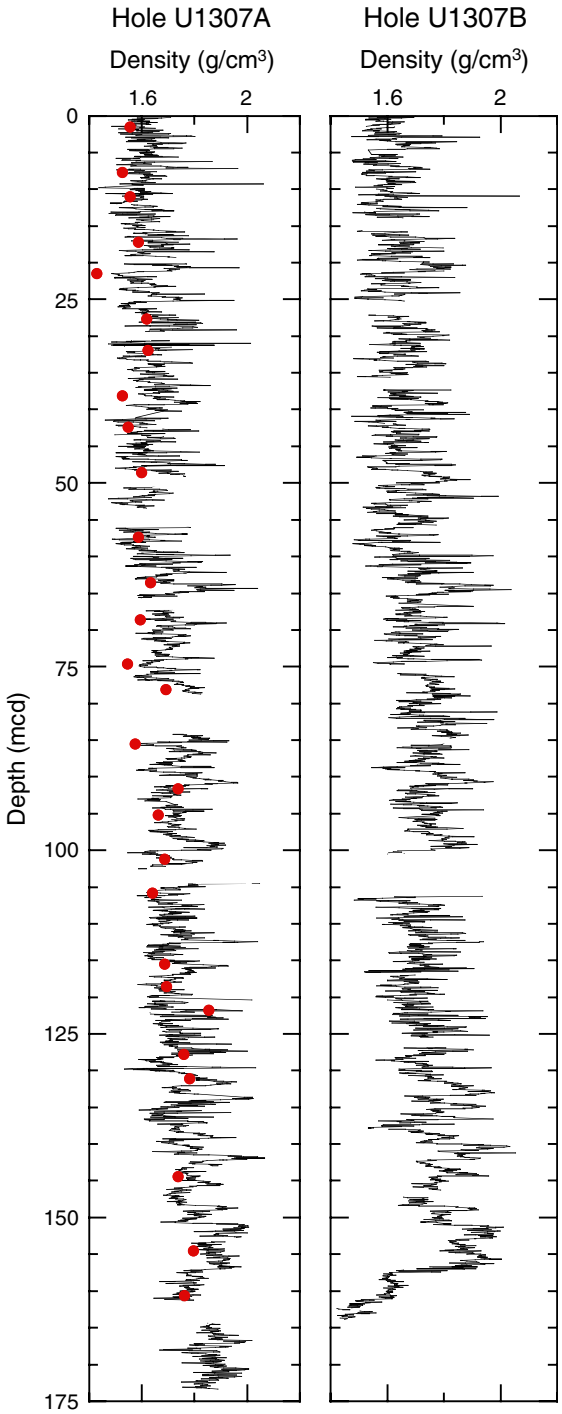

Figure F28. Natural gamma ray (NGR) counts from the multisensor track and bulk density from discrete measurements (red circles), Site U1307.

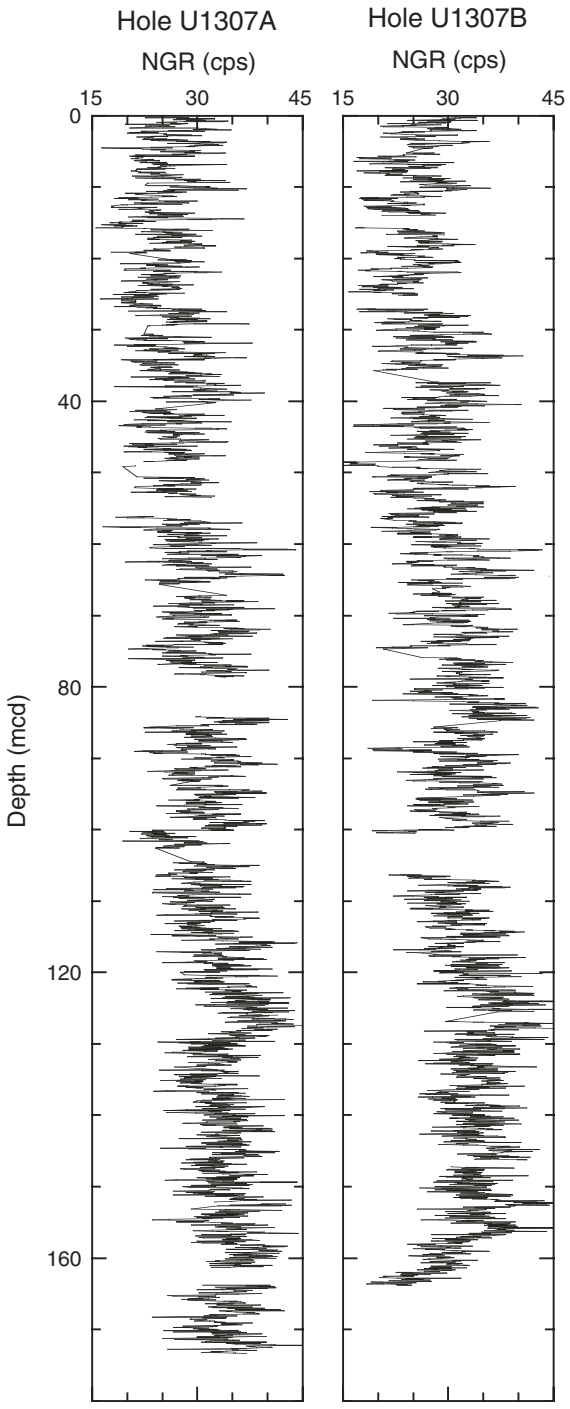

Figure F29. Downcore *P*-wave velocity records, Site U1307. Red circles = PWS3 discrete measurements.

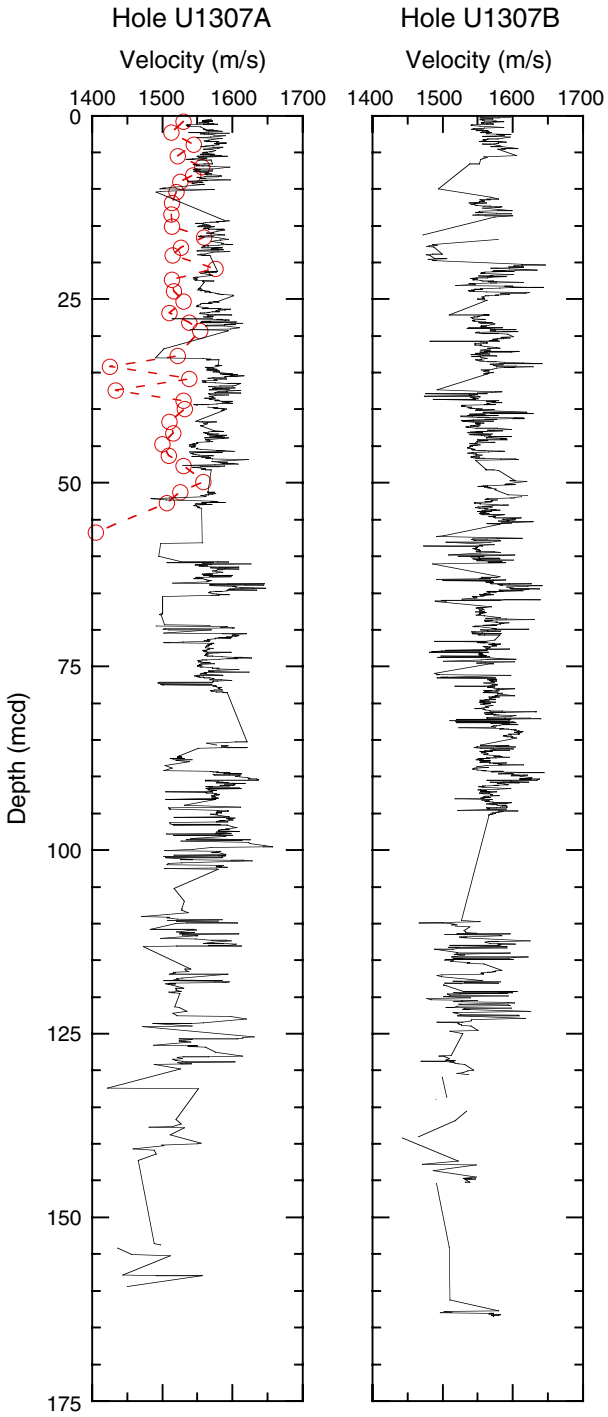

Figure F30. Downcore gamma ray attenuation–derived porosity calculations and discrete porosity measurements (red circles), Site U1307.

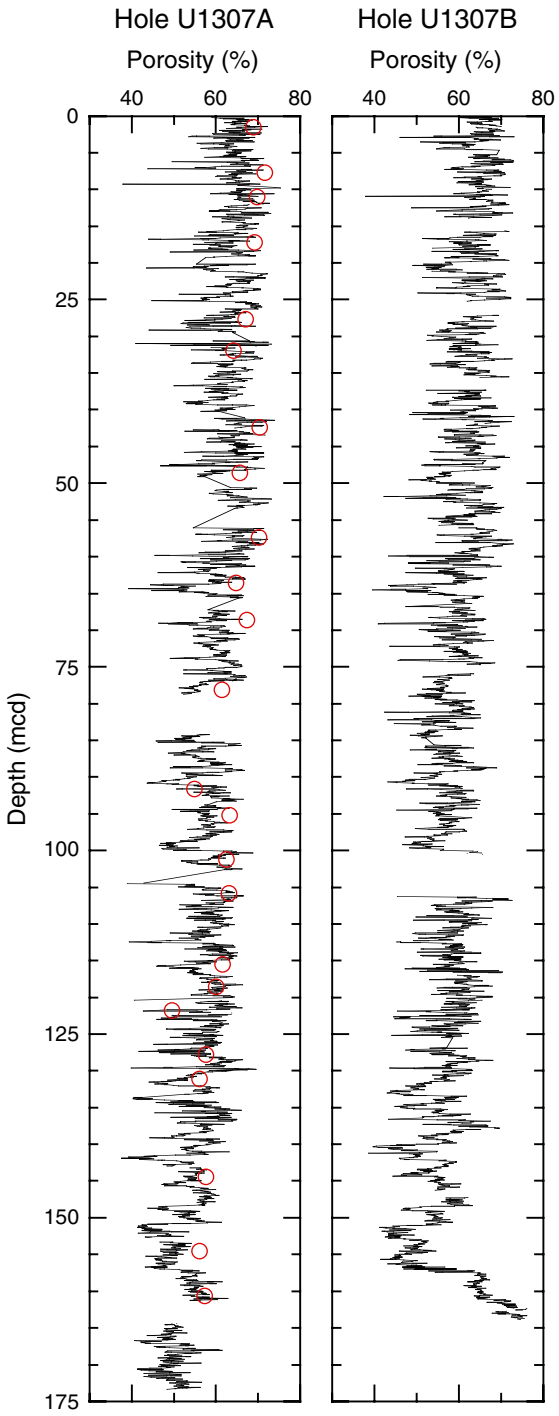

Table T1. Coring summary, Site U1307.

Hole U1307A
Latitude: 58°30.3468′N
Longitude: 46°24.0327′W
Time on site (h): 52.50 (0830 h, 28 October 2004–1300 h, 30 October 2004)
Time on hole (h): 27.42 (0830 h, 28 October 2004–1155 h, 29 October 2004)
Seafloor (drill pipe measurement from rig floor, mbrf): 2586.4
Distance between rig floor and sea level (m): 11.3
Water depth (drill pipe measurement from sea level, m): 2575.1
Total depth (drill pipe measurement from rig floor, mbrf): 2748.0
Total penetration (meters below seafloor, mbsf): 162.6
Total length of cored section (m): 156.6
Total length of drilled interval (m): 6.0
Total core recovered (m): 160.76
Core recovery (%): 102.7
Total number of cores: 19
Total number of drilled intervals: 2

Hole U1307B
Latitude: 58°0.3576′N
Longitude: 46°24.0540′W
Time on hole (h): 25.08 (1155 h, 29 October 2004–1300 h, 30 October 2004)
Seafloor (drill pipe measurement from rig floor, mbrf): 2586.6
Distance between rig floor and sea level (m): 11.3
Water depth (drill pipe measurement from sea level, m): 2575.3
Total depth (drill pipe measurement from rig floor, mbrf): 2741.2
Total penetration (meters below seafloor, mbsf): 154.6
Total length of cored section (m): 154.6
Total core recovered (m): 156.97
Core recovery (%): 101.5
Total number of cores: 17

Core	Date (Oct 2004)	Local time (h)	Depth (mbsf) Top	Depth (mbsf) Bottom	Length (m) Cored	Length (m) Recovered	Recovery (%)	Comments
303-U1307A-								
1H	28	1440	0.0	9.5	9.5	9.48	99.8	Nonmagnetic barrel
2H	28	1530	9.5	19.0	9.5	9.88	104.0	Nonmagnetic barrel
3H	28	1620	19.0	28.5	9.5	9.74	102.5	Oriented; nonmagnetic barrel
4H	28	1710	28.5	38.0	9.5	10.00	105.3	Oriented; nonmagnetic barrel
5H	28	1800	38.0	47.5	9.5	9.37	98.6	Oriented; nonmagnetic barrel; crushed liner
6H	28	1845	47.5	50.5	3.0	3.13	104.3	Oriented; nonmagnetic barrel
		*****Drilled 50.5 to 52.5 mbsf*****						
7H	28	1945	52.5	62.0	9.5	9.99	105.2	Oriented; nonmagnetic barrel
8H	28	2030	62.0	71.5	9.5	9.97	105.0	Oriented; nonmagnetic barrel
9H	28	2115	71.5	73.7	2.2	2.25	102.3	Oriented; nonmagnetic barrel
		*****Drilled 73.7 to 77.7 mbsf*****						
10H	28	2210	77.7	87.2	9.5	9.59	101.0	Oriented; nonmagnetic barrel
11H	28	2300	87.2	96.7	9.5	9.06	95.4	Oriented; nonmagnetic barrel
12H	28	2350	96.7	106.2	9.5	9.89	104.1	Oriented; nonmagnetic barrel
13H	28	0040	106.2	112.4	6.2	6.23	100.5	Oriented; nonmagnetic barrel
14H	28	0150	112.4	121.9	9.5	9.95	104.7	Oriented; nonmagnetic barrel
15H	28	0240	121.9	125.7	3.8	3.82	100.5	Oriented; nonmagnetic barrel
16H	28	0400	125.7	135.2	9.5	9.72	102.3	Oriented; nonmagnetic barrel
17H	28	0510	135.2	144.7	9.5	9.95	104.7	Oriented; nonmagnetic barrel
18H	28	0610	144.7	153.1	8.4	8.46	100.7	Oriented; nonmagnetic barrel
19H	28	1030	153.1	162.6	9.5	9.99	105.2	Oriented; nonmagnetic barrel; bit plugged; deployed center bit
				Cored:	156.6	160.47	102.5	
				Drilled:	6.0			
				Total:	162.6			
303-U1307B-								
1H	29	1315	0.0	4.8	4.8	4.83	100.6	Nonmagnetic barrel
2H	29	1400	4.8	14.3	9.5	8.94	94.1	Nonmagnetic barrel
3H	29	1445	14.3	23.8	9.5	9.88	104.0	Oriented; nonmagnetic barrel
4H	29	1530	23.8	33.3	9.5	8.80	92.6	Oriented; nonmagnetic barrel
5H	29	1615	33.3	42.8	9.5	10.05	105.8	Oriented; nonmagnetic barrel; crushed liner
6H	29	1710	42.8	52.3	9.5	9.47	99.7	Oriented; nonmagnetic barrel
7H	29	1800	52.3	61.8	9.5	9.90	104.2	Oriented; nonmagnetic barrel; expanding core
8H	29	1850	61.8	71.3	9.5	8.11	85.4	Oriented; nonmagnetic barrel

Table T1 (continued).

Core	Date (Oct 2004)	Local time (h)	Depth (mbsf) Top	Depth (mbsf) Bottom	Length (m) Cored	Length (m) Recovered	Recovery (%)	Comments
303-U1307B-								
9H	29	1935	71.3	80.8	9.5	10.05	105.8	Oriented; nonmagnetic barrel
10H	29	2030	80.8	90.3	9.5	10.17	107.1	Oriented; nonmagnetic barrel
11H	29	2125	90.3	99.8	9.5	9.95	104.7	Oriented; nonmagnetic barrel; split/crushed liner
12H	29	2230	99.8	109.3	9.5	9.85	103.7	Oriented; nonmagnetic barrel
13H	29	2320	109.3	118.8	9.5	9.96	104.8	Oriented; nonmagnetic barrel
14H	30	0025	118.8	128.3	9.5	9.85	103.7	Oriented; nonmagnetic barrel
15H	30	0210	128.3	137.8	9.5	9.96	104.8	Oriented; nonmagnetic barrel
16H	30	0320	137.8	147.3	9.5	9.91	104.3	Oriented; nonmagnetic barrel
17H	30	0515	147.3	154.6	7.3	7.29	99.9	Oriented; nonmagnetic barrel
				Totals:	154.6	156.97	101.5	

Table T2. Depth intervals and thicknesses of foraminifer ooze beds, Holes U1307A and U1307B.

Foraminifer ooze bed	Hole, core, section, interval (cm)	Depth (mcd) Top	Depth (mcd) Bottom	Thickness (cm)
1	U1307A-1H-3, 122–130	4.41	4.49	8
	U1307B-1H-4, 30–34	4.30	4.34	4
2	U1307B-2H-2, 37–59	7.07	7.29	22
3	U1307A-2H-5, 85–103	16.54	16.72	18
	U1307B-3H-1, 87–108	16.47	16.68	21
4	U1307A-3H-4, 0–85	24.58	25.43	85
5	U1307B-4H-2, 118–150	29.67	29.99	32
6	U1307A-4H-5, 0–13	36.54	36.67	13
7	U1307A-5H-2, 0–17	42.55	42.72	17
	U1307B-5H-4, 91–96	42.65	42.70	5
8	U1307A-5H-5, 140, to 5H-7, 33	48.42	49.52	110
	U1307B-6H-1, 120, to 6H-2, 102	48.37	49.45	107

Table T3. Distribution of calcareous nannofossils, Hole U1307A.

Core, section, interval (cm)	Age (Ma)	Abundance	Preservation	*Calcidiscus leptoporus*	*Calcidiscus macintyrei*	*Ceratolithus cristatus*	*Coccolithus streckerii*	*Coccolithus pelagicus*	*Cyclolithella annula*	*Discoaster asymmetricus*	*Discoaster brouweri*	*Discoaster pentaradiatus*	*Discoaster surculus*	*Discoaster tamalis*	*Discoaster variabilis*	*Discoaster* spp.	*Discolithina japonica*	*Discolithina* spp.	*Emiliania huxleyi*	*Gephyrocapsa caribbeanica*	*Gephyrocapsa oceanica*	*Gephyrocapsa parallela*	*Gephyrocapsa* spp. (small)	*Helicosphaera carteri*	*Helicosphaera sellii*	*Pseudoemiliania lacunosa*	*Reticulofenestra asanoi*	*Reticulofenestra ampla*	*Reticulofenestra* spp. (small)	*Rhabdosphaera clavigera*	*Syracosphaera pulchra*	*Umbilicosphaera sibogae*	Reworked species: *Reticulofenestra pseudoumbilicus*	Reworked species: *Eiffellithus eximius*	Reworked species: *Watznaueria barnesae*	Nannofossil datum age (Ma)
303-U1307A-																																				0.25
1H-CC	0~0.25	F	M	+			+	R											+		+	+	R	+												
2H-CC	0.41~0.85	A	G	+				+										+	?		F	R	C	R		+			+							0.41
3H-CC	0.41~0.85	F	M	+																	R	R	R	+		F						+				
4H-CC	0.41~0.85	F	M	R				R										+			R	R	F			F			+					r	r	0.85
5H-1, 10–11	0.85~0.95	C	G	R													F	+			C	C	A	R		F	A		R							
5H-2, 10–11	0.85~0.95	C	M	C													F	R			F	F	A	F		R	C									0.95
5H-3, 10–11	?	B																																		
5H-4, 10–11	?	B																																		
5H-5, 10–11	?	B																																		
5H-6, 10–11	0.95~1.16	F	M	F														+					F	R		C	F		C							
5H-7, 10–11	0.95~1.16	C	M	F													+						+	+		C	R		A	+	+					
5H-CC	0.95~1.16	F	M	R														+					+	R		F	R		R		+	+				
6H-1, 10–11	0.95~1.16	F	M																				+	R		F	R		C		R					1.16
6H-2, 10–11	?	B																																		
6H-CC	1.16~1.21	R	P																				+	+					+							
7H-1, 10–11	1.16~1.21	C	M	C				C									+									C			A			+				
7H-2, 10–11	?	B																																		1.21
7H-3, 10–11	?	B																																		1.45
7H-4, 10–11	?	B																																		
7H-5, 10–11	1.45~1.65	R	M	+													+				R	R	F			C			C							
7H-6, 10–11	1.45~1.65	B																																		
7H-CC	1.45~1.65	B																																		
8H-1, 10–11	1.45~1.65	B																																		
8H-2, 10–11	1.45~1.65	R	P	R																C	C		R		+	R			C							
8H-3, 10–11	1.45~1.65	F	M	R				C									+			F	R		F	+	R	R			C							
8H-4, 10–11	1.45~1.65	B																																		
8H-5, 10–11	1.45~1.65	B																																		
8H-6, 10–11	1.45~1.65	B																																		
8H-CC	1.45~1.65	C	G	R				R										+		R	F		R	R		+			R		+					
9H-CC	1.45~1.65	F	M					F												F	F		F	+		+			+							1.65
10H-CC	?	R	P	+				+																					+							1.73
11H-CC	1.73~2.74	A	G	+			F	A															+	+		+			R			+				
12H-CC	?	R	P					+																					+							
13H-CC	?	B																																		
14H-CC	?	B																																		2.74
15H-CC	2.74~3.85	C	M	R	R	+	+	F		+	+	+	+			+									+	R		R	A	R	+		r			
16H-CC	?	R	M	+	+			+																		+			+							
17H-CC	2.74~3.85	A	G	R	R		+	C	+	+	+	+	+	+		+	+								R	R			A		+				
18H-CC	?	R	P	+						+			+			+										+			+							
19H-CC	2.74~3.85	A	M	+	R		+	A		+	+	+	+	+	+		+	+						+	+	R		+	A							

Notes: Abundance: A = abundant, C = common, F = few, R = rare, B = barren, + = present, r = reworked. Preservation: G = good, M = moderate, P = poor.

Table T4. Distribution of calcareous nannofossils, Hole U1307B.

Core, section	Age (Ma)	Abundance	Preservation	*Calcidiscus leptoporus*	*Calcidiscus macintyrei*	*Ceratolithus cristatus*	*Coccolithus streckerii*	*Coccolithus pelagicus*	*Discoaster asymmetricus*	*Discoaster brouweri*	*Discoaster pentaradiatus*	*Discoaster surculus*	*Discoaster triradiatus*	*Discoaster* spp.	*Discolithina japonica*	*Discolithina* spp.	*Emiliania huxleyi*	*Gephyrocapsa caribbeanica*	*Gephyrocapsa oceanica*	*Gephyrocapsa parallela*	*Gephyrocapsa* spp. (large)	*Gephyrocapsa* spp. (small)	*Helicosphaera carteri*	*Helicosphaera sellii*	*Pseudoemiliania lacunosa*	*Reticulofenestra ampla*	*Reticulofenestra asanoi*	*Reticulofenestra* spp. (small)	Reworked species: *Reticulofenestra pseudoumbilicus*	Reworked species: *Cribrosphaerella ehrenbergii*	Reworked species: *Eiffellithus turriseiffeli*	Reworked species: *Watznaueria barnesae*	Nannofossil datum age (Ma)
303-U1307B-																																0.25
1H-CC	0~0.25	R	M														+		+			+										0.41
2H-CC	?	R	P																									+					
3H-CC	0.41~0.85	F	M	+				+								+			+			+	+		R			+		r	r	r	0.85 0.95
4H-CC	0.41~0.85	R	P	+																		+			+			+		r			1.16
5H-CC	0.95~1.16	F	M	R												+						+	R		R		F	F					1.21 1.45
6H-CC	?	R	P	+				+																	R			+		r			
7H-CC	?	B																															1.65
8H-CC	1.45~1.65	F	P	+				F										R	+			F	+		+			+				r	1.73
9H-CC	?	R	P																						+			+					
10H-CC	1.73~2.74	C	G				R	C														+	R	R	R			+		r	r	r	
11H-CC	?	R	P					+																				+					
12H-CC	?	B																															2.74
13H-CC	?	B																															
14H-CC	2.74~3.85	C	M	F	R	+	R	A	+	+	R	R	+	+	+								R	R	R	R		A	r				
15H-CC	?	B																															
16H-CC	?	B																															
17H-CC	2.74~3.85	C	M	F	+		R	C	+	+	+	+		+	+									+	R	+		A	r				

Notes: Abundance: A = abundant, C = common, F = few, R = rare, B = barren, + = present, r = reworked. Preservation: G = good, M = moderate, P = poor.

Table T5. Distribution of planktonic foraminifers, Hole U1307A.

Core, section	Overall abundance	Preservation	*Globigerina bulloides*	*Neogloboquadrina atlantica* (d)	*Neogloboquadrina atlantica* (s)	*Neogloboquadrina pachyderma* (d)	*Neogloboquadrina pachyderma* (s)	*Turborotalita quinqueloba* (d)	*Turborotalita quinqueloba* (s)	Biozone
303-U1307A-										
1H-CC	C	P	F			R	D	P	R	
2H-CC	A	P					D			
3H-CC	C	P				R	D			*N. pachyderma (s)*
4H-CC	R	P				R	A	P	P	
5H-CC	C	M				R	D			
6H-CC	B	—								
7H-CC	B	—								
8H-CC	R	G					F			
9H-CC	R	P					A			*N. pachyderma (s)*
10H-CC	R	M				F	D	P	P	
11H-CC	R	M				R	R		F	*G. inflata–G. bulloides*?
12H-CC	B	—								
13H-CC	B	—								
14H-CC	B	—								
15H-CC	R	M	R		D					
16H-CC	R	M	R		A					*N. atlantica*
17H-CC	R	M	R	P	D		F			
18H-CC	B	—								
19H-CC	B	—								

Notes: *Globorotalia inflata* does not occur at Site U1307, so *G. inflata* Zone and *Globigerina bulloides* Zone could not be verified by their zonal markers directly. Abundance: D = dominant, A = abundant, C = common, F = few, R = rare, P = present, B = barren. Preservation: G = good, M = moderate, P = poor (see "**Foraminifers**" in the "Site U1302–U1308 methods" chapter). s = sinistral, d = dextral.

Table T6. Distribution of planktonic foraminifers, Hole U1307B.

Core	Overall abundance	Preservation	*Globigerina bulloides*	*Neogloboquadrina atlantica* (d)	*Neogloboquadrina atlantica* (s)	*Neogloboquadrina pachyderma* (d)	*Neogloboquadrina pachyderma* (s)	*Turborotalita quinqueloba* (d)	*Turborotalita quinqueloba* (s)	Biozone
303-U1307B-										
1H	A	G					D			
2H	R	M	F			R	D		P	
3H	R	M				P	D			*N. pachyderma* (s)
4H	R	M	P			P	D	P		
5H	R	M	P			R	D			
6H	R	P				P	D			
7H	B	—								
8H	R	P				P	A			*N. pachyderma* (s)
9H	R	P				R	A			
10H	R	P					R	P	P	*G. inflata–G. bulloides*?
11H	B	—								
12H	B	—								
13H	B	—								
14H	R	M	R	R	D	P	P			*N. atlantica*
15H	R	M			F		R			
16H	B	—								
17H	R	M				P	F			*N. atlantica*?

Notes: Abundance: D = dominant, A = abundant, F = few, R = rare, P = present, B = barren. Preservation: G = good, M = moderate, P = poor (see "Foraminifers" in the "Site U1302–U1308 methods" chapter). d = dextral, s = sinistral.

Table T7. Distribution of benthic foraminifers, Holes U1307A and U1307B.

Core	*Bolivina translucens*	*Cassidulina crassa*	*Cassidulina minuta*	*Cassidulina teretis*	*Chilostomella* spp.	*Cibicides lobatulus*	*Cibicidoides* spp.	*Cibicidoides wuellerstorfi*	*Eggerelloides bradyi*	*Epistominella exigua*	*Fissurina* spp.	*Gavelinopsis praegeri*	*Gyroidina* spp.	*Hoeglundina elegans*	*Lenticulina* spp.	*Melonis barleeanum*	*Melonis pompiloides*	*Nodogenerina* sp.	*Nonion asterizans*	*Nonion* spp./*Astrononion* spp.	*Nuttallides umbonifera*	*Oridorsalis umbonatus*	*Pullenia bulloides*	*Pullenia quinqueloba*	*Pyrgo* spp./*Biloculina* spp.	*Stainforthia* sp.	*Uvigerina peregrina*	Indeterminate Lagenina	Indeterminate Miliolina	Indeterminate Rotaliina	Indeterminate Textulariina	Total
303-U1307A-																																
2H																	1				1										1	3
3H																						2										2
4H																				1			1						1			3
5H		2	1																													3
8H	2																															2
9H			2																											1		3
10H				1			1					1					1	2														6
11H	10	2	1			2						7		2			2		1	4	10	2		1						3		47
12H																		1														1
15H							1										1							1			1			1		5
16H														1																		1
17H														1	1			2		11		1	1	5				2		2		26
18H																										1						1
19H										1	1						1							1								4
303-U1307B-																																
1H							2	1																				1	1		4	9
2H							1																2									3
3H								1	1																							2
4H								1												1		2			1				2	1		8
5H		2	4							1		1										1										9
8H				1																												1
9H			2																													2
10H			18		1					19		2	1			1	1	1					1	5		2		3		4		59
14H			1									1				1															1	4
15H							1																									1
17H																					1											1

Notes: Numbers are total observations, which are not calibrated. Barren samples are not listed.

Table T8. Distribution of diatoms and silicoflagellates, Hole U1307A. (Continued on next page.)

			Diatoms																																		
Core, section, interval (cm)	Abundance	Preservation	*Actinocyclus curvatulus*	*Actinocyclus octonarius*	*Actinocyclus oculatus*	*Actinoptychus senarius*	*Actinoptychus vulgaris*	*Bacterosira fragilis*	*Cavitatus jouseanus*	*Chaetoceros bacteriastroides*	RS *Chaetoceros cinctus*	RS *Chaetoceros compresus*	RS *Chaetoceros constrictus*	RS *Chaetoceros debilis*	RS *Chaetoceros diadema*	RS *Chaetoceros dydimus*	RS *Chaetoceros lorenzianus*	RS *Chaetoceros radicans*	RS *Chaetoceros* spp.	*Chaetoceros setae*	*Cocconeis* spp.	*Coscinodiscus asteromphalus*	*Coscinodiscus argus*	*Coscinodiscus marginatus*	*Coscinodiscus oculus-iridis*	*Coscinodiscus radiatus*	*Delphineis kippae*	*Fallacia* sp.	*Fragilariopsis cylindrus*	*Fragilariopsis oceanica*	*Grammatophora oceanica*	*Hemidiscus cuneiformis*	*Navicula* sp.	*Neodenticula koizumii*	*Neodenticula seminae*	*Nitzschia* sp.	*Paralia sulcata*
303-U1307A-																																					
1H-2, 73	C	M	T							T	T			R										T						T							
1H-3, 72	F	M									T			T	R							T		T													
1H-3, 125	B																																				
1H-3, 140	B																																				
1H-4, 38	B																																				
1H-4, 112	A	G	R		T							T	T	T					C	*								T	T	T						T	
1H-5, 139	C	M	T				T							R	T							T	T	T		T											T
1H-CC	F	P	T											R	T					*										T							
2H-4, 140	B																																				
2H-5, 96	B																																				
2H-CC	B																																				
3H-CC	B																																				
4H-1, 36	B																																				
4H-CC	T	M	*											T																							
5H-CC	T	M												T																					T		T
6H-CC	T	M												T								T															*
7H-6, 110	T	M																																			*
7H-CC	T	P																																			T
8H-CC	B																																				
9H-CC	B																																				
10H-5, 70	B																																				
10H-6, 70	B																																				
10H-CC	B																																				
11H-CC	F	P	T		R									T			T		T	*		T		T						*			T				
12H-6, 63	T	M	T											T										T													
12H-6, 72	B																																				
12H-CC	T	P																	T						*												*
13H-CC	T	P																																*?			*
14H-1, 140	T	P																				*		T													
14H-7, 29	R	M														T			T	*																	
14H-CC	T	P																	*																		
15H-CC	C	M	T																C					*			*					*					*
16H-6, 70	F	P	T			T						T		R				T	R	*																	
16H-6, 130	C	P	T	T										R	T				R	*																	
16H-CC	R	P						*											R					T						*				*?			*
17H-6, 130	T	P	T	T										T							T			T													
17H-CC	A	G	T						*										A					*							*						
18H-1, 70	F	P	T											T					T	*		*															T
18H-3, 70	C	M	T									T							R	*				T													
18H-CC	A	G																	A											*							
19H-CC	R	P																	T																		

Notes: Abundance: A = abundant, C = common, F = few, R = rare, T = trace, B = barren. Preservation: G = good, M = moderate, P = poor. RS = resting spore. * = fragment present.

Table T8 (continued).

Core, section, interval (cm)	Abundance	Preservation	Diatoms: *Porosira glacialis*	*Proboscia alata* f. *indica*	*Rhizosolenia hebetata* f. *hiemalis*	*Rhizosolenia hebetata* f. *semispina*	*Rhizosolenia hebetata* f. *subacuta*	*Rhizosolenia* spp.	*Roperia tesselata*	*Stephanogonia* spp.	*Stephanopyxis turris*	*Thalassionema bacillare*	*Thalassionema frauenfeldii*	*Thalassionema nitzschioides* var. *nitzschioides*	*Thalassionema nitzschioides* var. *inflata*	*Thalassionema nitzschioides* var. *parva*	*Thalassiosira bipora*	*Thalassiosira gravida*	*Thalassiosira gravida* spore	*Thalassiosira jouseae*	*Thalassiosira leptopus*	*Thalassiosira lineata*	*Thalassiosira nidulus*	*Thalassiosira nordenskioeldii*	*Thalassiosira oestrupii* var. *oestrupii*	*Thalassiosira oestrupii* var. *venrickae*	*Thalassiosira trifulta*	*Thalassiosira* spp.	*Thalassiothrix/Lioloma* complex	Silicoflagellates: *Dictyocha fibula*	*Distephanus speculum*	*Octactis pulchra*	*Actiniscus pentasterias*
303-U1307A-																																	
1H-2, 73	C	M			T													T						T	T			F				
1H-3, 72	F	M			T	T												T						T			T	R				
1H-3, 125	B																																
1H-3, 140	B																																
1H-4, 38	B																																
1H-4, 112	A	G				T												T	R		T			T	T			T				
1H-5, 139	C	M	*			T			T									T	T							T	T	T					
1H-CC	F	P				T												T	T					T			T	T					
2H-4, 140	B																																
2H-5, 96	B																																
2H-CC	B																																
3H-CC	B																																
4H-1, 36	B																																
4H-CC	T	M					T																										
5H-CC	T	M					T																		T				T				
6H-CC	T	M																							T				T				
7H-6, 110	T	M																T											*				
7H-CC	T	P					T																										
8H-CC	B																																
9H-CC	B																																
10H-5, 70	B																																
10H-6, 70	B																																
10H-CC	B																																
11H-CC	F	P			T	T						*	*	T	T			T		T			T		T			T					T
12H-6, 63	T	M			T									T															*				
12H-6, 72	B																																
12H-CC	T	P									*																						
13H-CC	T	P									*			*															*				
14H-1, 140	T	P												*																			
14-7H, 29	R	M												T						T					T	T							
14-CC	T	P																															
15-CC	C	M			T			T			T			R			T				*				T					*			
16H-6, 70	F	P									T		*	T											T				T			T	T
16H-6, 130	C	P			T						T			R	T											T				T			T
16H-CC	R	P								*	T	*		T			T		*					*	*			*				
17H-6, 130	T	P																		T									*				
17H-CC	A	G			T	T				T	R	T		A			T		*			T		T	T			T					
18H-1, 70	F	P			T						T	*	T	T	T					T	T												T
18H-3, 70	C	M		T	T						R				T	T				T					T	T					T		T
18H-CC	A	G								T	R			R			T				T				T			T					
19H-CC	R	P								T	T			T																			

Table T9. Distribution of diatoms and silicoflagellates, Hole U1307B. (Continued on next page.)

Core, section, interval (cm)	Diatoms																																				
	Abundance	Preservation	*Actinocyclus curvatulus*	*Actinocyclus octonarius*	*Actinocyclus oculatus*	*Actinoptychus vulgaris*	*Asteromphalus imbricatus*	*Chaetoceros concavicornis*	RS *Chaetoceros affinis*	RS *Chaetoceros cinctus*	RS *Chaetoceros compresus*	RS *Chaetoceros coronatus*	RS *Chaetoceros debilis*	RS *Chaetoceros diadema*	RS *Chaetoceros lorenzianus*	RS *Chaetoceros radicans*	RS *Chaetoceros* spp.	*Chaetoceros setae*	*Cocconeis* spp.	*Coscinodiscus asteromphalus*	*Coscinodiscus marginatus*	*Coscinodiscus oculus-iridis*	*Diploneis bombus*	*Fragilariopsis oceanica*	*Fragilariopsis reinholdii*	*Grammatophora marina*	*Melosira albicans*	*Neodenticula seminae*	*Nitzschia bicapitata*	*Nitzschia* sp.	*Paralia sulcata*	*Planktoniella sol*	*Proboscia curvirostris*	*Rhaphoneis surirella*	*Rhizosolenia acicularis*	*Rhizosolenia acuminata*	*Rhizosolenia bergonii*
303-U1307B-																																					
1H-CC	F	M	R										T							*										*							
2H-CC	B		*																																		
3H-1, 70	B																																				
3H-5, 65	B																																				
3H-6, 24	B																																				
3H-CC	B																																				
4H-3, 10	B																																				
4H-CC	F	M	T							T			R	T										T				T									
5H-3, 90	B																																				
5H-CC	T	P																		T	T							*									
6H-6, 26	B																																				
6H-CC	B																																				
7H-5, 80	B																																				
7H-CC	T	P											T		T						*										T						
8H-3, 80	B																																				
8H-3, 123	B																																				
8H-5, 140	T	P											T				T	*			T										*						
8H-CC	R	P	T		T															*													*				
9H-4, 30	T	P																													T						
9H-4, 145	T	P																																			T
9H-CC	B																																				
10H-2, 115	R	M	T										T								T										*						
10H-4, 70	B																														*						
10H-5, 11	B																																				
10H-CC	T	P	T																	T	T										*						
11H-CC	B																																				
12H-CC	T	P																													T						
13H-CC	C	M	T				T						T			T		*		*	T			T							T						
14H-5, 10	R	M	T						T				T				T	*			T																
14H-5, 120	F	M	T						T		T		R					T	*		T													*			
14H-CC	C	G	*														C																				
15H-CC	B																																				
16H-5, 82	C	M	T	T						T			T								T								T							T	
16H-CC	F	P				R						T													T	T	T					T			T		
17H-CC	T	P				T		*														T	*														

Notes: Abundance: A = abundant, C = common, F = few, R = rare, T = trace, B = barren. Preservation: G = good, M = moderate, P = poor. RS = resting spore. * = fragment present.

Table T9 (continued).

Core, section, interval (cm)	Abundance	Preservation	Diatoms: *Rhizosolenia hebetata* f. *hiemalis*	*Rhizosolenia hebetata* f. *semispina*	*Rhizosolenia hebetata* f. *subacuta*	*Rhizosolenia* spp.	*Stephanogonia* spp.	*Stephanopyxis grunowii*	*Stephanopyxis turris*	*Thalassionema frauenfeldii*	*Thalassionema nitzschioides* var. *nitzschioides*	*Thalassionema nitzschioides* var. *inflata*	*Thalassiosira antiqua*	*Thalassiosira bipora*	*Thalassiosira conferta*	*Thalassiosira gravida*	*Thalassiosira gravida* spore	*Thalassiosira leptopus*	*Thalassiosira nidulus*	*Thalassiosira nordenskioeldii*	*Thalassiosira oestrupii* var. *oestrupii*	*Thalassiosira oestrupii* var. *venrickae*	*Thalassiosira trifulta*	*Thalassiosira* spp.	*Thalassiothrix/Lioloma* complex	Silicoflagellates: *Distephanus speculum*	*Actiniscus pentasterias*
303-U1307B-																											
1H-CC	F	M		T	T												T	T							*		
2H-CC	B																										
3H-1, 70	B																										
3H-5, 65	B																										
3H-6, 24	B																										
3H-CC	B																										
4H-3, 10	B																										
4H-CC	F	M		T							T					T	T						T		*		
5H-3, 90	B																										
5H-CC	T	P			T					*						T						T					
6H-6, 26	B																										
6H-CC	B																										
7H-5, 80	B																										
7H-CC	T	P																									
8H-3, 80	B																										
8H-3, 123	B																										
8H-5, 140	T	P								T	*									T					*		
8H-CC	R	P	*	T						R						T	T				T				*		
9H-4, 30	T	P																									
9H-4, 145	T	P																							*		
9H-CC	B																								*		
10H-2, 115	R	M															T										
10H-4, 70	B																										
10H-5, 11	B																										
10H-CC	T	P								*						T						T					
11H-CC	B																										
12H-CC	T	P																									
13H-CC	C	M	T						T	T	T	T	T			T	T			T	R	T	F			T	
14H-5, 10	R	M							T								T				T				T		
14H-5, 120	F	M									T						T					T	T			T	T
14H-CC	C	G					T		T		F	T		T			T						*	T			
15H-CC	B																										
16H-5, 82	C	M		R	R			T		T					T				*			T					
16H-CC	F	P				T																					
17H-CC	T	P																									

Table T10. Distribution of radiolarians, Hole U1307A.

Core, section	Abundance	Preservation	*Actinomma leptodermum*	*Actinomma* spp.	*Hexacontium enthacanthum*	*Stylatractus* sp.	*Axoprunum angelinum*	Other actinommids	*Stylochlamidium venustum*	*Stylodictya multispina*	*Spongodiscus* spp.	*Larcopyle butschlii* group	*Lithelius minor*	*Pylospira octopyle*	*Pylospira* spp.	*Pseudodictyophimus* spp.	*Cycladophora davisiana davisiana*	*Botryostrobus acquilonaris*	Radiolarian zone
303-U1307A-																			
1H-CC	T	P	T																?
2H-CC	T	P	T					T											
3H-CC	B																		
4H-CC	B																		
5H-CC	R	P	T					R	T			T					R		*C. d. davisiana*
6H-CC	C	P	A			T		R					R	T	R		A	R	
7H-CC	T	P	T																?
8H-CC	T	M													T				
9H-CC	T	P						T			T				T				
10H-CC	B																		
11H-CC	T	P						T			T			T	T				?
12H-CC	T	P						T									T		*C. d. davisiana*
13H-CC	T	P			T								T		T				?
14H-CC	T	M	T					T			T					T			
15H-CC	T	M						T		T				T					
16H-CC	T	M		T				T			T		T						
17H-CC	R	M		R	T	T	T	R	T	T	R				T				
18H-CC	T	M						T			T		T						
19H-CC	R	P					T	R	T	T	T		T		R				

Notes: Abundance: A = abundant, C = common, R = rare, T = trace, B = barren. Preservation: M = moderate, P= poor.

Table T11. Distribution of palynomorphs, Hole U1307A.

	Marine				Terrestrial					Reworked					Dinocyst assemblages																									
Core, section	Preservation	Dinocysts*	Foraminifer organic linings	Tasmanites	Preservation	Pollen	Spores of Pteridophytes	Spores of *Sphagnum*	*Pediastrum*	Acritarchs	Dinocysts	Angiosperm pollen	Bisaccate pollen	Trilete spores	*Brigantedinium* spp.	*Brigantedinium simplex*	*Islandinium minutum*	*Impagidinium aculeatum*	*Impagidinium paradoxum*	*Impagidinium plicatum*	*Impagidinium pallidum*	*Impagidinium* cf. *japonicum*	*Pentapharsodinium dalei*	*Bitectatodinium tepikeiense*	*Operculodinium centrocarpum*	*Operculodinium centrocarpum* (short process form)	*Nematosphaeropsis labyrinthus*	*Achomosphaera* sp.	*Achomosphaera andalousiense*	*Spiniferites frigidus*	*Spiniferites ramosus*	*Spiniferites* sp.	*Corrudinium? labradori*	cf. *Filisphaera filifera*	*Nematosphaeropsis* sp. 1 de Vernal and Mudie, 1989	*Operculodinium eirikianum*	*Barssidinium pliocenum*	*Cymatiosphaera? invaginata*	Incertae sedis sp. 1 de Vernal and Mudie, 1989	Correlation with zones at ODP Site 646 (cf. de Vernal and Mudie, 1989)
303-U1307A-																																								
1H-CC	M	x	x		G	XX	x	x	x				x	x	P	o	o							o	P				o	o	o	o								
2H-CC	?				?																																			
3H-CC	?				?	r					r																													I
4H-CC	M	x			G	r				x	x		x	XX											P				P			P								
5H-CC	M	x	r		G	x		r						x	P										o									o						
6H-CC	M	x			G	x	r	x					x	x								o			o		o						o							
7H-CC	M	x	x		G	x		r			x		r	x					o					o										P						
8H-CC	M	x	x		G	XX					r		x	x	P	P		o																						
9H-CC	M	XX			G	x		r	x			r	x	x	P	P		o							o							o		P						
10H-CC	?				G	r	r			x																														
11H-CC	G	x	r		G	x							r	r	o	o												o				o						P		
12H-CC	M	x			G	x		r	x					r	P		o							o			o							P				o		II
13H-CC	M	x			G	XX	x	x	x				r	r	P								o												o			P		
14H-CC	G	XXX	x	x	G	XX		x	x	r	r		r	r	x				r		r				r									r	XX			XXX		
15H-CC	G	XX		r	G	x							r	x	P				P	o	o	o			P		o								o			P		
16H-CC	G	XX			G	x		r						x	o			o	o						o										P			P	o	
17H-CC	G	XX	r	r	G	x		r							o										o									r				P	P	III
18H-CC	G	XX			G	x	x		x	r			x		x			r	r	r	r		r		r									r	XX			XXX	XX	
19H-CC	G	XXX		x	G	x				r					x							r	x		XX	x						r		r	r	r	r	XXX	XX	

Notes: * = *Cymatiosphaera* and *incertae sedis* sp. 1 included. Absolute abundances: XXXX = extremely abundant, XXX = abundant, XX = common, x = few, r = rare. Relative abundance of dinocyst taxa: XXX = dominant, XX = common, X = few, r = rare, P = presence, o = single occurrence.

Table T12. Polarity zonation, Holes U1307A and U1307B.

Polarity chron interpretation	Age (Ma)	Interval	Hole U1307A Core, section, interval (cm)	Hole U1307A Depth (mbsf)	Hole U1307A Depth (mcd)	Hole U1307B Core, section, interval (cm)	Hole U1307B Depth (mbsf)	Hole U1307B Depth (mcd)
			303-U1307A-			303-U1307B-		
C1n (b) Matuyama/Brunhes	0.78	Upper	4H-2, 65	30.65	32.69	4H-4, 135	29.65	32.84
		Lower	4H-2, 145	31.40	33.49	4H-5, 70	30.50	33.69
C1r.1n (t) Jaramillo	0.99	Upper	5H-2, 140	40.95	43.95	5H-5, 85	40.15	44.09
		Lower	5H-3, 125	42.22	45.27	5H-6, 60	41.40	45.34
C1r.1n (b) Jaramillo	1.07	Upper	5H-6, 30‡	45.77	48.82	6H-1, 100‡	43.80	48.17
		Lower	5H-7, 85	46.99	50.04	6H-2, 130	45.36	49.73
(t) Cobb Mountain	1.19*	Upper				6H-5, 100	49.56	53.93
		Lower				6H-6, 90	50.96	55.33
(b) Cobb Mountain	1.215*	Upper						
		Lower						
C2n (t) Olduvai	1.77	Upper	10H-3, 125	81.95	88.32	10H-3, 35	84.15	88.91
		Lower	10H-5, 70	84.40	90.77	10H-4, 80	86.10	90.86
C2n (b) Olduvai	1.945	Upper				11H-6, 100	97.88	103.08
		Lower				11H-7, 35	98.73	103.93
C2r.1n (t) Reunion	2.115†	Upper	12H-5, 45	103.15	110.83	12H-3, 140	104.20	110.62
		Lower	12H-5, 75	103.45	111.13	12H-4, 40	104.70	111.12
C2r.1n (b) Reunion	2.153†	Upper	12H-6, 60	104.80	112.48	12H-5, 10	105.90	112.32
		Lower	12H-6, 85	105.05	112.73	12H-5, 45	106.25	112.67
C2An.1n (t) Gauss/Matuyama	2.581	Upper	14H-3, 40	115.80	123.71	13H-6, 25	117.05	123.58
		Lower	14H-4, 15	117.05	124.10	13H-7, 25	118.55	125.08
C2An.1n (b)	3.04	Upper	17H-2, 55	137.25	145.11	15H-7, 60	137.90	146.15
		Lower	17H-2, 100	137.75	145.56	16H-1, 95**	138.75	148.07
C2An.2n (t)	3.11	Upper	17H-4, 55	140.25	148.11			
		Lower	17H-4, 90	140.60	148.46			
C2An.2n (b)	3.22	Upper	17H-5, 10	140.85	148.71			
		Lower	17H-4, 115	141.30	149.16			
C2An.3n (t)	3.33	Upper	18H-1, 80	145.50	153.89	16H-5, 50	144.30	153.62
		Lower	18H-2, 115	147.38	155.77	16H-6, 100	146.30	155.62
C2An.3n (b) Gauss/Gilbert	3.58	Upper	19H-6, 60	161.20	171.81			
		Lower	19H-6, 135	161.95	172.56			

Notes: (b) = bottom, (t) = top. Ages follow Cande and Kent (1995) except where indicated. * = Channell et al., 2002. † = Channell et al., 2003. ‡ = truncated by sand. ** = core break.

Table T13. Age interpretation, Site U1307.

Polarity chron interpretation	Age (Ma)	Depth (mcd)	Depth ± (m)
C1n (b) Matuyama/Brunhes	0.78	33	0.5
C1r.1n (t) Jaramillo	0.99	44.5	0.7
C1r.1n (b) Jaramillo	1.07	49.0	1
C2n (t) Olduvai	1.77	89.85	1
C2n (b) Olduvai	1.95	103.5	1
C2r.1n (t) Reunion	2.115	110.95	0.3
C2r.1n (b) Reunion	2.153	112.55	0.2
C2An.1n (t) Gauss/Matuyama	2.581	123.9	1
C2An.1n (b)	3.04	145.3	1
C2An.2n (t)	3.11	148.3	0.5
C2An.2n (b)	3.22	148.9	0.3
C2An.3n (t)	3.33	154.8	1
C2An.3n (b) Gauss/Gilbert	3.58	172.2	0.5

Note: b = bottom, t = top.

Table T14. Shipboard composite and corrected composite depths, Holes U1307A and U1307B.

Core	Top depth (mbsf)	Offset (m)	Top depth (mcd)	Top depth (cmcd)
303-U1307A-				
2H	9.50	0.19	9.69	9.14
3H	19.00	1.08	20.08	18.94
4H	28.50	2.04	30.54	28.81
5H	38.00	3.05	41.05	38.73
6H	47.50	3.05	50.55	47.69
7H	52.50	3.55	56.05	52.88
8H	62.00	5.13	67.13	63.33
9H	71.50	5.13	76.63	72.29
10H	77.70	6.37	84.07	79.31
11H	87.20	6.52	93.72	88.42
12H	96.70	7.68	104.38	98.47
13H	106.20	7.85	114.05	107.59
14H	112.40	7.91	120.31	113.50
15H	121.90	7.77	129.67	122.33
16H	125.70	7.86	133.56	126.00
17H	135.20	7.86	143.06	134.96
18H	144.70	8.39	153.09	144.42
19H	153.10	10.61	163.71	154.44
303-U1307B-				
1H	0.00	0.00	0.00	0.00
2H	4.80	0.40	5.20	4.91
3H	14.30	1.30	15.60	14.72
4H	23.80	3.19	26.99	25.46
5H	33.30	3.94	37.24	35.13
6H	42.80	4.37	47.17	44.50
7H	52.30	4.37	56.67	53.46
8H	61.80	4.91	66.71	62.93
9H	71.30	4.54	75.84	71.55
10H	80.80	4.76	85.56	80.72
11H	90.30	5.20	95.50	90.09
12H	99.80	6.42	106.22	100.21
13H	109.30	6.53	115.83	109.27
14H	118.80	7.98	126.78	119.60
15H	128.30	8.25	136.55	128.82
16H	137.80	9.32	147.12	138.79
17H	147.30	9.32	156.62	147.75

Table T15. Sampling splice tie points, Site U1307.

Hole, core, section, interval (cm)	Depth (mbsf)	Depth (mcd)		Hole, core, section, interval (cm)	Depth (mbsf)	Depth (mcd)
1307B-1H-2, 23.1	1.92	1.92	Tie to	1307A-1H-2, 41.7	1.73	1.92
1307A-1H-5, 93.10	6.93	7.12	Tie to	1307B-2H-2, 41.90	6.72	7.12
1307B-2H-5, 40.50	11.20	11.60	Tie to	1307A-2H-2, 41.10	11.41	11.60
1307A-2H-6, 51.20	17.51	17.70	Tie to	1307B-3H-2, 59.60	16.40	17.70
1307B-3H-5, 81.90	21.12	22.42	Tie to	1307A-3H-2, 84.10	21.34	22.42
1307A-3H-6, 73.20	27.23	28.31	Tie to	1307B-4H-1, 132.00	25.12	28.31
1307B-4H-5, 88.10	30.68	33.87	Tie to	1307A-4H-3, 32.10	31.83	33.87
1307A-4H-6, 64.40	36.64	38.68	Tie to	1307B-5H-1, 144.00	34.74	38.68
1307B-5H-4, 63.40	38.43	42.37	Tie to	1307A-5H-1, 132.00	39.32	42.37
1307A-5H-5, 133.70	45.31	48.36	Tie to	1307B-6H-1, 118.50	43.99	48.36
1307B-6H-7, 77.30	52.11	56.48	Append to	1307B-7H-1, 0.00	52.30	56.67
1307B-7H-7, 63.30	61.98	66.35	Append to	1307B-8H-1, 0.00	61.80	66.71
1307B-8H-4, 18.60	66.49	71.40	Tie to	1307A-8H-3, 126.60	66.27	71.40
1307A-8H-7, 31.30	71.31	76.44	Tie to	1307B-9H-1, 60.00	71.90	76.44
1307B-9H-7, 25.30	80.55	85.09	Tie to	1307A-10H-1, 102.00	78.72	85.09
1307A-10H-5, 95.50	84.66	91.03	Tie to	1307B-10H-4, 96.70	86.27	91.03
1307B-10H-7, 5.20	89.85	94.61	Tie to	1307A-11H-1, 88.50	88.09	94.61
1307A-11H-4, 22.80	91.93	98.45	Tie to	1307B-11H-2, 144.50	93.25	98.45
1307B-11H-7, 99.10	99.48	104.68	Tie to	1307A-12H-1, 30.00	97.00	104.68
1307A-12H-3, 18.10	99.88	107.56	Tie to	1307B-12H-1, 132.00	101.14	107.56
1307B-12H-7, 60.60	109.41	115.83	Tie to	1307B-13H-1, 0.00	109.30	115.83
1307B-13H-5, 131.60	116.62	123.15	Tie to	1307A-14H-2, 133.90	115.24	123.15
1307A-14H-6, 23.00	120.13	128.04	Tie to	1307B-14H-1, 126.00	120.06	128.04
1307B-14H-7, 60.20	128.40	136.38	Append to	1307B-15H-1, 0.00	128.30	136.55
1307B-15H-7, 70.00	138.00	146.25	Append to	1307B-16H-1, 0.00	137.80	147.12
1307B-16H-5, 145.00	145.25	154.57	Tie to	1307A-18H-1, 145.00	146.18	154.57
1307A-18H-6, 70.00	152.93	161.32	Append to	1307A-19H-1, 0.00	153.10	163.71
1307A-19H-7, 71.00	162.81	173.42				

Table T16. Depth ranges and sedimentation rates, Site U1307.

Depth interval (mcd)	Sedimentation rate (cm/k.y.)
0–33.0	4.2
33.0–44.5	5.5
44.5–49.0	5.6
49.0–54.6	4.7
54.6–89.9	6.1
89.9–103.5	7.6
103.5–111.0	4.5
111.0–112.6	4.2
112.6–123.9	2.7
123.9–145.3	4.7
145.3–148.3	4.3
148.3–148.9	0.5
148.9–154.6	5.2
154.6–172.2	7.0

Table T17. Headspace hydrocarbon gases, Hole U1307A.

Core, section, interval (cm)	Depth (mbsf)	Depth (mcd)	C_1/C_2	C_1 (ppmv)	C_2 (ppmv)
303-U1307A-					
1H-2, 0.0–5.0	1.50	1.69		216	0.0
2H-2, 0.0–5.0	11.00	11.19		132	0.0
3H-2, 0.0–5.0	20.50	21.58		53	0.0
4H-2, 0.0–5.0	30.00	32.04		33	0.0
5H-2, 0.0–5.0	39.50	42.55		27	0.0
6H-2, 0.0–5.0	49.00	52.05		34	0.0
7H-2, 0.0–5.0	54.00	57.55		31	0.0
8H-2, 0.0–5.0	63.50	68.63		36	0.0
9H-2, 0.0–5.0	73.00	78.13		49	0.0
10H-2, 0.0–5.0	79.20	85.57		89	0.0
11H-2, 0.0–5.0	88.70	95.22		1,987	0.0
12H-2, 0.0–5.0	98.20	105.88	3,551	6,391	1.8
13H-2, 0.0–5.0	107.70	115.55	4,023	10,459	2.6
14H-2, 0.0–5.0	113.90	121.81	2,566	14,627	5.7
15H-2, 0.0–5.0	123.40	131.17	3,593	7,186	2.0
16H-4, 0.0–5.0	130.20	138.06	3,844	23,830	6.2
17H-2, 0.0–5.0	136.70	144.56	3,462	23,194	6.7
18H-2, 0.0–5.0	146.23	154.62	3,906	22,264	5.7
19H-2, 0.0–5.0	154.60	165.21	3,716	26,015	7.0

Table T18. Bulk sedimentary carbon and nitrogen, Hole U1307A.

Core, section, interval (cm)	Depth (mbsf)	Depth (mcd)	Carbon (wt%) Inorganic	$CaCO_3$	Total	Organic	Nitrogen (wt%)	Organic C/N
303-U1307A-								
1H-1, 138–139	1.38	1.57	1.06	8.85	1.12	0.06	0.00	
1H-6, 3–4	7.53	7.72	0.68	5.69	0.57		0.03	
2H-1, 138–139	10.88	11.07	0.68	5.64	0.64		0.00	
2H-6, 3–4	17.03	17.22	0.42	3.51	0.26		0.03	
3H-1, 138–139	20.38	21.46	1.27	10.61	1.22		0.00	
3H-6, 3–4	26.53	27.61	0.59	4.95	0.52		0.05	
4H-1, 138–139	29.88	31.92	0.32	2.68	0.36	0.04	0.04	1.09
4H-6, 3–4	36.03	38.07	0.22	1.85	0.27	0.05	0.05	1.07
5H-1, 138–139	39.38	42.43	0.25	2.05	0.26	0.01	0.05	0.12
5H-6, 3–4	45.50	48.55	6.92	57.64	7.29	0.37	0.00	
7H-1, 138–139	53.88	57.43	0.09	0.78	0.18	0.09	0.00	
7H-6, 3–4	60.03	63.58	0.19	1.61	0.31	0.12	0.05	2.21
8H-1, 149–150	63.49	68.62	0.29	2.38	0.32	0.03	0.05	0.67
8H-6, 0–1	69.50	74.63	0.20	1.63	0.25	0.05	0.03	1.73
9H-1, 147–148	72.97	78.10	0.35	2.96	0.45	0.10	0.07	1.40
10H-1, 143–144	79.13	85.50	0.22	1.80	0.25	0.03	0.03	1.03
10H-6, 1–2	85.21	91.58	0.14	1.21	0.56	0.42	0.08	4.94
11H-1, 149–150	88.69	95.21	0.12	0.97	0.44	0.32	0.08	4.16
11H-6, 1–2	94.71	101.23	1.42	11.84	1.51	0.09	0.03	2.82
12H-1, 149–150	98.19	105.87	0.93	7.79	0.78		0.05	
13H-1, 144–145	107.64	115.49	0.08	0.67	0.19	0.11	0.05	2.24
13H-4, 1–2	110.71	118.56	0.04	0.35	0.27	0.23	0.06	4.00
14H-1, 147–148	113.87	121.78	0.06	0.50	0.35	0.29	0.07	4.38
14H-6, 1–2	119.91	127.82	0.03	0.28	0.44	0.41	0.08	5.49
15H-1, 143–144	123.33	131.10	0.93	7.78	1.05	0.12	0.05	2.27
16H-6, 3–4	133.23	141.09	0.33	2.76	0.57	0.24	0.07	3.71
17H-1, 143–144	136.63	144.49	0.20	1.65	0.40	0.20	0.06	3.49
17H-6, 3–4	142.73	150.59	1.43	11.92	1.57	0.14	0.04	3.36
18H-1, 143–144	146.13	154.52	0.29	2.43	0.44	0.15	0.04	3.85
18H-6, 3–4	152.26	160.65	0.33	2.78	0.51	0.18	0.06	3.13
19H-1, 138–139	154.48	165.09	0.45	3.76	0.55	0.10	0.03	3.02

Table T19. Interstitial water geochemistry, Hole U1307A.

Core, section, interval (cm)	Depth (mbsf)	Depth (mcd)	Anions (mM) SO_4^{2-}	Anions (mM) Cl^-	pH	Alkalinity (mM)	Salinity (g/kg)	Major cations (mM) Na^+	K^+	Mg^{2+}	Ca^{2+}	Minor and trace constituents (µM) NH_4^+	B	Ba^{2+}	Fe^{2+}	Li^+	Mn^{2+}	H_4SiO_4	Sr^{2+}	Ratios (µM/mM) Sr/Ca	Li/Ca
303-U1307A-																					
1H-1, 145.0–150.0	1.45	1.64	29.06	560	7.22	2.86	35	488	11.35	50.88	10.11	11	428	0.7	0.1	22.9	0.2	338	86.6	8.57	2.27
2H-1, 145.0–150.0	10.95	11.14	25.51	563	7.34	3.72	35	486	11.30	50.01	10.16	131	412	0.6	13.4	14.2	93.5	493	86.2	8.48	1.39
3H-1, 145.0–150.0	20.45	21.53	22.11	566	7.52	4.22	35	485	11.06	48.30	10.81	252	372	0.3	10.9	11.4	44.9	416	83.4	7.71	1.05
4H-1, 145.0–150.0	29.95	31.99	18.22	567	7.36	4.88	34	488	10.90	45.95	8.93	344	427	0.4	12.8	10.4	31.5	461	82.6	9.26	1.16
5H-1, 145.0–150.0	39.45	42.50	14.11	568	7.44	5.77	34	486	10.70	44.13	8.27	469	397	0.4	17.1	11.5	24.6	545	83.0	10.03	1.39
6H-1, 145.0–150.0	48.95	52.00	9.19	568	7.76	7.51	34	487	10.66	40.67	7.58	691	338	0.5	3.5	12.4	20.6	472	81.3	10.72	1.64
7H-1, 145.0–150.0	53.95	57.50	9.51	569	7.94	7.65	34	487	11.06	40.98	7.52	665	321	0.5	1.7	12.5	19.1	458	79.5	10.58	1.66
10H-1, 145.0–150.0	79.15	85.52	1.58	569	7.79	10.08	33	487	9.96	37.42	5.27	1002	355	5.9	2.9	11.8	8.6	520	75.9	14.42	2.23
13H-1, 145.0–150.0	107.65	115.50	0.56	571	7.45	9.99	34	488	9.66	36.82	5.34	1334	384	10.1	13.5	15.9	10.4	823	81.1	15.20	2.98
16H-3, 145.0–150.0	130.15	138.01	0.89	574	7.46	9.77	34	491	9.39	37.09	5.46	1590	405	10.8	11.6	20.1	8.3	848	82.9	15.19	3.68
19H-1, 145.0–150.0	154.55	165.16	0.80	575	7.32	8.89	34	493	8.88	36.57	5.60	1895	393	9.6	19.6	23.5	2.7	886	83.0	14.82	4.20